Politecnico di Milano

Scuola di Ingegneria Civile, Ambientale e Territoriale

Laurea Magistrale in
Ingegneria Civile - Civil Engineering

Non linear distributions of temperature and their long term creep-relaxation behaviour interaction in R.C. homogeneous and composite R.C.-steel bridges.

Luca Forni Mat. 945575

Advisor:
Prof. Franco Mola

Academic Year 2020/2021

INDEX

ABSTRACT **11**

SOMMARIO **13**

SOMMARIO ESTESO **15**

1 AIM OF THE RESEARCH **21**

2 THERMAL ACTIONS ON STRUCTURES **23**

2.1 Introduction 23

2.2 Climatic factors influencing the thermal response of a structure 23

2.2.1 Air temperature 23

2.2.2 Wind velocity 25

2.2.3 Short wave radiation (solar radiation) 25

2.2.4 Long wave radiation (thermal radiation) 25

2.3 Thermal distribution computation 26

2.3.1 Heat transfer equations 27

2.3.2 Boundary conditions 28

2.3.3 Numerical integration of the Fourier Equation 31

2.4 Thermal actions in prismatic structures 32

2.4.1 Deformations suppression method 32

2.4.2 Alternative procedure to the deformations suppression method 36

2.4.3 General definition of thermal action 38

2.4.4 Classification of thermal actions 39

2.5 Code provisions 40

3 ELASTIC FIELD **45**

3.1 Introduction 45

3.2 Compatibility stresses due to non-linear temperature variations 45

3.3 Additional stresses due to redundant restraints 47

3.4 Examples of applications 47

3.4.1 Example 1 47

3.4.2 Example 2 55

3.4.3 Example 3 67

3.4.4 Example 4 71

4 VISCOELASTIC FIELD **75**

4.1 Introduction 75

4.2 Computation of stresses due to imposed deformations 76

4.2.1 Exact formulation 76

4.2.2 Algebraic approach 78

4.2.3 Fundamental Theorem 81

4.3 Numerical solution of the Volterra Integral Equation 85

4.3.1 Algorithm for the computation of the stresses 85

4.3.2 Time step definition 89

4.3.3 Example of application 91

4.4 Application of the Fundamental Theorem 95

4.4.1 Example of application with temperature distributions variable in time 95

4.4.2 Example of application with temperature distributions constant in time 99

5 VISCOELASTIC FIELD AND SINUSOIDAL TEMPERATURE VARIATIONS **103**

5.1 Introduction 103

5.2 Sinusoidal temperature variations 103

5.3 Numerical solution of the Volterra Integral Equation 110

5.4 Example of application 112

6 CASE STUDIES **119**
6.1 Introduction 119
6.2 Case study 1: Multi-span continuous box girder bridge 119
6.2.1 Description of the structure 119
6.2.2 Analysis of the structure in the elastic field 122
6.2.3 Analysis of the structure in the viscoelastic field 128
6.3 Case study 2: Simply supported bridge with composite deck 131
6.3.1 Description of the structure 131
6.3.2 Analysis of the structure in the elastic field 132
6.3.3 Analysis of the structure in the viscoelastic field 137

7 CONCLUSIONS AND FUTURE RESEARCH **143**

REFERENCES **145**

INDEX OF FIGURES

Figure 1- Daily variations of shade air temperature 24
Figure 2 - Annual variation of average monthly temperatures 24
Figure 3 – Air temperature and fictitious sun-air temperature example 30
Figure 4 – Approximation of the daily variation of air temperature 31
Figure 5 - Long prismatic body of finite length 33
Figure 6 – Generic cross section 36
Figure 7 – Correlation between shade air temperature and the average effective temperature of bridges according to EC1 (based on the results by M.Emerson) 41
Figure 8 – Heating temperature profile (left) and cooling temperature profile (right) adopted by the British code 42
Figure 9 – Temperature profiles adopted by the New Zealand code (above) and by the Australian code (below) 43
Figure 10 – Homogeneous rectangular cross section subject to a parabolic temperature distribution over its depth 48
Figure 11 – Compatibility stresses distribution over the depth of the cross section 50
Figure 12 – Total deformation of the cross section 50
Figure 13 - Two times redundant static scheme and relative redundant variables 51
Figure 14 – Total stresses distribution over the depth of the cross section 53
Figure 15 - One time redundant static scheme and relative redundant variable 53
Figure 16 – Total stresses distribution over the depth of the cross section 54
Figure 17 – Homogeneous rectangular section subject to a discontinuous temperature distribution over its depth 55
Figure 18 – Compatibility stresses distribution over the depth of the cross section 57
Figure 19 – Total deformation of the cross section 57
Figure 20 - One time redundant static scheme and relative redundant variable 59
Figure 21 - Total stresses distribution over the depth of the cross section 60
Figure 22 - Two times redundant static scheme and relative redundant variables 60
Figure 23 - Total stresses distribution over the depth of the cross section 62
Figure 24 - Three times redundant static scheme and relative redundant variables 62
Figure 25 - Total stresses distribution over the depth of the cross section 64
Figure 26 - Total stresses distribution over the depth of the cross section 64
Figure 27 - Four times redundant static scheme with elastic restraints and relative redundant variables 65
Figure 28 - Total stresses distribution over the depth of the cross section 66
Figure 29 - Total stresses distribution over the depth of the cross section 67
Figure 30 - Homogeneous T-shaped cross section subject to an exponential temperature distribution over its depth 68
Figure 31 – Compatibility stresses distribution over the depth of the cross section 69

Figure 32 - Total deformation of the cross section 70
Figure 33 - Homogeneous T-shaped cross section subject to a discontinuous non-linear temperature distribution over its depth 72
Figure 34 – Compatibility stresses distribution over the depth of the cross section..... 74
Figure 35 – Total deformation of the cross section 74
Figure 36 – Creep Function $J(t, t0)$ 88
Figure 37– Relaxation Function $R(t, t0)$ 89
Figure 38 – Time step amplitude according to CEB bulletin 142-142bis 90
Figure 39 – Time variation of the parameter $T0$..... 92
Figure 40 – Compatibility stresses comparison 93
Figure 41 – Total stresses comparison (Static scheme 1) 94
Figure 42 - Total stresses comparison (Static scheme 2)..... 94
Figure 43 – Comparison of the solutions in the viscoelastic field 96
Figure 44 – Compatibility stresses comparison 96
Figure 45 - Comparison of the solutions in the viscoelastic field..... 97
Figure 46 – Total stresses comparison (Static scheme 1) 97
Figure 47 - Comparison of the solutions in the viscoelastic field..... 98
Figure 48 – Total stresses comparison (Static scheme 2) 98
Figure 49 - Compatibility stresses comparison..... 101
Figure 50 – Total stresses comparison (Static scheme 1) 101
Figure 51 - Total stresses comparison (Static scheme 2)..... 102
Figure 52 – Temperature function (casting of the structure in Spring) 104
Figure 53 - Temperature function over the period of 1 year..... 105
Figure 54 – Temperature function (casting of the structure in Autumn) 106
Figure 55 - Temperature function over the period of 1 year..... 106
Figure 56 – Temperature function (casting of the structure in Winter) 107
Figure 57 - Temperature function over the period of 1 year..... 108
Figure 58 – Temperature function (casting of the structure in Summer) 109
Figure 59 - Temperature function over the period of 1 year..... 109
Figure 60 – Time step amplitude (casting of the structure in Spring or Autumn)..... 111
Figure 61 – Time step amplitude (casting of the structure in Summer or Winter)..... 112
Figure 62 - Variation in time of the compatibility stress 114
Figure 63 - Comparison of elastic and viscoelastic solutions..... 114
Figure 64 - Variation in time of the compatibility stress 115
Figure 65 - Comparison of elastic and viscoelastic solutions..... 115
Figure 66 - Variation in time of the compatibility stress 116
Figure 67 - Comparison of elastic and viscoelastic solutions..... 116
Figure 68 - Variation in time of the compatibility stress 117
Figure 69 - Comparison of elastic and viscoelastic solutions..... 117
Figure 70 – Case study 1: Multi-span continuous box girder bridge..... 120
Figure 71 – Cross section shape and dimensions (in cm)..... 120
Figure 72 – Eurocode 1 non-linear temperature distribution (heating) 121
Figure 73 – Compatibility stresses distribution over the depth of the cross section..... 124

Figure 74 – Total deformation of the cross section 124
Figure 75 – Static scheme of the multi-span bridge 126
Figure 76 - Static scheme of the multi-span bridge and relative redundant variables 127
Figure 77 – Total stresses distribution over the depth of the cross section 128
Figure 78 – Compatibility stresses comparison 130
Figure 79 – Total stresses comparison 130
Figure 80 – Cross section of the composite deck (dimensions in mm) 131
Figure 81 - I-shaped steel beam (dimensions in mm) 131
Figure 82 – Compatibility stresses distribution over the depth of the cross section 135
Figure 83 – Total deformation of the cross section 135
Figure 84 – Compatibility stresses comparison 140
Figure 85– Total deformation of the cross section comparison 141

ABSTRACT

The analysis of the response of bridges to thermal actions is a particularly relevant topic, as confirmed by several cases of damages suffered by this type of structures reported in literature. Bridge structures are subject to non-linear temperature distributions generating compatibility stresses in order to satisfy the plane section hypothesis under Bernoulli beam bending. Moreover when redundant structures are considered, the effect of thermal actions produces additional stresses due to the reactions of the redundant restraints. In this framework, the aim of the present work is to evaluate the influence of the long term creep-relaxation behaviour of concrete on these stresses. In order to do this, various techniques for the analysis in the viscoelastic field are studied with reference to this particular problem, arriving to define the exact formulation which should be adopted in the case in which the sinusoidal variation in time of the temperature distributions is considered. However, in addition to the exact formulation, also approximate solutions, more suitable for the engineering practice, are explored. In particular, in order to show the application of the procedures for the long-term analysis in the viscoelastic field to real bridge structures, two case studies are analysed: a multi-span box girder bridge and a simply supported bridge with composite deck. Moreover this second structure allows to show the extension of the procedure to the case of non-homogenous cross sections, in order to provide the necessary tools to analyse also composite reinforced concrete-steel bridges.

Key words:

Reinforced Concrete and Composite Bridges; Thermal Variation; Creep; Integral Equations; Algebraic Approach; Fundamental Theorem.

SOMMARIO

L'analisi della risposta dei ponti alle azioni termiche è una tematica particolarmente rilevante, come confermato da diversi casi di gravi danni subiti da strutture di questo tipo e documentati in letteratura. Le strutture da ponte sono soggette a distribuzioni di temperatura non lineari che generano sforzi di compatibilità necessari affinché sia soddisfatta l'ipotesi di sezione piana secondo la teoria della trave inflessa di Bernoulli. Inoltre, quando si considerano strutture iperstatiche, l'effetto delle azioni termiche produce sollecitazioni aggiuntive dovute alle reazioni dei vincoli iperstatici. In questo quadro, lo scopo del presente lavoro è valutare l'influenza del comportamento a lungo termine del calcestruzzo su queste sollecitazioni. A tal fine vengono studiate diverse tecniche di analisi in campo viscoelastico, con riferimento a questo particolare problema, arrivando a definire la formulazione esatta che dovrebbe essere adottata nel caso in cui si consideri la variazione sinusoidale nel tempo delle distribuzioni di temperatura. Tuttavia, oltre alla formulazione esatta, vengono esplorate anche soluzioni approssimate, più adatte alla pratica ingegneristica. In particolare, al fine di mostrare l'applicazione delle procedure per l'analisi a lungo termine in campo viscoelastico a strutture da ponte reali, sono stati analizzati due casi studio: un ponte a cassone con travata continua su più campate ed un ponte in semplice appoggio con sezione mista acciaio-calcestruzzo. Questa seconda struttura permette inoltre di mostrare l'estensione della procedura descritta al caso di sezioni trasversali non omogenee, al fine di fornire gli strumenti necessari per analizzare anche i ponti con sezione mista acciaio-calcestruzzo.

Parole chiave:

Ponti in Calcestruzzo Armato e a Sezione Mista; Variazione Termica; Deformazioni Viscose; Equazioni Integrali; Formulazioni Algebriche; Teorema Fondamentale.

SOMMARIO ESTESO

L'analisi della risposta dei ponti alle azioni termiche è una tematica particolarmente rilevante, come confermato da diversi casi di gravi danni subiti da strutture di questo tipo e documentati in letteratura. Le strutture da ponte sono soggette a distribuzioni di temperatura non lineari che generano sforzi di compatibilità necessari affinché sia soddisfatta l'ipotesi di sezione piana secondo la teoria della trave inflessa di Bernoulli. Inoltre, quando si considerano strutture iperstatiche, l'effetto delle azioni termiche produce sollecitazioni aggiuntive dovute alle reazioni dei vincoli iperstatici. In questo quadro, lo scopo del presente lavoro è valutare l'influenza del comportamento a lungo termine del calcestruzzo su queste sollecitazioni.

Il presente lavoro di tesi si sviluppa in sette capitoli i cui contenuti sono brevemente illustrati nel prosieguo.

Il **primo capitolo** è dedicato all'introduzione della problematica oggetto di studio, delineando inoltre le fasi secondo cui la ricerca si è sviluppata.

Nel **secondo capitolo** viene fornita una panoramica degli aspetti necessari a definire le azioni termiche agenti sulle strutture, prestando particolare attenzione al caso delle strutture da ponte. La corretta definizione delle azioni termiche dovute al clima è infatti un presupposto necessario al fine di trattare correttamente le problematiche affrontate nei capitoli successivi.

Inizialmente si sono considerati i fattori climatici che influenzano la risposta termica delle strutture, tra i quali particolare importanza è ricoperta dalla temperatura dell'aria, la quale presenta variazioni annuali e giornaliere con andamento prossimo a quello di una sinusoide.

Si descrive quindi brevemente il problema del calcolo delle distribuzioni di temperatura nelle strutture.

Viene poi presentato il metodo di soppressione delle deformazioni che permette di definire, nota la distribuzione di temperatura sulla sezione di un corpo prismatico a cui possono essere assimilati gli impalcati da ponte, le azioni geometriche agenti su di esso. Un'alternativa a tale metodo, utilizzato per la definizione delle deformazioni imposte su di una struttura a causa della temperatura, viene inoltre presentata in quanto adottata per le successive analisi.

Infine una breve rassegna delle normative riguardanti le azioni termiche sulle strutture è illustrata.

Nel **terzo capitolo** si presenta l'analisi in campo elastico di strutture omogenee soggette a distribuzioni di temperatura non lineari. Sulla base della procedura alternativa al metodo della soppressione delle deformazioni precedentemente descritta, si illustra dal punto di vista teorico il

calcolo degli sforzi di compatibilità dovuti alla non linearità della distribuzione di temperatura. Inoltre viene presentata la procedura per il calcolo delle sollecitazioni aggiuntive da considerarsi nel caso di strutture iperstatiche.

Avendo definito compiutamente gli aspetti teorici necessari al calcolo delle sollecitazioni che nascono nelle strutture omogenee soggette a distribuzioni di temperatura non lineari, si analizzano diversi casi di applicazione considerando vari tipi di sezioni soggette a differenti distribuzioni di temperatura non lineari, calcolando allo stesso tempo gli sforzi aggiuntivi associati ad alcuni schemi strutturali iperstatici. Attraverso tali esempi di applicazione ci si propone infatti di mostrare l'applicabilità della procedura presentata alle più svariate situazioni, ponendo in evidenza, di volta in volta, le complicazioni che nascono a causa della particolare sezione considerata o della particolare distribuzione di temperatura applicata.

Il **quarto capitolo** è dedicato all'analisi in campo viscoelastico di strutture omogenee soggette a distribuzioni di temperatura non lineari, al fine di valutare l'influenza del comportamento a lungo termine del calcestruzzo sugli sforzi che nascono nei ponti a causa delle azioni termiche. Gli aspetti teorici necessari ad effettuare questo tipo di analisi sono dettagliatamente discussi nel contesto della viscoelasticità lineare.

In particolare tre procedure alternative per il calcolo degli sforzi dovuti a deformazioni imposte variabili nel tempo vengono presentate e specializzate alla problematica in esame delle strutture omogenee soggette a distribuzioni di temperatura non lineari. Tali procedure sono rappresentate dalla formulazione esatta, basata sulla risoluzione di un'Equazione Integrale di Volterra, dall'approccio algebrico ed infine dal Teorema Fondamentale.

Risulta tuttavia importante precisare che, sulla base di quanto discusso nel capitolo 2 con riferimento alle azioni climatiche sulle strutture, l'analisi rigorosa delle problematiche oggetto di studio dovrebbe prendere in considerazione una variazione nel tempo delle deformazioni imposte che abbia un andamento sinusoidale. Tuttavia tale aspetto introduce diverse complicazioni nell'analisi in campo viscoelastico perciò, al fine di discutere compiutamente le strategia da adottare per poter far fronte a queste situazioni, si rimanda al capitolo 5, proponendosi di considerare nel quarto capitolo variazioni nel tempo della distribuzione di temperatura più convenzionali.

Dal momento che la formulazione esatta porta alla scrittura di un'Equazione Integrale di Volterra, si è presentata in dettaglio la procedura numerica che è stata implementata par la sua risoluzione. Si sono presentati inoltre i risultati in campo viscoelastico in termini di sollecitazioni generate dalle azioni termiche a 10000 giorni ottenuti con la procedura implementata per uno degli esempi analizzati nel capitolo 3 con riferimento al campo elastico. In questo modo è stato quindi possibile valutare la riduzione degli sforzi in campo viscoelastico attraverso un confronto tra quanto calcolato precedentemente in campo elastico e quanto risulta dalla procedura numerica di integrazione dell'Equazione Integrale di Volterra.

Si applica inoltre, per la risoluzione dello stesso problema, il Teorema Fondamentale, il quale fornisce una soluzione approssimata del problema in esame. I risultati così ottenuti sono stati comparati con quelli derivanti dalla formulazione esatta, attraverso la risoluzione dell'Equazione Integrale di Volterra, permettendo quindi di evidenziare l'eccellente livello di approssimazione associato al Teorema Fondamentale. Tale considerazione, unitamente alla semplicità di applicazione di tale metodo che consiste sostanzialmente nella sovrapposizione di tre soluzioni elastiche opportunamente combinate, permette di identificare nel Teorema Fondamentale un valido strumento da applicarsi nella pratica ingegneristica.

Infine lo stesso teorema è stato applicato al caso di distribuzioni di temperatura costanti nel tempo in quanto le normative nazionali ed internazionali fornisco gradienti di temperatura da adottarsi nell'analisi delle problematiche in esame che risultano appunto costanti nel tempo. Tale procedura sarà infatti adottata in seguito, nel sesto capitolo, per l'analisi di due casi studio su reali strutture da ponte.

Nel **quinto capitolo** si giunge a definire la formulazione esatta per l'analisi in campo viscoelastico delle problematiche in esame. Come già anticipato, una trattazione rigorosa del problema del calcolo delle sollecitazioni che nascono nelle strutture da ponte a causa di distribuzioni di temperatura non lineari prevederebbe l'adozione di una variazione di temperatura con legge sinusoidale, la quale permette di riprodurre con sufficiente precisione la variazione stagionale delle azioni climatiche. In questo contesto il Teorema Fondamentale non risulta applicabile e perciò la formulazione esatta risulta l'unica via percorribile per la soluzione del problema.

Al fine di approcciare correttamente la definizione delle variazioni di temperatura sinusoidali, si sono considerate quattro diverse funzioni di temperatura variabili nel tempo secondo legge sinusoidale, associate a quattro diversi scenari riguardanti la stagione dell'anno in cui avviene il getto dell'opera.

Tuttavia, nonostante si sia già ampiamente discussa nel capitolo 4 la tecnica numerica per la risoluzione dell'Equazione Integrale di Volterra che governa il problema, si è reso necessario rivedere tale procedura, adattando opportunamente gli intervalli di integrazione, al fine di ottenere risultati affidabili anche nel caso di storie di deformazioni variabili con legge sinusoidale a causa della particolare variabilità temporale considerata per la distribuzione di temperatura.

La procedura implementata così modificata è stata quindi adottata, allo scopo di fornire un esempio di applicazione, per risolvere il medesimo problema considerato per le analisi in campo viscoelastico riportate nel capitolo 4. In questo caso è stata però adottata una variazione della distribuzione di temperatura con andamento sinusoidale e perciò si è ritenuto più significativo presentare graficamente i risultati dell'evoluzione delle sollecitazioni nel tempo, piuttosto che i risultati in termini di distribuzione delle sollecitazioni sulla sezione trasversale. Inoltre l'analisi di tale problema è stata svolta considerando i diversi scenari relativi alla stagione dell'anno in cui avviene il getto dell'opera, mettendo in evidenza le differenze che si possono riscontrare in termini di sollecitazioni nei vari casi.

Infine il **sesto capitolo** è dedicato all'analisi di due casi studio riguardanti la valutazione della risposta a lungo termine di strutture reali da ponte soggette alle azioni termiche. In particolare si sono considerati il caso di un ponte a cassone con travata continua su più campate e di un ponte in semplice appoggio con sezione mista acciaio-calcestruzzo.

Il primo caso studio ha permesso di mostrare l'applicabilità delle procedure discusse in presenza della distribuzione di temperatura non-lineare fornita dalla normativa europea mentre il secondo caso studio ha permesso di mostrare l'estensione della procedura, precedentemente discussa con riferimento al caso di sezioni omogenee, al caso di sezioni miste acciaio-calcestruzzo.

Nel **capitolo 7** sono riportate le conclusioni ed un breve accenno a possibili ricerche future nell'ambito del lavoro svolto.

1 AIM OF THE RESEARCH

Structures are subject to temperature distributions which are, generally, complicated functions of the spatial coordinates and of time. As a consequence, due to the strong non-linearity of the temperature distributions, compatibility stresses are generated to satisfy the plane section hypothesis under Bernoulli beam bending. Moreover, in the case of redundant structures, the effect of thermal actions produces an additional state of stress due to the reactions of the additional restraints. The knowledge of the stresses caused by temperature variations is of paramount importance both in the design phase as well as in the verification stage. As a matter of fact, it is not possible to ignore thermal effects due to climatic actions in structures as they can influence not only the durability and functionality of the structure itself but they can also reduce the safety margin at collapse. Thermal actions can indirectly compromise the safety of a reinforced concrete structure when they lead to severe cracking, causing the corrosion of rebars and, in the case of beams, when the cracking is so extended over the depth of the section to compromise the shear resistance.

Despite the importance and complexity of this topic, climatic thermal actions have often been approached in a simplistic way, as well explained by Froli [1] and testified by many references that can be found in literature. In particular, in 1979, Leonhardt [2] drew the attention to the damages caused in structures, primarily in bridges, due to an inadequate design against thermal actions. This topic, in fact, has particular relevance when dealing with bridges as confirmed by several cases of severe damages suffered by this type of structures.

In this framework, the aim of the present work is to evaluate the influence of the long-term behaviour of concrete on the stresses which arise in bridges due to thermal actions.

An introduction aimed at describing the climatic actions on structures will be provided, highlighting in particular their cyclic behaviour which will be a key aspect to consider when dealing with the analysis performed in the viscoelastic field. In addition to this, a brief overview of code prescriptions from various country regarding thermal actions will be also provided.

The analysis of the compatibility stresses due to non-linear temperature distributions, as well as the analysis of the additional stresses which arise in presence of thermal actions in redundant structures, will be first addressed with reference to the elastic field for the case of homogeneous sections. The results obtained in this way will allow to set a reference for the computations performed in the viscoelastic field, in order to take into account the influence of the long-term behaviour of concrete.

The applicability to this particular problem of the various techniques which can be adopted for the analysis in the viscoelastic field, will be then discussed. In fact, because of the peculiar cyclic

variation in time of the thermal actions, special considerations must be done in approaching the problem of the long-term response of the structure.

Finally, after having discussed in detail all the theoretical aspects characterizing the problem of the evaluation of the long-term response of bridges to thermal actions, two real structures will be analysed: a multi-span box girder bridge, characterized by a redundant static scheme, and a bridge with composite deck and simply supported static scheme. This will allow also to show the extension of the procedure, previously discussed with reference to homogeneous cross sections, to the case of non-homogenous cross sections, in order to provide the necessary tools to analyse also bridges with composite decks.

2 THERMAL ACTIONS ON STRUCTURES

2.1 Introduction

The aim of the present chapter is to provide an overview of the theoretical aspects necessary to define the thermal actions on structures, paying particular attention to the case of bridge structures, on the basis of the research done by Froli [1] and on the basis of the Bulletin n.170 of the Italian National Research Council (CNR) [3].

The correct definition of the thermal actions due to the climate, acting on bridge structures, is in fact a fundamental step for the work presented in the following chapters.

2.2 Climatic factors influencing the thermal response of a structure

The knowledge of the climatic factors which influence the thermal response of a structure is necessary in order to define with sufficient accuracy the boundary conditions for the computation of the induced thermal fields.

The main climatic factors are:

- shade air temperature;
- wind velocity;
- short wave radiation (solar radiation), which can be decomposed in direct and diffused radiation;
- long wave radiation (thermal radiation), due to the radiation emitted by the atmosphere and by the environment.

2.2.1 Air temperature

The shade air temperature, for sake of simplicity called air temperature in the following, depends on the season, on the latitude and it is strongly influenced by local climatic conditions. Due to this fact it is evident the importance of making reference to in situ measurements over a long time span, in order to obtain reliable information.

A very important aspect for the following developments is the fact that both the daily variation of the mean air temperature as well as the annual variation of it show a wave-like shape. This particular characteristic depends on the alternation of day and night and on the alternation of the seasons. In order to appreciate these trends in temperature variations *Figure 1* shows an example of daily variations of air temperature while *Figure 2* shows an example of the annual variation of average monthly temperatures for three Italian cities.

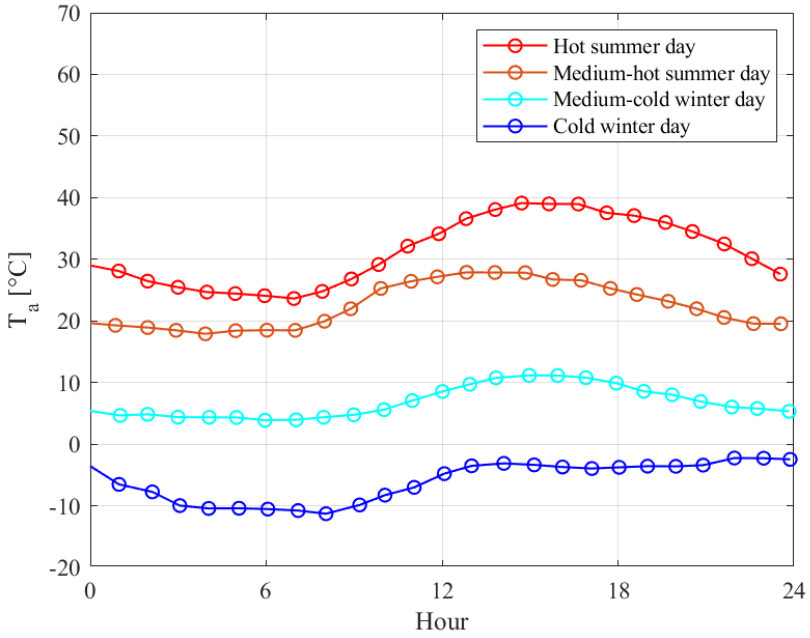

Figure 1- Daily variations of shade air temperature

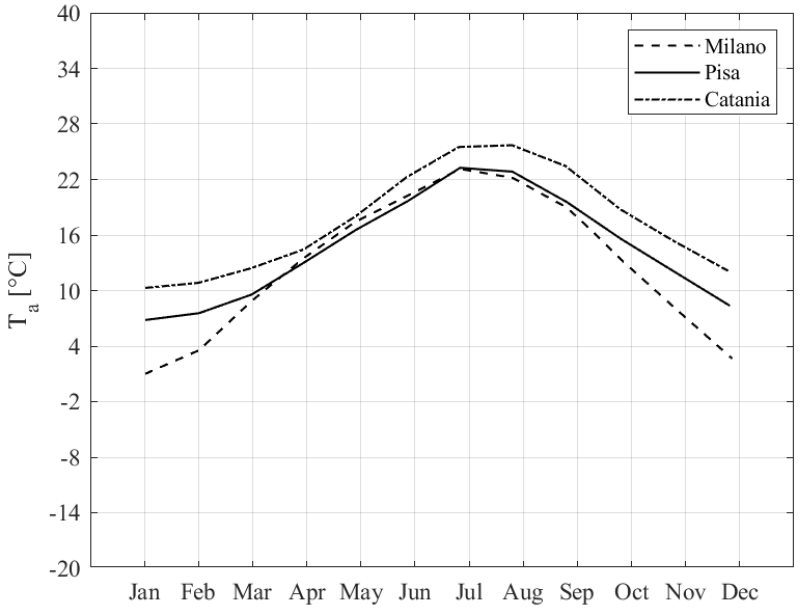

Figure 2 - Annual variation of average monthly temperatures

2.2.2 Wind velocity

The wind velocity deeply affects the thermal response of a structure since from it depends the convection heat exchange. Depending on the situation, a low or an high wind velocity can bring to the most unfavourable situation: for instance the highest temperatures will be reached on the surface of a structure exposed to the sun in a clear summer day if, contemporarily, the wind velocity will be low, so that the exchange of heat to the environment will be low. On the contrary, the lowest temperature will be reached in clear winter nights, when the air temperature becomes lower than the one of the surface if, contemporarily, the wind velocity is high.

2.2.3 Short wave radiation (solar radiation)

The solar radiation can be decomposed in two parts

- direct solar radiation I
- diffused solar radiation D

The sum of these two components provides the so called global radiation r_s:

$$r_s = I + D \quad (1)$$

Both the components depend on the geographic location, on the season, on the cloudiness and on the opacity of the air. Moreover the direct radiation acting on a surface depends on its orientation.

2.2.4 Long wave radiation (thermal radiation)

Thermal radiation is emitted by any solid or gaseous medium due to the fact that it is endowed with a certain temperature. This phenomenon can be described by means of Stefan-Boltzmann law:

$$r = \epsilon\, C_s\, T^4 \quad (2)$$

where:

- r = thermal power radiated per unit surface $[W/m^2]$
- C_s = Stefan-Boltzmann constant
- ϵ = emission coefficient of the body
- T = absolute temperature of the body $[°K]$

Furthermore Kirchoff law applies and establishes the relationship between the emission coefficient ϵ and the absorption coefficient a.

$$\epsilon = a \quad (3)$$

The structure for which it is requested the determination of the temperature distribution receives and absorbs thermal radiation from the surrounding environment (such as the soil and other

constructions) and from the atmosphere while emitting itself thermal radiations. As it is not possible to evaluate precisely the quantity of heat radiated by the atmosphere and by the soil surface because of the fact that their temperature distributions are not known, it is necessary to adopt some approximate evaluations starting from the shade air temperature. Since this temperature depends on the climatic conditions of the site, it is possible to treat, among the meteorological quantities, also the atmospheric and terrestrial thermal radiations.

In particular for what concerns the atmospheric thermal radiation, the heat quantity radiated by the atmosphere can be expressed as follow:

$$r_a = \epsilon_a \, C_s \, T_a^4 \qquad (4)$$

where:

- r_a = thermal power per unit surface of the structure radiated by the atmosphere $[W/m^2]$
- ϵ_a = emissivity of the atmosphere ($\epsilon_a = 0{,}86$ for clear sky, $\epsilon_a = 0{,}94$ for cloudy sky)
- T_a = shade air temperature $[°K]$

Analogously, for the terrestrial thermal radiation it can be written:

$$r_t = \epsilon_t \, C_s \, T_a^4 \qquad (5)$$

where:

- r_t = thermal power per unit surface of the structure radiated by the soil $[W/m^2]$
- ϵ_a = emissivity of the soil ($\epsilon_a = 0{,}86$ for clear sky, $\epsilon_a = 0{,}94$ for cloudy sky)

2.3 Thermal distribution computation

For what concerns heat transmission, a generic structure can be considered as a solid body whose boundary is in contact with other bodies of various nature or with fluids. The heat exchange is due to conduction in those portions of the boundary in contact with other solids while it is due to convection and radiation in those portions in contact with liquids or air. Furthermore exothermal (e.g. cement hydration) or endothermal chemical processes can take place inside the mass of the structure. These processes, together with the superficial heat exchange, can lead to temperature distributions which are generally not uniform, causing therefore an internal heat flux due to conduction.

Since both the superficial exchange as well as the internal chemical processes are rarely stationary, the temperature in the structure results, other than variable in space, variable from time to time:

$$\mathrm{T} = f(\mathrm{x}, \mathrm{y}, \mathrm{z}, \mathrm{t}) \qquad (6)$$

where:

- T = temperature inside the body
- x, y, z = coordinates of the generic point P inside the volume of the structure
- t = time variable

2.3.1 Heat transfer equations

From the mathematical point of view, the problem of the determination of the function T for an assigned structure is described inside the body by the Fourier heat conduction equation:

$$\frac{\partial^2 \lambda_x T}{\partial \mathrm{x}^2} + \frac{\partial^2 \lambda_y T}{\partial y^2} + \frac{\partial^2 \lambda_z T}{\partial \mathrm{z}^2} + \dot{q} = \rho C_p \frac{\partial \mathrm{T}}{\partial \mathrm{t}} \quad (7)$$

While the equation (7) holds for every point inside the body, on the boundary, for each element of surface, the principle of energy conservation is applied:

$$\frac{\partial \lambda_x T_s}{\partial x} n_x + \frac{\partial \lambda_y T_s}{\partial y} n_y + \frac{\partial \lambda_z T_s}{\partial z} n_z + q = 0 \quad (8)$$

In the previous equations the various symbols are:

- T_s = superficial temperature $[°C]$
- $\lambda_x, \lambda_y, \lambda_z$ = thermal transfer coefficients along x, y, z
- $\dot{q}$ = thermal power produced per unit volume of the body $[W/m^3]$
- ρ = material density $[kg/m^3]$
- C_p = specific heat of the material $[Wh/kg\,°C]$
- n_x, n_y, n_z = direction cosines of the normal to the surface in point P, oriented outward
- q = thermal power exchanged per unit surface of the boundary $[W/m^2]$

The simplifying hypothesis of thermally homogeneous and isotropic body is usually accepted, allowing to write equations (7) and (8) in the following form where the conduction coefficients are reduced to only one coefficient.

$$\frac{\partial^2 T}{\partial \mathrm{x}^2} + \frac{\partial^2 T}{\partial y^2} + \frac{\partial^2 T}{\partial \mathrm{z}^2} + \dot{q} = \frac{1}{\beta} \frac{\partial \mathrm{T}}{\partial \mathrm{t}} \quad (9)$$

$$\lambda \left[\frac{\partial T_s}{\partial x} n_x + \frac{\partial T_s}{\partial y} n_y + \frac{\partial T_s}{\partial z} n_z \right] + q = 0 \quad (10)$$

Where:

- $\beta = \frac{\lambda}{C_p \rho}$ is the thermal diffusivity $[m^2/h]$

It is important to underline that equation (9) must be applied to the whole volume of the body and equation (10) must be applied to the external surface and to the surface of eventual internal holes.

In order to obtain a good prediction of the thermal fields induced in a structure, it is necessary to model in an accurate way the superficial heat transfers, generally indicated with the symbol q in the previous equations. In the following paragraph all the contributions of superficial heat transfer will be therefore analysed in detail.

2.3.2 Boundary conditions

For what concerns the convection heat exchanges in a structure, they are mainly those between the surface and the air. The heat quantity exchanged through this mechanism is essentially influenced by the air velocity and by the difference in temperature between the air and the surface of the structure. In particular the convection mechanism is classified as natural convection or forced convection, depending on the fact that the air movement around the body is caused by the difference in temperature of the air in proximity of the interface or it is due to external causes such as wind.

The convection heat exchange can be described by the Newton's law of cooling:

$$q_c = \alpha(T_s - T_a) \quad (11)$$

where:

- q_c = thermal power exchanged by convection per unit surface $[W/m^2]$
- T_s = surface temperature $[°C]$
- T_a = surrounding air temperature $[°C]$
- α = adduction coefficient of the surface $[W/m^2\,°C]$

It is worth noting that the adduction coefficient takes into account the effect of the velocity of the air around the surface of the body on the convection heat exchange between the air and the surface itself. Rigorously α is a function and not a constant value, depending on various factors such as: surface orientation, velocity, density and viscosity of the air, difference in temperature between the solid surface and the air. However, in the framework of the computation of the temperature distribution for structural analysis, various authors agree in considering sufficiently accurate an expression of α depending only on the air velocity, for which a constant value between 0 and $5\ m/s$ is adopted. In particular, in the CEB-FIP Bulletin [4], it is proposed the following relation:

$$\alpha = 5.6 + 4.0\,V \quad [W/m^2\,°C] \quad (12)$$

with: $V \leq 5\ m/s$

In the case of velocities greater than $5\ m/s$, the same Bulletin suggests the following expression:

$$\alpha = 7.15\,V^{0.78} \quad [W/m^2\,°C] \quad (13)$$

However the major part of the heat absorbed by a structure is the one due to radiation phenomena among which the solar radiation is the dominant one. In this framework it is possible to make the hypothesis that the heat absorption due to radiation takes place just on the surface of the body and it is considered to be directly proportional to the radiating power acting on the surface.

- <u>Solar radiation (short wave radiation)</u>

  If r_s is the global radiating solar power, sum of the direct and diffused radiating power, the absorbed thermal power per unit of surface is expressed by:

$$q_{rs} = a \cdot r_s \quad (14)$$

where a is the absorption coefficient of the surface, depending on the material and on the colour of the surface itself. In the case of concrete, the coefficient a is assumed to be equal to 0,8.

- Thermal radiation (long wave radiation)

In an analogous way to what happens for the solar radiation , the thermal power absorbed by the structure because of thermal radiations, respectively atmospheric and terrestrial, will be given by:

$$q_{ra} = a \cdot r_a \quad (15)$$

$$q_{rt} = a \cdot r_t \quad (16)$$

where r_a and r_t are the atmospheric and the terrestrial radiating power.

- Thermal radiation emitted by the body

Finally the surface of the structure itself radiates heat towards the surrounding environment and the thermal power emitted by the surface, expressed in $[W/m^2]$, is given by:

$$q_{re} = -\epsilon_s \, C_S \, T_s^4 \quad (17)$$

where ϵ_s is the emission coefficient of the surface of the structure ($\epsilon = a$).

In conclusion, the total thermal power exchanged on an elementary portion of the external surface, in the most general case, is given by:

$$q = q_c + q_{rs} + q_{ra} + q_{rt} + q_{re} = \alpha(T_s - T_a) - a(I + D + \epsilon_a C_s T_a^4 + \epsilon_t C_s T_a^4 - C_s T_s^4) \quad (18)$$

in which the positive sign is related to the case of thermal power going out of the body.

From the practical point of view it is convenient to express equation (18) by means of a purely convective thermal exchange between the surface of the body, characterized by a temperature T_s, and the air, for which it is considered a fictitious temperature T^*.

$$q = \alpha(T_s - T^*) = \alpha(T_s - T_a) - a(I + D + \epsilon_a C_s T_a^4 + \epsilon_t C_s T_a^4 - C_s T_s^4) \quad (19)$$

from which derives:

$$T^* = T_a + \frac{a}{\alpha}(I + D + \epsilon_a C_s T_a^4 + \epsilon_t C_s T_a^4 - C_s T_s^4) \quad (20)$$

The previous equation represents a boundary condition in which the temperature (even though fictitious) of the external fluid and a law describing the thermal power exchange between fluid and the surface of the structure are assigned.

The temperature $T^*$is called fictitious sun-air temperature and represents the temperature at which the air should be in order that the convective thermal exchange between the external surface and the air itself results the same as the effective total thermal exchange caused by convection and by the various radiation phenomena. For sake of example *Figure 3* shows shade air temperature and the fictitious sun-air temperature in the average day of August, in the Italian city of Pisa, for the case of horizontal surfaces.

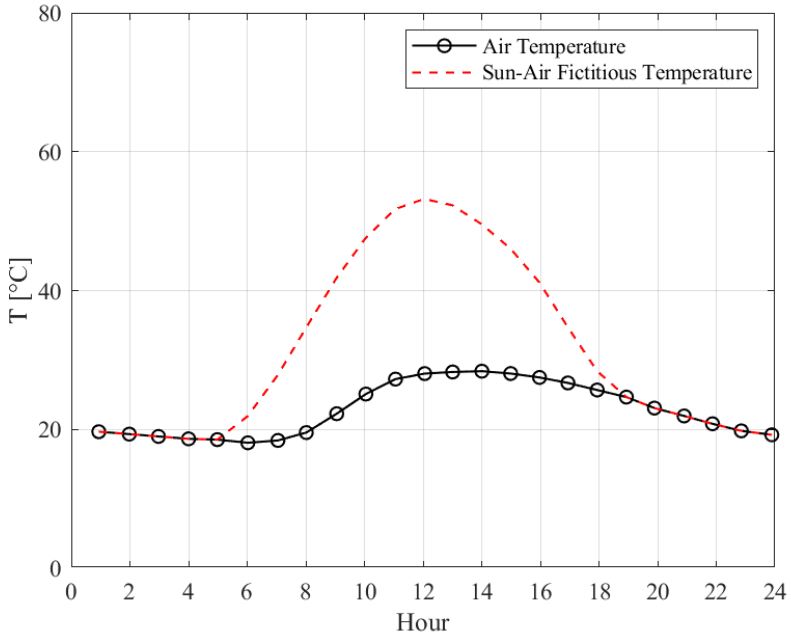

Figure 3 – Air temperature and fictitious sun-air temperature example

Furthermore it is possible to neglect the fourth order terms which are not very significant, leading to the following expression for equation (19):

$$q = \alpha(T_s - T^*) = \alpha(T_s - T_a) - a(I + D) \quad (21)$$

Remembering that I and D depend on t, it is therefore possible to write:

$$T^*(t) = T_a(t) + \frac{a}{\alpha}(I + D) \quad (22)$$

The daily variation of the air temperature can be expressed by means of Fourier series developments truncated at the first harmonic. The approximation, obtained proceeding in this way, is quite good, as it can be appreciated from *Figure 4*.

$$T_a(t) = T_m + \Delta T \cdot cos\left[\frac{2\pi \cdot (t+\omega)}{P}\right] \quad (23)$$

where T_m and ΔT are respectively the mean value and the semi-difference between the maximum and the minimum measured values.

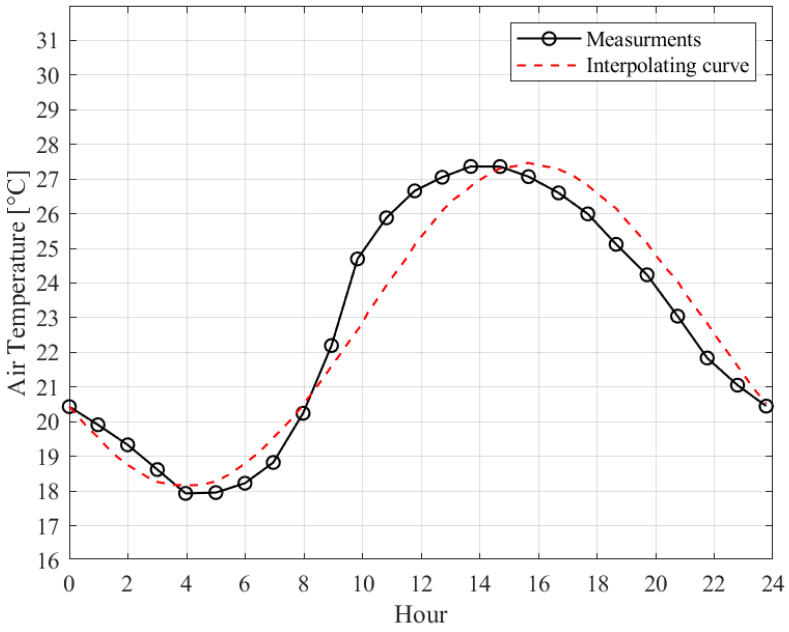

Figure 4 – Approximation of the daily variation of air temperature

2.3.3 Numerical integration of the Fourier Equation

The solution of the Fourier Equation over a domain characterized by a complex shape, having boundary conditions which are in general variable in time and space, such as in the case of bridge structures, can be performed only by means of numerical integration. Various researchers have studied this problem, always considering the hypothesis of null heat flux in the longitudinal direction of the bridge. This hypothesis has been confirmed to be accurate by the results of an analysis carried out by Mirambell and Aguado [5].

The technique which can be adopted for this kind of analysis is the Finite Element Method; in fact, analogously to what happens in the field of continuum mechanics, also in the case of heat transfer problems, the Finite Element Method is widely used. In particular, this technique has been adopted in the researches carried out in New Zealand (Lanigan [6]) and in Canada (Elbadry, Ghali [7], [8]) in which procedures for plane heat transfer problems have been developed in order to compute the temperature distributions due to climatic actions in bridges.

Under the hypothesis that the bridge analysed is an isotropic and homogeneous prismatic body with a longitudinal axis z, having a temperature distribution which is constant along its axis, without any internal source of heat, the Fourier heat transfer equation is written as follow:

$$\nabla^2 T = \frac{1}{\beta}\frac{\partial T}{\partial t} \qquad (24)$$

where:

- $\beta = \frac{\lambda}{C_v \rho}$ is the thermal diffusivity $[m^2/h]$
- ρ = mass density $[kg/m^3]$
- Cv = specific heat coefficient $[Wh/kg\,°C]$
- λ = thermal transfer coefficient $[W/m\,°C]$

The previous equation has to be associated to the boundary conditions and the simplifying considerations, presented in the previous paragraph with reference to the fictitious temperature, are also taken into account.

The solution of this problem by means of the Finite Element Method can be described by making a parallelism with the same method used in the field of structural analysis. In both cases, in fact, the domain is subdivided in various elements of opportune dimensions and shapes and the following relations between causes and effects are defined respectively for the structural analysis problem and for the thermal problem:

$$\underline{F} = \underline{\underline{K}}\,\underline{\delta} \qquad (25)$$

$$\underline{\varphi} = \underline{\underline{H}}\,\underline{T} \qquad (26)$$

The first equation, referred to the structural analysis problem, expresses the relation between forces ($\underline{F}$) and displacements ($\underline{\delta}$) by means of the stiffness matrix ($\underline{\underline{K}}$) while the second equation, referred to the thermal problem, expresses the relation between thermal fluxes ($\underline{\varphi}$) and temperatures ($\underline{T}$) by means of a thermal transfer matrix ($\underline{\underline{H}}$).

Thanks to this method it is therefore possible to obtain the temperature values in all the nodes of the mesh used to discretise the domain. The temperature T in any point of an element of the mesh will be then obtained as a function of the temperature in the nodes of that element by means of shape functions.

2.4 Thermal actions in prismatic structures

2.4.1 Deformations suppression method

The temperature acting on a structure, which can be defined according to the theoretical concepts presented in the previous paragraphs, is taken into account in structural analysis by means of imposed deformations. In order to define these geometrical actions on structures, caused by temperature, the deformation suppression method is adopted.

Consider a prismatic body, indefinitely long, in which the temperature is independent on time and on the z coordinate, that means having a steady heat flow parallel to the x-y plane. According to

these hypothesis the prismatic body under consideration is in a state of plain strain and it can be demonstrated, as done by Timoshenko [9], that the only stress different from zero is σ_z.

In the case of a long prismatic body of finite length, an approximate solution can be found by making the hypothesis that, at a sufficient distance from the ends, sections remain plane. To this latter model several real structures can be assimilated such as, in particular, bridge girders for which, as already stated, the hypothesis of independence of the temperature from the z coordinate is well accepted. The hypothesis of steady state is not that realistic, however, since temperature in massive structures varies quite slowly, it can be considered approximately constant in proximity of the time instants in which it assumes extreme values.

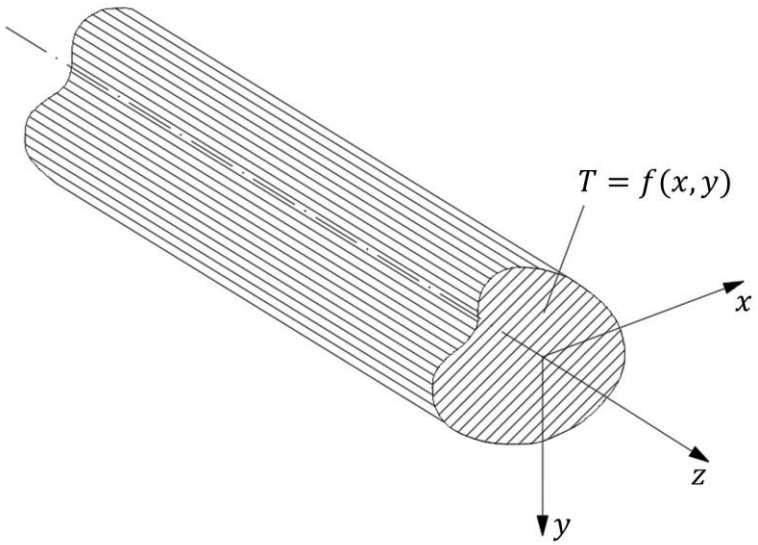

Figure 5 - Long prismatic body of finite length

Having defined A as the area of the section of the prismatic body, E the Young modulus of the material and α its coefficient of thermal expansion, it is considered a distribution of temperature $T(x, y)$ acting instantaneously over A.

If the axial fibres would be free to expand, their thermal deformation would be:

$$\varepsilon_z^{(T)} = \alpha T(x, y) \tag{27}$$

According to the deformation suppression method (Timoshenko [9]), in order to eliminate these thermal deformations it is sufficient to apply to each axial fiber a normal stress equal to:

$$\sigma_z^{(T)} = -\alpha E T(x, y) \tag{28}$$

To this stresses distribution correspond an axial force $N^{(T)}$, a bending moment $M_x^{(T)}$ around the x axis and a bending moment $M_y^{(T)}$ around the y axis:

$$N^{(T)} = \int_A \sigma_z^{(T)} dA \quad (29)$$

$$M_x^{(T)} = \int_A \sigma_z^{(T)} y dA \quad (30)$$

$$M_y^{(T)} = \int_A \sigma_z^{(T)} x dA \quad (31)$$

However in reality the ends of the prismatic body are free from forces. It is therefore possible to imagine to apply to the ends an axial force $N^{(S)}$ and two bending moments $M_x^{(S)}$, $M_y^{(S)}$ so that:

$$N^{(T)} + N^{(S)} = 0 \quad (32)$$

$$M_x^{(T)} + M_x^{(S)} = 0 \quad (33)$$

$$M_y^{(T)} + M_y^{(S)} = 0 \quad (34)$$

Due to the Saint-Venant principle, at a sufficient distance from the ends, $N^{(S)}$, $M_x^{(S)}$, $M_y^{(S)}$ will produce some linear deformations:

$$\varepsilon_z^{(S)} = \varepsilon_0 + \left(\frac{d\phi_x}{dz}\right) y + \left(\frac{d\phi_y}{dz}\right) x \quad (35)$$

to which correspond the following stresses:

$$\sigma_z^{(S)} = E\left[\varepsilon_0 + \left(\frac{d\phi_x}{dz}\right) y + \left(\frac{d\phi_y}{dz}\right) x\right] \quad (36)$$

Equation (32) can be therefore written as follow:

$$\int_A \left(\sigma_z^{(T)} + \sigma_z^{(S)}\right) dA = 0 \quad (37)$$

and substituting the expressions (28) and (36) of the normal stresses:

$$E\int_A \left\{-\alpha T(x,y) + \left[\varepsilon_0 + \left(\frac{d\phi_x}{dz}\right) y + \left(\frac{d\phi_y}{dz}\right) x\right]\right\} dA = 0 \quad (38)$$

Since x and y are centroidal axes, it results:

$$\int_A \left[\left(\frac{d\phi_x}{dz}\right) y + \left(\frac{d\phi_y}{dz}\right) x\right] dA = 0 \quad (39)$$

Therefore it is finally obtained that:

$$\varepsilon_0 = \frac{\alpha}{A}\int_A T(x,y)\, dA \quad (40)$$

which is the axial deformation of the fiber at the level of the centroid due to temperature.

Proceeding in an analogous way, starting from equation (33):

$$\int_A \left(\sigma_z^{(T)} y + \sigma_z^{(S)} y\right) dA = 0 \quad (41)$$

$$E \int_A \left\{-\alpha T(x,y) \cdot y + \left[\varepsilon_0 + \left(\frac{d\phi_x}{dz}\right) y + \left(\frac{d\phi_y}{dz}\right) x\right] \cdot y\right\} dA = 0 \quad (42)$$

$$E \int_A \left\{-\alpha T(x,y) \cdot y + \varepsilon_0 y + \left(\frac{d\phi_x}{dz}\right) y^2 + \left(\frac{d\phi_y}{dz}\right) xy\right\} dA = 0 \quad (43)$$

Since x and y are centroidal axes:

$$\int_A \varepsilon_0 y \, dA = 0 \quad (44)$$

and having chosen as x and y the principal reference axes:

$$\int_A \left(\frac{d\phi_y}{dz}\right) xy \, dA = 0 \quad (45)$$

Therefore it is finally obtained that:

$$\chi_x = \frac{d\phi_x}{dz} = \frac{\alpha}{I_x} \int_A T(x,y) \cdot y dA \quad (46)$$

which is the thermal curvature in the plane z-y, where I_x is the moment of inertia of the section with respect to x axis.

Starting instead from equation (34) it is obtained:

$$\chi_y = \frac{d\phi_y}{dz} = \frac{\alpha}{I_y} \int_A T(x,y) \cdot x dA \quad (47)$$

which is the thermal curvature in the plane z-x, where I_y is the moment of inertia of the section with respect to y axis.

Moreover it is possible to define the following quantities:

$$T_m = \frac{1}{A} \int_A T(x,y) dA \quad (48)$$

$$DT_y = \frac{1}{I_x} \int_A T(x,y) \cdot y dA \quad (49)$$

$$DT_x = \frac{1}{I_y} \int_A T(x,y) \cdot x dA \quad (50)$$

which are respectively the average effective temperature of the body $[°C]$, the global effective linear thermal gradient of the body along y direction $[° C/m]$ and the global effective linear thermal gradient of the body along x direction $[° C/m]$. The first one is responsible of the axial deformation of the fiber at the level of the centroid while the second one and the third one are responsible of the thermal curvatures in z-y and z-x planes. These quantities will be recalled in paragraph 2.4.4 where a brief overview of code provisions from different countries in the world will be provided. However in the following developments the gradient DT_x will not be taken into account since, as arise from the research done by Froli on a real bridge structure in Italy carried

out with an extensive thermal monitoring campaign (see [1] – Chapter IV), it results of one order of magnitude lower than the gradient DT_y.

2.4.2 Alternative procedure to the deformations suppression method

In addition to the method for the definition of the imposed deformations on a structure due to temperature, presented in paragraph 2.4.1 and adopted by Froli [1], it is also possible to follow a different approach which is the one applied for the analysis presented in the following chapters.

Consider a generic cross section for which the centroid corresponds to the origin of the principal reference system. The temperature distribution $T(x, y, t)$ acting over the section is in general, as already discussed, a complicated function of the spatial coordinates and of time.

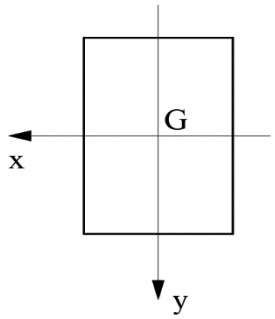

Figure 6 – Generic cross section

The total deformation under the hypothesis that the section remains plane can be written as follow:

$$\varepsilon = \underline{\rho}^T \underline{\psi} \qquad (51)$$

with:

$$\underline{\rho} = \begin{bmatrix} 1 \\ y \\ x \end{bmatrix}$$

$$\underline{\psi} = \begin{bmatrix} \varepsilon_0 \\ \chi_x \\ \chi_y \end{bmatrix}$$

The deformation generating stresses is given by the difference between the total deformation ε and the thermal deformation $\alpha T(x, y, t)$:

$$\varepsilon_\sigma = \underline{\rho}^T \underline{\psi} - \alpha T(x, y, t) \qquad (52)$$

The associated stresses in the elastic field, positive if in tension, are given by:

$$\sigma = E\left[\underline{\rho}^T \underline{\psi} - \alpha T(x,y,t)\right] \quad (53)$$

Equation (53) represents a system of self-equilibrated stresses to which correspond null axial force and null bending moment. It is therefore imposed the equilibrium:

$$\int_A \underline{\rho}\sigma dA = 0 \quad (54)$$

which, substituting expression (53), is written as follow:

$$E\int_A \underline{\rho}\,\underline{\rho}^T dA \cdot \underline{\psi} - E\int_A \alpha T(x,y,t)\cdot \underline{\rho}\, dA = 0 \quad (55)$$

where:

- $$\underline{\rho}\,\underline{\rho}^T = \begin{bmatrix}1\\ y\\ x\end{bmatrix}\begin{bmatrix}1 & y & x\end{bmatrix} = \begin{bmatrix}1 & y & x\\ y & y^2 & xy\\ x & xy & x^2\end{bmatrix} \quad (56)$$

  and therefore, it follows:

  $$E\int_A \underline{\rho}\,\underline{\rho}^T dA = E\begin{bmatrix}1 & 0 & 0\\ 0 & I_x & 0\\ 0 & 0 & I_y\end{bmatrix} = \underline{\underline{B}} \quad (57)$$

  which is the stiffness matrix, where A is the area of the section while I_x and I_y are the moments of inertia of the section.

- $$E\int_A \alpha T(x,y,t)\cdot \underline{\rho}\, dA = \begin{bmatrix}E\alpha\int_A T(x,y,t)dA\\ E\alpha\int_A T(x,y,t)\cdot y dA\\ E\alpha\int_A T(x,y,t)\cdot x dA\end{bmatrix} = \underline{S}(t) \quad (58)$$

  which is a vector function of time depending on the temperature acting on the structure.

On the basis of equations (57) and (58), equation (55) can be written as:

$$\underline{\underline{B}}\,\underline{\psi} = \underline{S}(t) \quad (59)$$

which represents a set of three decoupled equation, as the stiffness matrix $\underline{\underline{B}}$ is a diagonal matrix, which can be solved in order to get $\underline{\psi}$.

$$\underline{\psi} = \underline{\underline{B}}^{-1}\,\underline{S}(t) \quad (60)$$

The three components of the vector $\underline{\psi}$ found according to this procedure are:

$$\psi_1 = \varepsilon_0 = \frac{\alpha}{A}\int_A T(x,y,t)dA \quad (61)$$

$$\psi_2 = \chi_x = \frac{\alpha}{I_x}\int_A T(x,y,t)\cdot y dA \quad (62)$$

$$\psi_3 = \chi_y = \frac{\alpha}{I_y}\int_A T(x,y,t)\cdot x dA \quad (63)$$

which are respectively the axial deformation of the fiber at the level of the centroid due to temperature, the thermal curvature in the plane z-y and the thermal curvature in the plane z-x, exactly equal to those found with the deformations suppression method.

2.4.3 General definition of thermal action

An important observation about the definition of thermal action is the fact that, known the temperature distribution acting in a certain instant t and consequently computed the quantities defined by the expressions (48), (49) and (50), in general, they don't yet represent the thermal actions of interest for structural analysis.

In fact, at the generic instant t, the thermal effect of interest will not be dependent on the actual thermal distribution $T(x,y,t)$ but it will be dependent on the difference $\Delta T(x,y,t)$ between the thermal distribution at time t and the one at time t_0, that is the time instant to which correspond the initial time of action for the considered thermal effect.

$$\Delta T(x,y,t) = T(x,y,t) - T(x,y,t_0) \quad (64)$$

The expressions (48), (49) and (50) will be therefore the ones referred to $\Delta T(x,y,t)$ instead of $T(x,y,t)$:

$$T_m = \frac{1}{A}\int_A \Delta T(x,y,t)dA \quad (65)$$

$$DT_y = \frac{1}{I_x}\int_A \Delta T(x,y,t)\cdot y dA \quad (66)$$

$$DT_x = \frac{1}{I_y}\int_A \Delta T(x,y,t)\cdot x dA \quad (67)$$

The same concept applies to the computation of the axial deformation of the fiber at the level of the centroid due to temperature and to the computation of the thermal curvatures.

For what concern the selection of the correct instant t_0, it depends on the acquisition of the restraints by the structure during its construction. For instance when considering a bridge with a simply supported girder, the initial time t_0 to be considered for the computation of the axial thermal displacements, in order to correctly design the expansion joints and the bearing supports, is the time instant in which the girder is placed on its supports. If instead a continuous girder on multiple supports is considered and the aim is to compute the stresses due to temperature, the initial time

t_0 will correspond to the time in which the structure reaches the final condition of redundancy of the restraints.

2.4.4 Classification of thermal actions

According to Froli [1], thermal actions can be classified with reference both to their spatial and to their time distribution.

For what concerns the spatial classification, thermal actions on bridge girders can be distinguished in:

- Global actions (or longitudinal)

  They are given by the expressions (65), (66) and (67) on the basis of the difference of the thermal field at a generic instant t and at the initial time t_0. These actions, due to the non-linearity of the thermal field, are responsible of the arising of compatibility stresses as well as of an additional state of stress in the case of redundant structures, as it will be described in detail in chapter 3. Moreover in bridge structures these stresses can reach the same order of magnitude of those caused by the traffic loads (Mirambell, Aguado [10]) and will be the ones studied in the following developments.

  These actions, in fact, have greater importance with respect to the local actions, as testified by the fact that in the Eurocode 1 [11] the provided prescriptions on thermal actions in bridges are mainly referred to the global actions.

- Local actions (or transversal)

  They can arise in the case of box girder bridges, due to the non-uniform distribution of temperature on the box walls.

For what concerns the temporal classification, thermal actions can be distinguished in:

- Long duration actions

  Because of the alternation of seasons during the year with the consequent variations in the climatic conditions, it is possible to observe an average variation, characterized by a slow evolution in time, of the components T_m, DT_y, DT_x which are therefore classified as long duration components of the thermal actions. The average annual variation of DT_y, DT_x is generally small while the average annual variation of T_m is much more significative.

- Short duration actions

  The global actions T_m, DT_y, DT_x, due to the alternation of day and night, are also characterized by daily oscillations which are therefore classified as short duration components of the thermal action.

2.5 Code provisions

The aim of the present paragraph is to provide a brief overview of the code provisions regarding thermal actions in bridges from different countries in the world; however, for a more detailed analysis of this topic, it possible to make reference to [1].

The first systematic research program about the thermal response of bridges aimed at producing code provisions is the one by Mary Emerson, which is based on the continuous and prolonged measurement of thermal fields in different kinds of bridges, in various locations in Great Britain. The fundamental results obtained by Emerson [12], [13], related to the study of the global actions in bridge girders, have been traduced in code prescriptions in the British standards BS5400 [14].

The characteristic values of the component T_m are determined by Emerson finding, in an empirical way, on the basis of the great number of observations collected, a functional dependence between the component T_m itself and the extreme values of the shade air temperature [15].

This functional dependence can be represented by means of two groups of three curves, as shown in *Figure 7*. The three curves are referred respectively to steel decks, composite decks and concrete decks, independently from the shape and dimension of the cross section. Once the dependence between the shade air temperature and the average effective temperature T_m is defined, it is sufficient to consider the isothermal maps of the extreme values of the shade air temperature at the level of the sea, associated with a return period of 50 years, to obtain the correspondent extreme values of T_m with the same return period, in a certain location. Moreover, in order to consider different return periods, it is possible to adopt corrective coefficients and the altitude of the site is taken into account by means of assigned altimetric gradients of the air temperature.

The simplicity of this method, together with the fact that it is on the safe side since it considers the same sensitivity to the thermal variations for massive bridge structures as well as for light bridge structures, has led to the adoption of it by the Project Team in charge of the redaction of the section related to thermal actions of Eurocode 1.

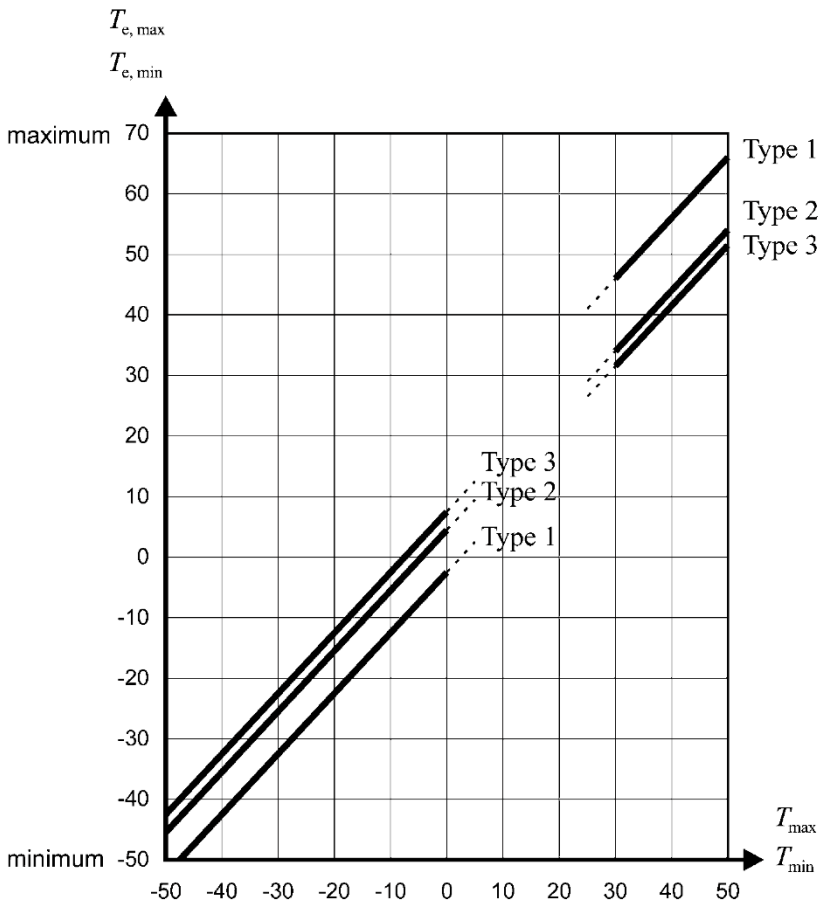

Figure 7 – Correlation between shade air temperature and the average effective temperature of bridges according to EC1 (based on the results by M.Emerson)

For what concerns the global effective thermal gradient, the Project Team has instead introduced two different approaches which the designer can adopt depending on the importance of the bridge and the accuracy required for its thermal analysis. The first approach, which is the simplified one, is based on the method adopted by the DIN regulations in Germany while the second approach, more complex and accurate, is based on the method of the British regulations.

- Simplified approach

  The bridges are subdivided in three categories: steel decks, composite decks, concrete decks. For each category the characteristic values of DT_y are given as temperature differences between the extrados and the intrados, independently from the type of

section and from its depth. The non-linearity of the thermal fields is disregarded in this approach and the influence of the surfacing (both for road and for railway bridges) is taken into account by a corrective coefficient which depends on the thickness of the surfacing itself.

- Complex approach

  The bridges are subdivided in the three categories adopted also for the simplified approach. For each category the characteristic values of the temperature profiles which depart from the uniformity are given on the basis of the type of section and on its depth.

As already mentioned temperature distributions are complicated functions of the spatial coordinates and of time. In particular the temperature profiles result to be strongly non-linear over the depth of the cross section and the extension of the zone in which the profile is non-linear, under the same climatic condition, results to be almost equal for each section category, independently from its depth [16]. This aspect is well addressed in some codes from different countries such as the British regulations [14], the New Zealand regulations [17] and the Australian regulations [18]. These codes, in fact, provide in a schematic way the profiles, over the depth of the cross section, of the extreme differences of the thermal field with respect to uniformity (under the implicit assumption that the initial thermal field, even though unknown, is uniform). A schematic representation of the profiles adopted by these codes are reported in the following figures where h is the depth of the cross section.

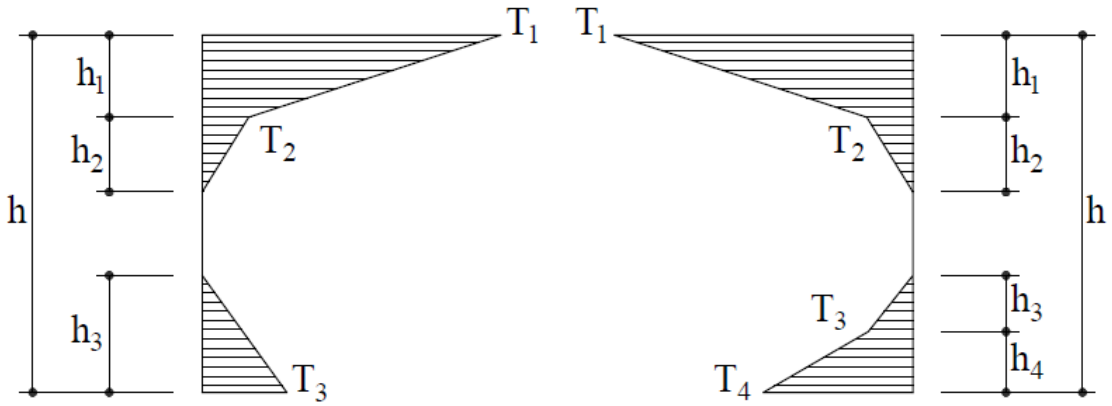

Figure 8 – Heating temperature profile (left) and cooling temperature profile (right) adopted by the British code

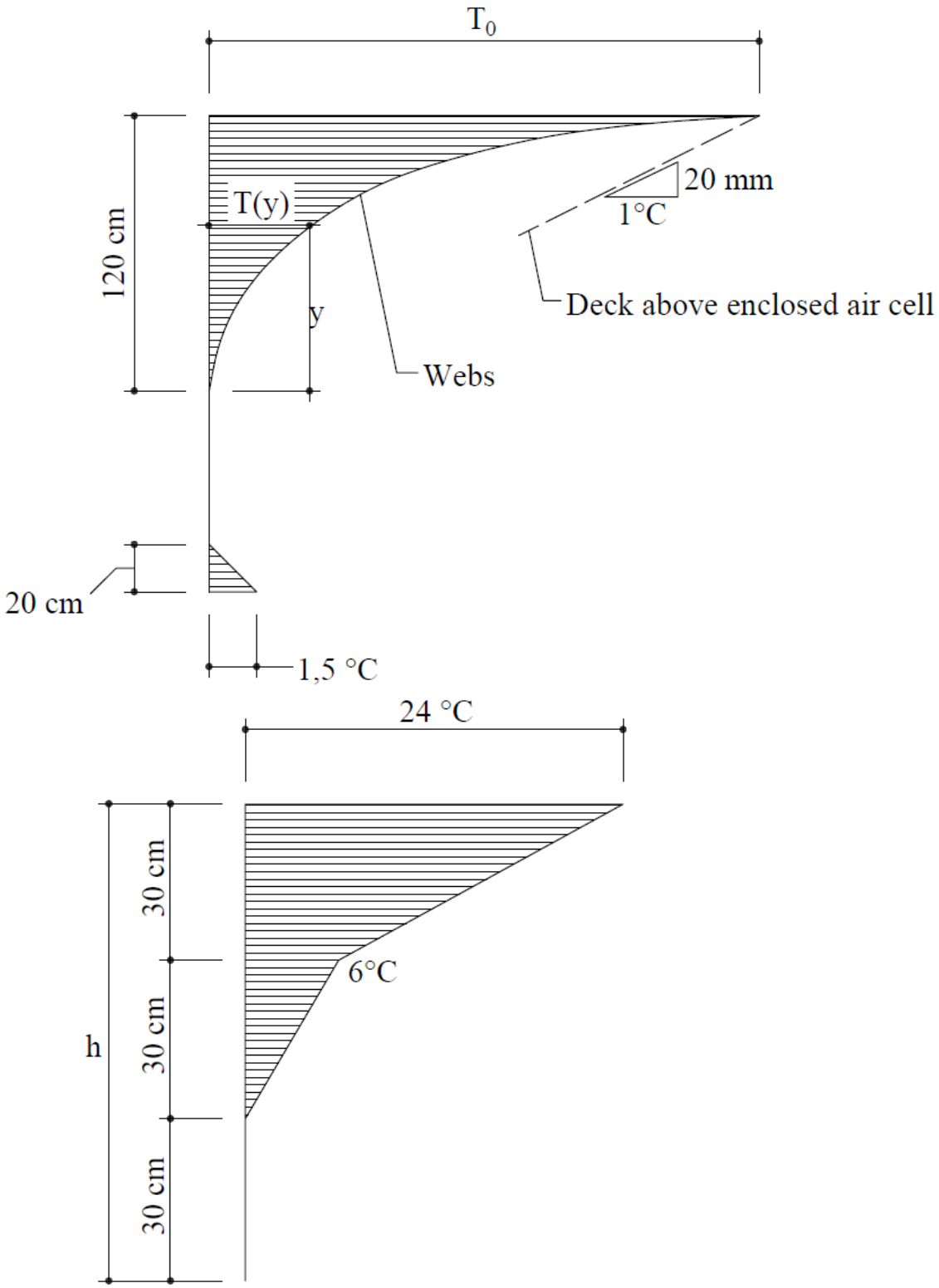

Figure 9 – Temperature profiles adopted by the New Zealand code (above) and by the Australian code (below)

3 ELASTIC FIELD

3.1 Introduction

The analysis in the elastic field of homogeneous structures subject to non-linear temperature distributions over the depth of the cross section is presented in this chapter. Depending on the type of structure, this problem may be analysed at two different levels. In fact, due to the non-linearity of the thermal field over the depth of the cross section, compatibility stresses will always arise at the sectional level; however, at the structural level, in presence of redundant static schemes, an additional state of stress is generated by the thermal actions.

The theoretical concepts presented in paragraphs 3.2 and 3.3 will be applied in paragraph 3.4 in order to solve some significative examples. The results obtained in this way will be then used as a reference to be compared with the ones obtained for the same problems in the viscoelastic field in chapters 4 and 5, in order to determine the influence of the long-term behaviour of concrete.

3.2 Compatibility stresses due to non-linear temperature variations

Consider a generic homogeneous cross section, subject to a non-linear temperature distribution along its depth y, for which the plane section hypothesis is assumed. In order to satisfy this assumption, due to the non-linearity of the thermal field, compatibility stresses are generated and can be computed according to equation (53) presented in paragraph 2.4.2:

$$\sigma_e(y) = E_0 \left[\underline{\rho}^T \underline{\psi}_e - \alpha T(y, t_0) \right] \quad (68)$$

Since the elastic field is considered, the subscript "e" is adopted and the Young modulus considered in the previous equation is the one at initial time t_0 which is indicated as E_0; for the same reason also the temperature distribution, which is variable in time, is computed for $t = t_0$.

An important difference with respect to the generic formulation presented in paragraph 2.4.2 is the fact that, in this case, the curvature in the z-x plane is not taken into account since, as already discussed, the gradient DT_x, which causes it, results of one order of magnitude lower than the gradient DT_y and can be neglected in practical cases. The vectors $\underline{\rho}^T$ and $\underline{\psi}_e$ are therefore defined as follow:

$$\underline{\rho} = \begin{bmatrix} 1 \\ y \end{bmatrix}$$

$$\underline{\psi}_e = \begin{bmatrix} \varepsilon_0 \\ \chi_x \end{bmatrix}$$

As already discussed the compatibility stresses given by equation (68) are self-equilibrated and are associated to the difference between the total deformation and the non-linear deformation over the depth of the cross section $\alpha T(y, t_0)$:

$$\varepsilon_\sigma(y) = \underline{\rho}^T \underline{\psi}_e - \alpha T(y, t_0) \qquad (69)$$

In the previous equations the vector $\underline{\psi}_e$ can be computed on the basis of the procedure explained in paragraph 2.4.2, according to which, by imposing the equilibrium, the following relation is obtained:

$$\underline{\psi}_e = \underline{\underline{B}}_e^{-1} \underline{S}(t_0) \qquad (70)$$

where the stiffness matrix in the elastic field $\underline{\underline{B}}_e$ is computed with reference to the Young modulus at initial time E_0:

$$\underline{\underline{B}}_e = E_0 \begin{bmatrix} A & 0 \\ 0 & I \end{bmatrix}$$

where A is the area of the cross section and I is the moment of inertia of the cross section with respect to the x axis.

Due to the fact that, for the specific problem under examination, the vector $\underline{\psi}_e$ has only two components, expression (70) represents a system of two decoupled equations instead of a system of three equations as it happens in the case of the generic formulation. In particular, the two equations obtained in this case are:

$$\psi_{1e} = \varepsilon_0 = \frac{\alpha}{A} \int_A T(y, t_0) dA \qquad (71)$$

$$\psi_{2e} = \chi_x = \frac{\alpha}{I} \int_A T(y, t_0) \cdot y dA \qquad (72)$$

By substituting the vector $\underline{\psi}_e$ in expression (68) and by developing the product between the vector $\underline{\rho}$ and the vector $\underline{\psi}_e$ it is finally found:

$$\sigma_e(y) = E_0 \left[\frac{\alpha}{A} \int_A T(y, t_0) dA + \frac{\alpha}{I} \int_A T(y, t_0) \cdot y dA \cdot y - \alpha T(y, t_0) \right] \qquad (73)$$

From the previous equation it is clear that the compatibility stresses arise at the sectional level just in presence of non-linear temperature distributions. In fact, in the case in which $T(y, t_0)$ is linear along the depth of the cross section, the sum of the terms in the square brackets of the previous equation is null and therefore no compatibility stresses arise. Moreover the distribution of stresses σ_e over the cross section appears to be non-linear, due to the presence of the non-linear term $\alpha T(y, t_0)$.

Once the vector $\underline{\psi_e}$ is known, also the total deformation of the cross section in the elastic field, due to the presence of the non-linear temperature distribution, under the plane section hypothesis, can be computed as follow:

$$\varepsilon_e(y) = \underline{\rho}^T \underline{\psi_e} = \psi_{1e} + \psi_{2e} \cdot y = \frac{\alpha}{A}\int_A T(y,t_0)dA + \frac{\alpha}{I}\int_A T(y,t_0)\cdot y dA \cdot y \qquad (74)$$

3.3 Additional stresses due to redundant restraints

In addition to the compatibility stresses presented in the previous paragraph, which arise at the sectional level independently on the static scheme of the structure to which the section under analysis belongs, in the case of redundant structures, the effect of thermal actions produces an additional state of stress due to the reactions of the redundant restraints.

As already explained, the compatibility stresses arise in order to satisfy the plane section hypothesis according to which the total deformation of the section is defined by equation (74). To this deformation correspond an axial deformation due to temperature ψ_{1e} and the thermal curvature in the plane z-y given by ψ_{2e}. At the structural level both of these geometrical actions, determined at the sectional level according to the procedure shown in the previous paragraph, can be then considered in performing the structural analysis of the redundant static scheme. By operating in this way it is possible to compute the reactions of the redundant restraints due to the non-linear temperature distribution acting on the structure, which will finally correspond to additional stresses at the sectional level.

3.4 Examples of applications

Some significant examples of applications of the method, explained in the previous paragraphs for the computation in the elastic field of the compatibility stresses and of the additional stresses in presence of redundant static schemes, will be here presented. In order to show the applicability of the procedure to the most general situations, different kinds of sections subjected to various non-linear temperature distributions will be considered along with different redundant static schemes. For sake of simplicity in the writing of the equations, the variability in time of the temperature distribution is here neglected since, in the elastic field, the temperature is always computed, as already mentioned, for $t = t_0$. The variability in time will be then considered when dealing with the analysis in the viscoelastic field in chapter 4 and chapter 5.

3.4.1 Example 1

Consider an homogeneous rectangular cross section subject to a parabolic temperature distribution over its depth, whose dimensions are those indicated in *Figure 10*. The values assumed by the temperature function in correspondence of the top, centroidal and bottom fibers are respectively T_s, T_G and T_i.

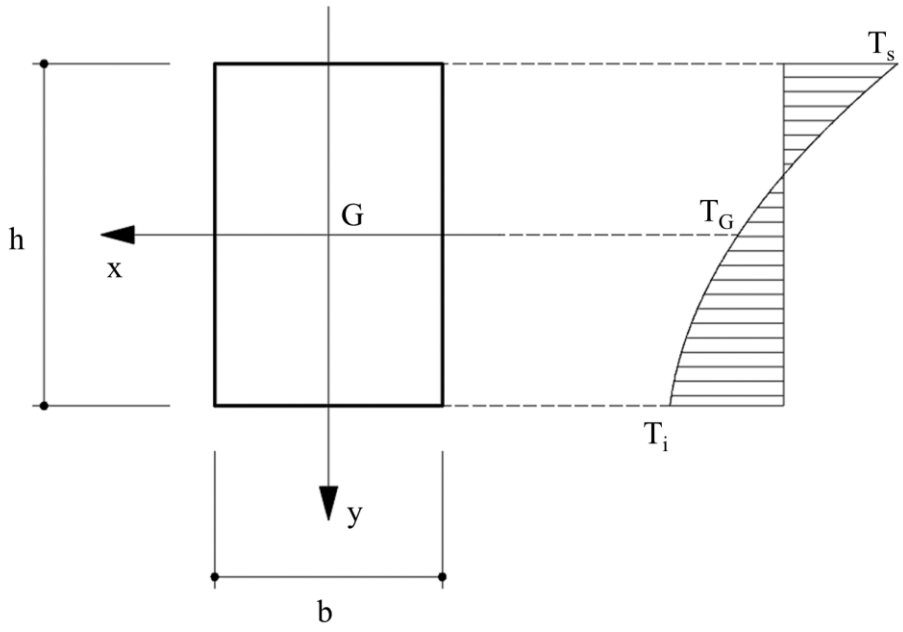

Figure 10 – Homogeneous rectangular cross section subject to a parabolic temperature distribution over its depth

The origin of the reference system is fixed in correspondence of the centroid of the cross section and the expression of the parabolic function defining the temperature distribution along the depth of the section is determined by imposing that the temperature assumes the values T_s, T_G and T_i in correspondence of the coordinates $y = -h/2$, $y = 0$ and $y = -h/2$.

$$T = Ay^2 + By + C \tag{75}$$

$$y = -\frac{h}{2} \qquad T = T_s \qquad A\frac{h^2}{4} - B\frac{h}{2} + C = T_s \tag{76}$$

$$y = 0 \qquad T = T_G \qquad C = T_G \tag{77}$$

$$y = \frac{h}{2} \qquad T = T_i \qquad A\frac{h^2}{4} + B\frac{h}{2} + C = T_i \tag{78}$$

After some simple computations the expression of the function defining the temperature distribution along the coordinate y is:

$$T(y) = (T_s + T_i - 2T_G)\frac{2y^2}{h^2} + (t_i - T_s)\frac{y}{h} + T_G \tag{79}$$

Knowing the expression of $T(y)$ it is possible to compute the two components of vector $\underline{\psi_e}$ according to equations (71) and (72):

$$\psi_{1e} = \frac{\alpha}{A}\int_A T dA = \frac{\alpha b}{A}\cdot\int_{-\frac{h}{2}}^{\frac{h}{2}}\left[(T_s + T_i - 2T_G)\frac{2y^2}{h^2} + (t_i - T_s)\frac{y}{h} + T_G\right]dy \quad (80)$$

$$\psi_{1e} = \frac{\alpha}{6}(T_s + T_i + 4T_G) \quad (81)$$

$$\psi_{2e} = \frac{\alpha}{I}\int_A T y dA = \frac{\alpha b}{I}\cdot\int_{-\frac{h}{2}}^{\frac{h}{2}}\left[(T_s + T_i - 2T_G)\frac{2y^2}{h^2} + (t_i - T_s)\frac{y}{h} + T_G\right]\cdot y\, dy \quad (82)$$

$$\psi_{2e} = \frac{\alpha(T_i - T_s)}{h} \quad (83)$$

The compatibility stresses in the elastic field are computed according to equation (68):

$$\sigma_e(y) = E_0[\psi_{1e} + \psi_{2e}\cdot y - \alpha\cdot T(y)] \quad (84)$$

Substituting the expressions (81), (83) and (79) in the previous equation it is obtained:

$$\sigma_e(y) = E_0\alpha\left[\frac{T_s + T_i + 4T_G}{6} + \frac{(T_i - T_s)y}{h} - 2(T_s + T_i - 2T_G)\frac{y^2}{h^2} - (T_i - T_s)\frac{y}{h} - T_G\right] \quad (85)$$

which, after some simplifications, is finally written as follow:

$$\sigma_e(y) = E_0\alpha\left[-2(T_s + T_i - 2T_G)\frac{y^2}{h^2} + \frac{T_s + T_i - 2T_G}{6}\right] \quad (86)$$

For sake of simplicity all the parameters defining the temperature function are considered to be dependent on a single parameter T_0 as follow:

- $T_s = -T_0$
- $T_G = T_0$
- $T_i = 2T_0$

The quantities previously computed will therefore become:

$$T(y) = T_0\left(-2\frac{y^2}{h^2} + 3\frac{y}{h} + 1\right) \quad (87)$$

$$\psi_{1e} = \frac{\alpha T_0}{6}(-1 + 2 + 4) = \frac{5}{6}\alpha T_0 \quad (88)$$

$$\psi_{2e} = 3\frac{\alpha T_0}{h} \quad (89)$$

$$\sigma_e(y) = E_0\alpha T_0\left(2\frac{y^2}{h^2} - \frac{1}{6}\right) \quad (90)$$

The compatibility stresses distribution over the depth of the cross section for the case under examination is reported in *Figure 11* where the coordinate y is normalized with respect to the depth h of the section and the stresses are normalized with respect to $E_0 \alpha T_0$.

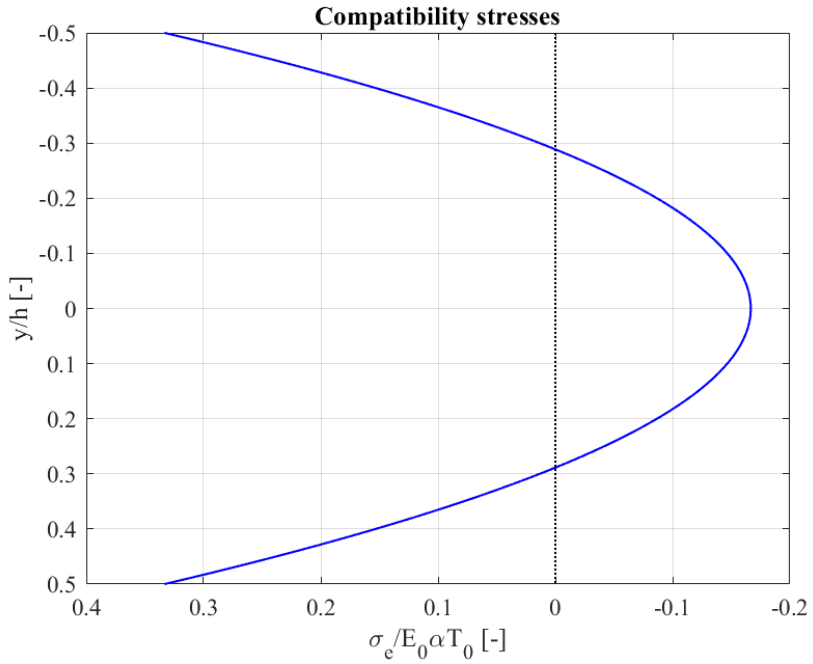

Figure 11 – Compatibility stresses distribution over the depth of the cross section

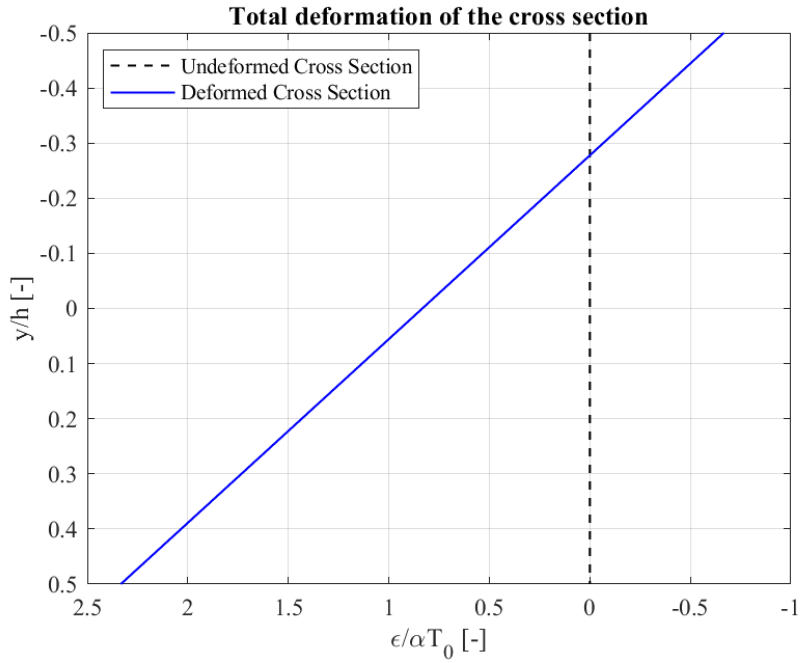

Figure 12 – Total deformation of the cross section

Once the components of the vector $\underline{\psi}_e$ are known, also the total deformation of the cross section under the plane section hypothesis can be computed according to equation (74). The result obtained for the case under examination is reported in *Figure 12* where the coordinate y is normalized with respect to the depth h of the section and the deformation is normalized with respect to αT_0.

An effective way to verify the computations carried out is to exploit the fact that the compatibility stresses σ_e are self-equilibrated by checking that the equilibrium equations are satisfied:

$$\int_A \underline{\rho}\sigma dA = 0 \qquad (91)$$

which for the example under consideration are:

$$\int_{-h/2}^{h/2} \sigma_e b dy = E_0 \alpha T_0 b \left|\frac{2}{3}\frac{y^3}{h^2} - \frac{1}{6}y\right|_{-\frac{h}{2}}^{\frac{h}{2}} = 0 \qquad (92)$$

$$\int_{-\frac{h}{2}}^{\frac{h}{2}} \sigma_e y b dy = E_0 \alpha T_0 b \left|\frac{2y^4}{4h^2} - \frac{y^2}{12}\right|_{-\frac{h}{2}}^{\frac{h}{2}} = 0 \qquad (93)$$

The equilibrium equations are satisfied, therefore the compatibility stresses computed are correct.

In order to show the application of the procedure for the computation of the additional stresses due to redundant restraint, it is possible to consider the case in which the section under examination is the one adopted for the elements composing the following redundant static schemes:

- Scheme 1

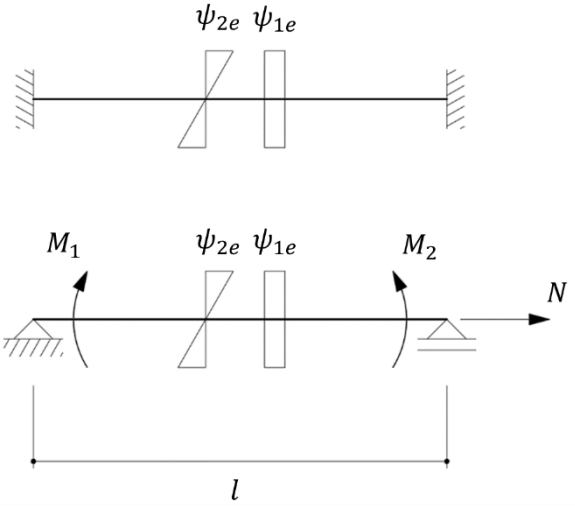

Figure 13 - Two times redundant static scheme and relative redundant variables

The static scheme reported in *Figure 13* is two times redundant and the geometrical actions ψ_{1e} and ψ_{2e}, previously determined at the sectional level, are applied. Moreover in the same figure the redundant variables M_1, M_2 and N have been highlighted. By performing the structural analysis of this structural scheme it is possible to compute the reactions of the redundant restraints due to the non-linear temperature distribution, which will finally lead to additional stresses at the sectional level.

Since the geometrical action ψ_{2e} is constant along the beam axis, the static scheme under examination is characterized by a central symmetry and therefore it is possible to state that M_1 is equal to M_2. The compatibility equations, necessary to compute the redundant variables, are therefore just two:

$$M_1 \left(\frac{l}{3E_0 I} + \frac{l}{6E_0 I}\right) + \psi_{2e} \frac{l}{2} = 0 \quad (94)$$

$$N \frac{l}{E_0 A} + \psi_{1e} l = 0 \quad (95)$$

from which it is obtained:

$$M_1 = -\psi_{2e} E_0 I \quad (96)$$

$$N = -\psi_{1e} E_0 A \quad (97)$$

The axial force and the bending moment along the beam are constant and respectively equal to N and M_1. It is therefore necessary to consider, for each section of the beam, an additional stresses distribution $\Delta\sigma_e(y)$ along the depth of the cross section, corresponding to the effect of the redundant variables just computed.

$$\Delta\sigma_e(y) = E_0 \left(\frac{N}{E_0 A} + \frac{M_1}{E_0 I} \cdot y\right) \quad (98)$$

which, by substituting the values of the redundant variables M_1 and N, becomes:

$$\Delta\sigma_e(y) = -\psi_{1e} E_0 - \psi_{2e} E_0 y = E_0 \alpha T_0 \left(-\frac{5}{6} - 3\frac{y}{h}\right) \quad (99)$$

The total stresses at the sectional level are therefore computed by making the sum of the compatibility stresses $\sigma_e(y)$ and of the additional stresses $\Delta\sigma_e(y)$ due to the redundant restraints as it can be appreciated in *Figure 14*. Moreover it is possible to observe that, as the beam considered in scheme 1 is completely restrained, the total stresses at the sectional level are simply given by $-E_0 \alpha T(y)$.

$$\sigma_{e,tot}(y) = \sigma_e(y) + \Delta\sigma_e(y) = E_0 \alpha T_0 \left(2\frac{y^2}{h^2} - 3\frac{y}{h} - 1\right) = -E_0 \alpha T(y) \quad (100)$$

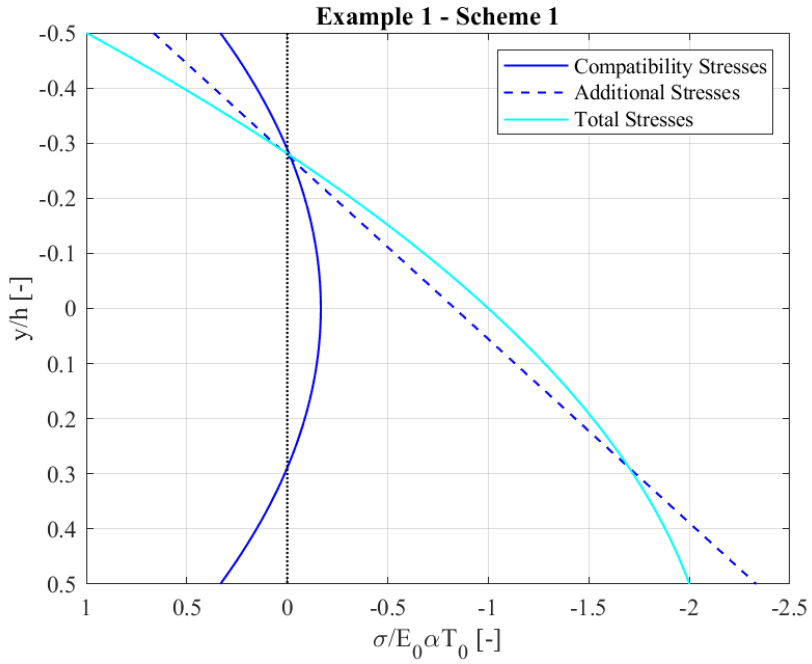

Figure 14 – Total stresses distribution over the depth of the cross section

- Scheme 2

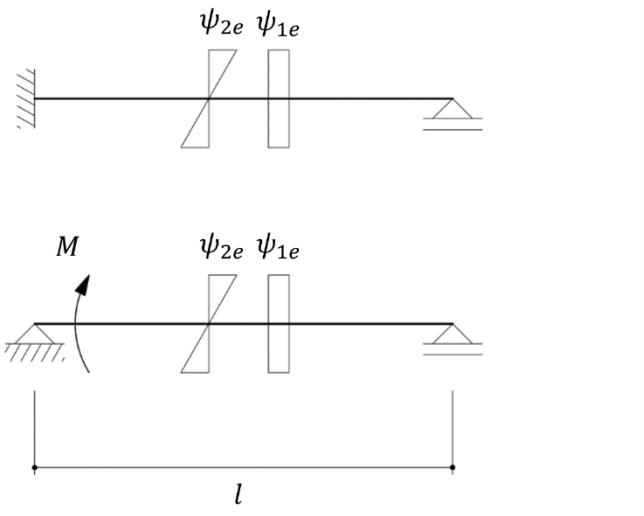

Figure 15 - One time redundant static scheme and relative redundant variable

The second structural scheme analyzed in presence of the geometrical actions ψ_{1e} and ψ_{2e} is only one time redundant. The compatibility equation, necessary to compute the redundant variable M, is the following:

$$M\frac{l}{3E_0I} + \psi_{2e}\frac{l}{2} = 0 \qquad (101)$$

from which it is obtained:

$$M = -\frac{3}{2}E_0I\psi_{2e} \qquad (102)$$

Since, due to the configuration of the restraints of the static scheme under analysis, no redundant axial variables are present, the geometrical action ψ_{1e} does not appear in the compatibility equation and does not influence the additional stresses distribution.

The additional stresses distribution, over the depth of the section in correspondence of which the redundant variable M is applied, is the following:

$$\Delta\sigma_e(y) = -\frac{3}{2}E_0\psi_{2e}y = E_0\alpha T_0\left(-\frac{9}{2}\frac{y}{h}\right) \qquad (103)$$

The total stresses at the sectional level are computed by making the sum of the compatibility stresses $\sigma_e(y)$ and of the additional stresses $\Delta\sigma_e(y)$ due to the redundant restraint as it can be appreciated in *Figure 16*.

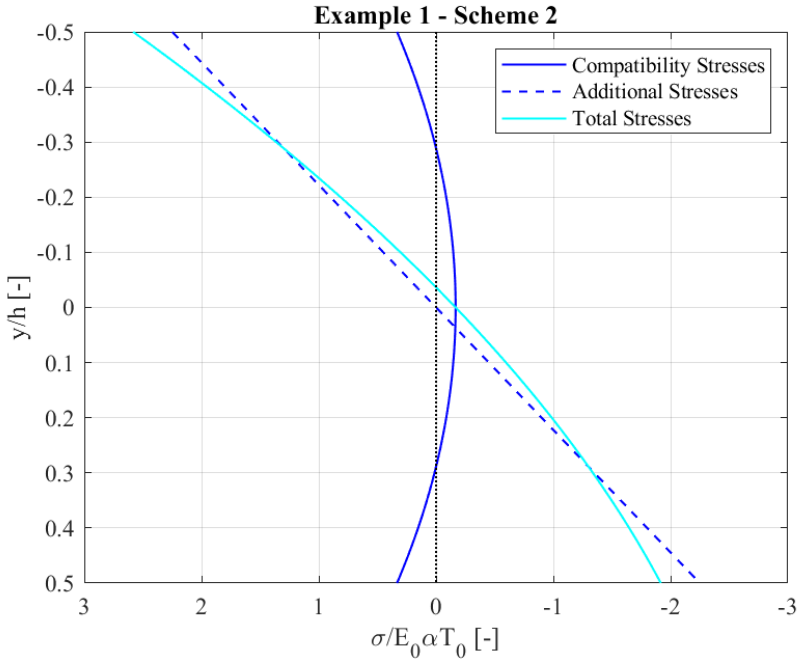

Figure 16 – Total stresses distribution over the depth of the cross section

3.4.2 Example 2

Consider the same homogeneous rectangular cross section analysed in example 1, subject to a discontinuous, non-linear temperature distribution over its depth. In particular the temperature distribution in the portion of the cross section above the centroid G is defined by means of a sinusoidal function of y coordinate, while the temperature distribution in the portion below the centroid is defined by means of a linear function of y coordinate. The aim of this example is to show the application of the method to the cases in which the non-linear temperature distribution is characterized by the additional complexity of being a discontinuous function.

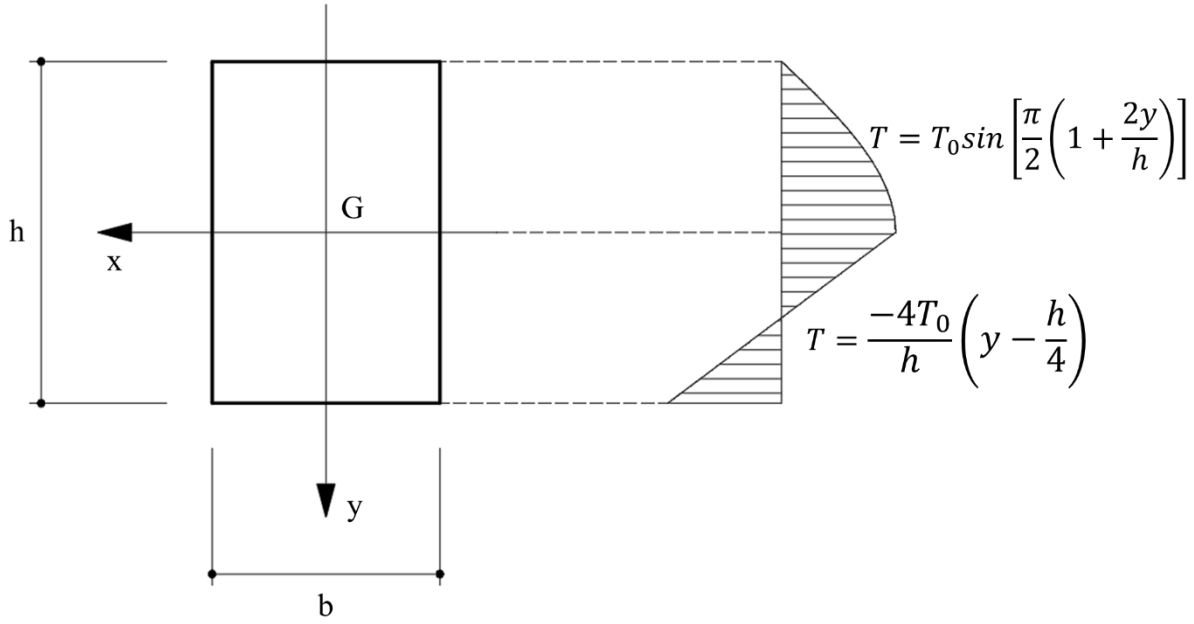

Figure 17 – Homogeneous rectangular section subject to a discontinuous temperature distribution over its depth

The components of the vector $\underline{\psi_e}$ are computed according to equations (71) and (72) in which the integration is opportunely performed in order to deal with the discontinuity in the temperature distribution:

$$\psi_{1e} = \frac{\alpha}{A}\int_A T dA = \frac{\alpha}{A}\left\{\int_{-\frac{h}{2}}^{0} T_0 sin\left[\frac{\pi}{2}\left(1+\frac{2y}{h}\right)\right] b dy + \int_0^{\frac{h}{2}} -\frac{4T_0}{h}\left(y-\frac{h}{4}\right) b dy\right\} =$$

$$= \frac{\alpha}{A}\left\{\int_{-\frac{h}{2}}^{0} T_0 \sin\left(\frac{\pi}{2}+\frac{\pi y}{h}\right) b dy + \int_0^{\frac{h}{2}}\left(-\frac{4T_0}{h} yb + T_0 b\right) dy\right\} =$$

$$= \frac{\alpha}{A}\left\{\int_{-\frac{h}{2}}^{0} T_0 \cos\left(\frac{\pi y}{h}\right) b dy + \int_{0}^{\frac{h}{2}} \left(-\frac{4T_0}{h} y b + T_0 b\right) dy\right\} =$$

$$= \frac{\alpha}{A}\left\{\left|T_0 \frac{h}{\pi} \sin\left(\frac{\pi y}{h}\right) b dy\right|_{-\frac{h}{2}}^{0} + \left|-\frac{2T_0}{h} y^2 b + T_0 b y\right|_{0}^{\frac{h}{2}}\right\} = \frac{\alpha}{\pi} T_0 \qquad (104)$$

$$\psi_{2e} = \frac{\alpha}{\mathrm{I}} \int_A T y dA = \frac{\alpha}{I}\left\{\int_{-\frac{h}{2}}^{0} T_0 sin\left[\frac{\pi}{2}\left(1 + \frac{2y}{h}\right)\right] b y dy + \int_{0}^{\frac{h}{2}} -4\frac{T_0}{h}\left(y - \frac{h}{4}\right) b y dy\right\} =$$

$$= \frac{\alpha}{I}\left\{\int_{-\frac{h}{2}}^{0} T_0 cos\left(\frac{\pi y}{h}\right) b y dy + \int_{0}^{\frac{h}{2}} \left(-\frac{4T_0}{h} y^2 b + T_0 y b\right) dy\right\} =$$

$$= \frac{\alpha}{I}\left\{\left|T_0 \frac{h}{\pi} sin\left(\frac{\pi y}{h}\right) b y\right|_{-\frac{h}{2}}^{0} - \int_{-\frac{h}{2}}^{0} T_0 \frac{h}{\pi} \sin\left(\frac{\pi y}{h}\right) b dy + \int_{0}^{\frac{h}{2}} \left(-\frac{4T_0}{h} y^2 b + T_0 y b\right) dy\right\} =$$

$$= \frac{\alpha}{I}\left\{-T_0 \frac{h}{\pi} b \frac{h}{2} - \left|-T_0 \frac{h^2}{\pi^2} cos\left(\frac{\pi y}{h}\right) b\right|_{-\frac{h}{2}}^{0} + \left|-\frac{4}{3}\frac{T_0}{h} y^3 b + \frac{1}{2} T_0 y^2 b\right|_{0}^{\frac{h}{2}}\right\} =$$

$$= \frac{\alpha}{I}\left\{-\frac{T_0}{2}\frac{h^2 b}{\pi} + T_0 \frac{h^2 b}{\pi^2} - \frac{4}{3}\frac{T_0}{h}\frac{h^3}{8} b + \frac{1}{2} T_0 \frac{h^2}{4} b\right\} = \frac{\alpha}{I} T_0 \left(\frac{h^2 b}{\pi^2} - \frac{1}{2}\frac{h^2 b}{\pi} - \frac{1}{24} h^2 b\right) \qquad (105)$$

The compatibility stresses in the elastic field are computed according to equation (68) which, due to the discontinuity in the temperature distribution leads to the following expressions:

for $-\frac{h}{2} \le y \le 0$

$$\sigma_e(y) = E_0\left\{\frac{\alpha}{\pi} T_0 + \frac{\alpha}{I} T_0 \left(\frac{h^2 b}{\pi^2} - \frac{1}{2}\frac{h^2 b}{\pi} - \frac{1}{24} h^2 b\right) y - \alpha T_0 sin\left[\frac{\pi}{2}\left(1 + \frac{2y}{h}\right)\right]\right\} \qquad (106)$$

for $0 \le y \le \frac{h}{2}$

$$\sigma_e(y) = E_0\left\{\frac{\alpha}{\pi} T_0 + \frac{\alpha}{I} T_0 \left(\frac{h^2 b}{\pi^2} - \frac{1}{2}\frac{h^2 b}{\pi} - \frac{1}{24} h^2 b\right) y + \frac{4\alpha T_0}{h}\left(y - \frac{h}{4}\right)\right\} \qquad (107)$$

The compatibility stresses distribution over the depth of the cross section for the case under examination is reported in *Figure 18* where the coordinate y is normalized with respect to the depth h of the section and the stresses are normalized with respect to $E_0 \alpha T_0$. In *Figure 19* the total

deformation of the cross section under the plane section hypothesis, normalized with respect to αT_0, is also reported.

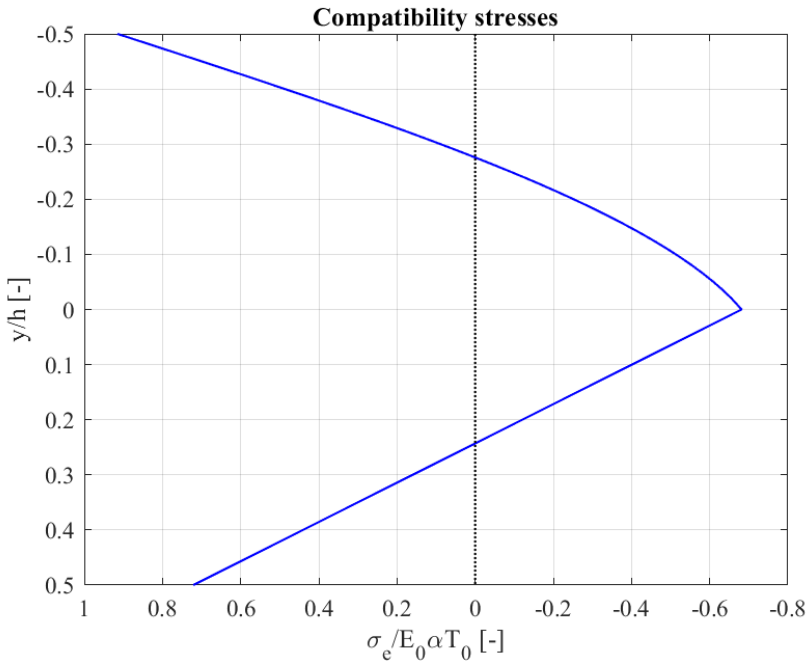

Figure 18 – Compatibility stresses distribution over the depth of the cross section

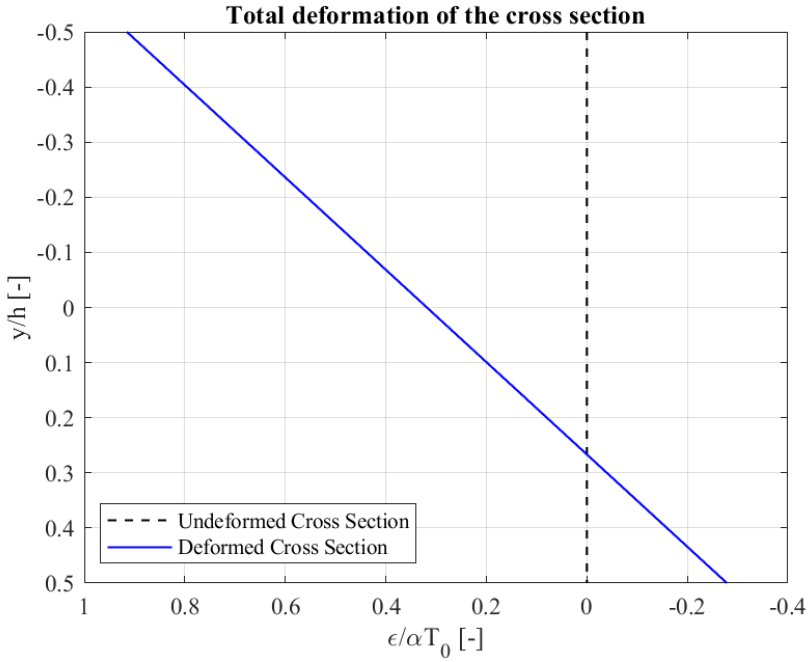

Figure 19 – Total deformation of the cross section

The computations carried out are verified by checking that the equilibrium equations are satisfied:

$$\int_A \underline{\rho}\sigma dA = 0 \qquad (108)$$

which for the example under consideration are:

$$\int_{-h/2}^{h/2} \sigma_e b dy = E_0 \alpha T_0 \left\{ \int_{-h/2}^{0} \left[\frac{1}{\pi} + \frac{12}{bh^3} bh^2 \left(\frac{1}{\pi^2} - \frac{1}{2\pi} - \frac{1}{24} \right) y - \sin\left(\frac{\pi}{2} + \frac{\pi y}{h} \right) \right] b dy + \right.$$

$$\left. + \int_{0}^{h/2} \left[\frac{1}{\pi} + \frac{12}{bh^3} bh^2 \left(\frac{1}{\pi^2} - \frac{1}{2\pi} - \frac{1}{24} \right) y + \frac{4y}{h} - 1 \right] b dy \right\} =$$

$$= E_0 \alpha T_0 \left\{ \left| \frac{b}{\pi} y + \frac{6}{h} b y^2 \left(\frac{1}{\pi^2} - \frac{1}{2\pi} - \frac{1}{24} \right) - \frac{h}{\pi} sin\left(\frac{\pi y}{h} \right) b \right|_{-\frac{h}{2}}^{0} + \left| \frac{b}{h} y + \frac{6}{h} b y^2 \left(\frac{1}{\pi^2} - \frac{1}{2\pi} - \frac{1}{24} \right) + \right.$$

$$\left. + \frac{2y^2 b}{h} - yb \right|_{0}^{\frac{h}{2}} =$$

$$= E_0 \alpha T_0 \left\{ \frac{b}{\pi} \frac{h}{2} + \frac{6}{h} b y^2 \left(\frac{1}{\pi^2} - \frac{1}{2\pi} - \frac{1}{24} \right) + \frac{b}{\pi} \frac{h}{2} - \frac{6}{h} b y^2 \left(\frac{1}{\pi^2} - \frac{1}{2\pi} - \frac{1}{24} \right) - \frac{h}{\pi} b + \frac{hb}{2} - \frac{hb}{2} \right\} = 0 \qquad (109)$$

$$\int_{-h/2}^{h/2} \sigma_e y b dy = E_0 \alpha T_0 \left\{ \int_{-h/2}^{h/2} \left[\frac{yb}{\pi} + \frac{12}{bh^3} bh^2 \left(\frac{1}{\pi^2} - \frac{1}{2\pi} - \frac{1}{24} \right) y^2 b \right] dy + \right.$$

$$\left. - \int_{-h/2}^{0} sin\left[\frac{\pi}{2} \left(1 + \frac{2y}{h} \right) \right] y b dy + \int_{0}^{h/2} \frac{4}{h} \left(y - \frac{h}{4} \right) y b dy \right\} =$$

$$= E_0 \alpha T_0 \left\{ \left| \frac{y^2}{2} \frac{b}{\pi} + \frac{12}{h} \left(\frac{1}{\pi^2} - \frac{1}{2\pi} - \frac{1}{24} \right) \frac{y^3}{3} b \right|_{-h/2}^{h/2} - \int_{-h/2}^{0} cos\left(\frac{\pi y}{h} \right) y b dy + \right.$$

$$\left. + \int_{0}^{h/2} \left(\frac{4}{h} y^2 b - yb \right) dy \right\} =$$

$$= E_0 \alpha T_0 \left\{ \frac{h^2}{8} \frac{b}{\pi} + \frac{12}{h} \left(\frac{1}{\pi^2} - \frac{1}{2\pi} - \frac{1}{24} \right) \frac{h^3}{24} b - \frac{h^2}{8} \frac{b}{\pi} + \frac{12}{h} \left(\frac{1}{\pi^2} - \frac{1}{2\pi} - \frac{1}{24} \right) \frac{h^3}{24} b + \right.$$

$$\left. - \int_{-h/2}^{0} cos\left(\frac{\pi y}{h} \right) y b dy + \left| \frac{4}{3} \frac{y^3 b}{h} - \frac{y^2 b}{2} \right|_{0}^{h/2} \right\} =$$

$$= E_0 \alpha T_0 \left\{ \left(\frac{1}{\pi^2} - \frac{1}{2\pi} - \frac{1}{24} \right) h^2 b + \frac{h}{\pi} \frac{h}{2} b - \frac{h^2}{\pi^2} b + \frac{4}{3} \frac{b}{h} \frac{h^3}{8} - \frac{1}{2} b \frac{h^2}{4} \right\} = 0 \qquad (110)$$

The equilibrium equations are satisfied, therefore the compatibility stresses computed are correct.

For what concerns this second example, 4 static schemes have been considered for the application of the procedure for the computation of the additional stresses due to redundant restraint.

- Scheme 1

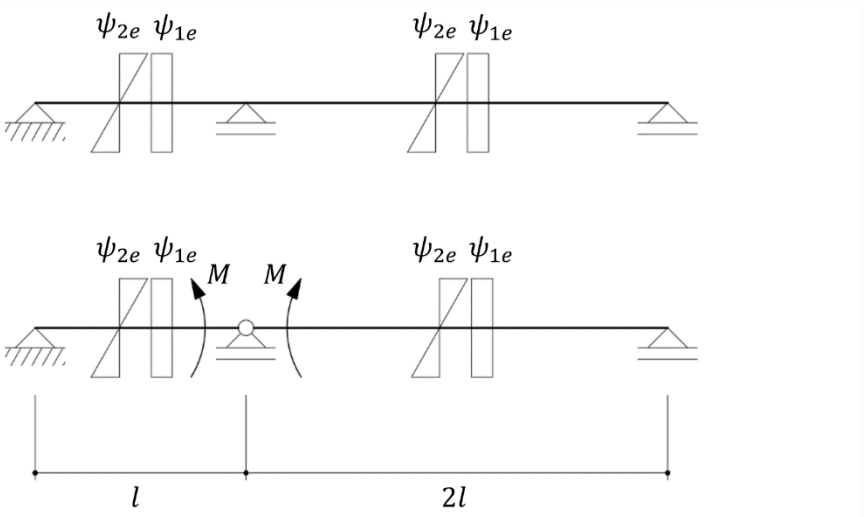

Figure 20 - One time redundant static scheme and relative redundant variable

Analogously to what has already been presented for the first example, the structural scheme is analysed in presence of the geometrical actions ψ_{1e} and ψ_{2e}. The structural scheme is only one time redundant and the compatibility equation, necessary to compute the redundant variable M, is the following:

$$M\left(\frac{l}{3E_0I}+\frac{2l}{3E_0I}\right)+\ \psi_{2e}\frac{l}{2}+\psi_{2e}\frac{2l}{2}=0 \qquad (111)$$

from which it is obtained:

$$M=-\psi_{2e}\frac{3}{2}l\frac{E_0I}{l}=-\psi_{2e}\frac{3}{2}E_0I \qquad (112)$$

As stated before with reference to the second static scheme analyzed in the first example, also in this case no redundant axial variables are present and therefore the geometrical action ψ_{1e} does not appear in the compatibility equation and does not influence the additional stresses distribution.

The additional stresses distribution for the section in correspondence of the central support is therefore given by:

$$\Delta\sigma_e(y)=-\frac{3}{2}E_0\psi_{2e}y=-18E_0\alpha T_0\left(\frac{1}{\pi^2}-\frac{1}{2\pi}-\frac{1}{24}\right)\frac{y}{h} \qquad (113)$$

The total stresses at the sectional level, given by the sum of the compatibility stresses $\sigma_e(y)$ and of the additional stresses $\Delta\sigma_e(y)$, are represented in non-dimensional form in *Figure 21*.

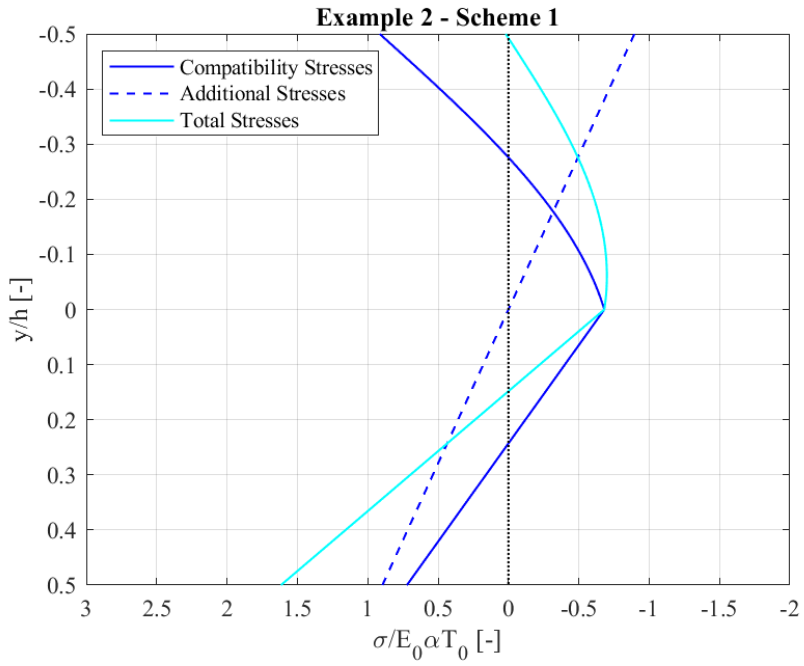

Figure 21 - Total stresses distribution over the depth of the cross section

- Scheme 2

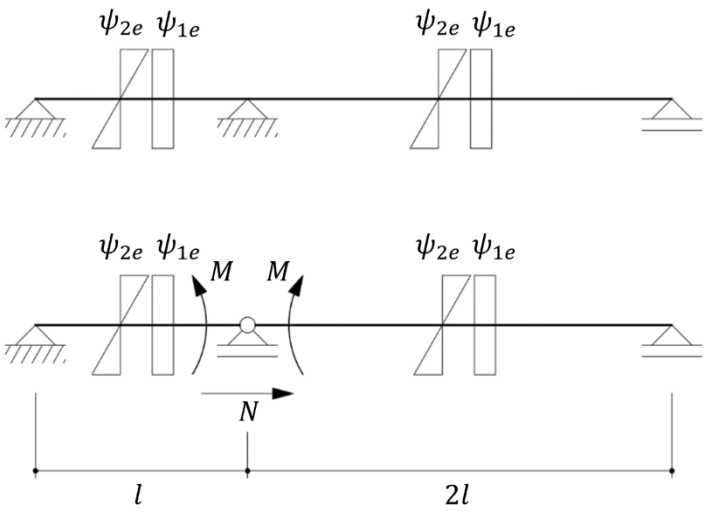

Figure 22 - Two times redundant static scheme and relative redundant variables

This second static scheme differs from the first one because of the fact that the central support of the two span continuous beam is no longer a roller but it is a simple support. This lead to an additional redundant variable represented by the horizontal action in the central support. The compatibility equations are written as follow:

$$M\left(\frac{l}{3E_0I}+\frac{2l}{3E_0I}\right)+\ \psi_{2e}\frac{l}{2}+\psi_{2e}\frac{2l}{2}=0 \quad (114)$$

$$N\frac{l}{E_0A}+\psi_{1e}l=0 \quad (115)$$

from which it is obtained:

$$M=-\psi_{2e}\frac{3}{2}E_0I \quad (116)$$

$$N=-\psi_{1e}E_0A \quad (117)$$

As already done for the first static scheme analysed, consider for instance the section in correspondence of the central support. The computation of the additional stresses distribution over that cross section, due to the presence of the redundant restraints, needs to be performed distinguishing if it is considered the section immediately on the left side or on the right side of the central support, because of the discontinuity in the value of the axial force in the two spans of the scheme.

For the section immediately on the left side of the central support, it is found:

$$\Delta\sigma_{e,left}(y)=-E_0\psi_{1e}-\frac{3}{2}E_0\psi_{2e}y=E_0\alpha T_0\left[-\frac{1}{\pi}-18\left(\frac{1}{\pi^2}-\frac{1}{2\pi}-\frac{1}{24}\right)\frac{y}{h}\right] \quad (118)$$

The total stresses at the sectional level given by the sum of the compatibility stresses $\sigma_e(y)$ and of the additional stresses $\Delta\sigma_{e,left}(y)$ are represented in non-dimensional form in *Figure 23*.

For what concerns the section immediately on the right side of the central support, since the axial force in correspondance of that section is null and the bending moment M coincides with the one computed for the static scheme 1, the additional stresses distribution is exactly the same as the one computed for the scheme 1.

$$\Delta\sigma_{e,right}(y)=-\frac{3}{2}E_0\psi_{2e}y=-18E_0\alpha T_0\left(\frac{1}{\pi^2}-\frac{1}{2\pi}-\frac{1}{24}\right)\frac{y}{h} \quad (119)$$

Since both the compatibility stresses $\sigma_e(y)$ and the additional stresses $\Delta\sigma_{e,right}(y)$ are respectively coincident with the compatibility stresses and the additional stresses computed for the static scheme 1, also the total stresses distribution will be the same and it is therefore possible to make reference to *Figure 21* also for what concerns total stresses diagram of the section immediately on the right side of the central support.

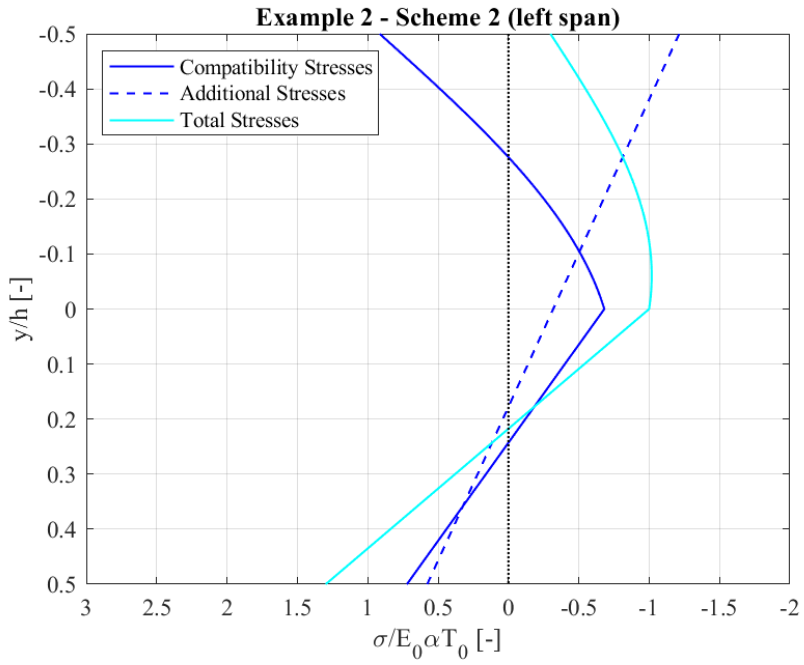

Figure 23 - Total stresses distribution over the depth of the cross section

- Scheme 3

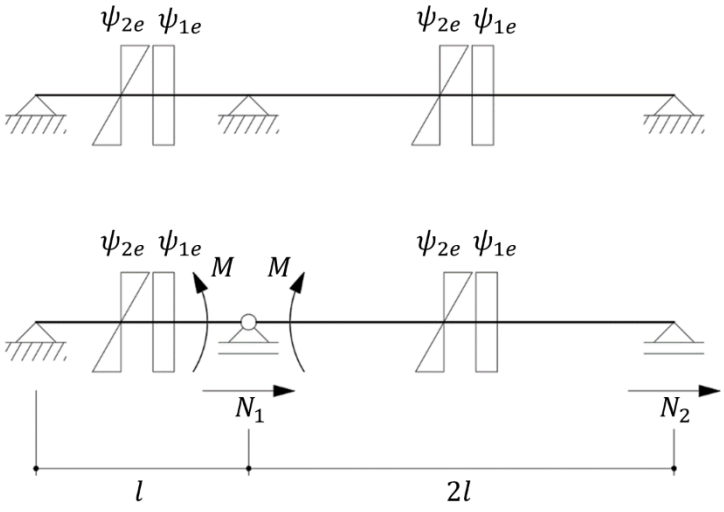

Figure 24 - Three times redundant static scheme and relative redundant variables

The third static scheme differs from the second one because of the fact that the right end support of the two span continuous beam is no longer a roller but it is a simple support. This lead to an additional redundant variable represented by the horizontal action in the right end support and the scheme is therefore a three times redundant static scheme. The compatibility equations, necessary to compute the three redundant variables, are written as follow:

$$M\left(\frac{l}{3E_0I}+\frac{2l}{3E_0I}\right)+\ \psi_{2e}\frac{l}{2}+\psi_{2e}\frac{2l}{2}=0 \tag{120}$$

$$\begin{cases} N_1\left(\frac{l}{E_0A}+\frac{2l}{E_0A}\right)+N_2\left(-\frac{2l}{E_0A}\right)+\psi_{1e}(l-2l)=0 \\ N_1\left(-\frac{2l}{E_0A}\right)+N_2\left(\frac{2l}{E_0A}\right)+\psi_{1e}2l=0 \end{cases} \tag{121}$$

from which it is obtained:

$$M=-\psi_{2e}\frac{3}{2}E_0I \tag{122}$$

$$N_1=-E_0A\psi_{1e} \tag{123}$$

$$N_2=-2E_0A\psi_{1e} \tag{124}$$

As observed also in the analysis of the scheme 2, when computing the additional stresses due to the redundant restraints, the discontinuity in the axial force value in correspondence of the central support is responsible for the necessity of distinguishing between the cross section immediately on the left side of the central support and the cross section immediately on the right side of the central support.

For the section immediately on the left side of the central support, it is found:

$$\Delta\sigma_{e,left}(y)=-3E_0\psi_{1e}-\frac{3}{2}E_0\psi_{2e}y=E_0\alpha T_0\left[-\frac{3}{\pi}-18\left(\frac{1}{\pi^2}-\frac{1}{2\pi}-\frac{1}{24}\right)\frac{y}{h}\right] \tag{125}$$

The total stresses at the sectional level given by the sum of the compatibility stresses $\sigma_e(y)$ and of the additional stresses $\Delta\sigma_{e,left}(y)$ are represented in non-dimensional form in *Figure 25*.

For the section immediately on the right side of the central support, it is found:

$$\Delta\sigma_{e,right}(y)=-2E_0\psi_{1e}-\frac{3}{2}E_0\psi_{2e}y=E_0\alpha T_0\left[-\frac{2}{\pi}-18\left(\frac{1}{\pi^2}-\frac{1}{2\pi}-\frac{1}{24}\right)\frac{y}{h}\right] \tag{126}$$

The total stresses at the sectional level given by the sum of the compatibility stresses $\sigma_e(y)$ and of the additional stresses $\Delta\sigma_{e,right}(y)$ are represented in non-dimensional form in *Figure 26*.

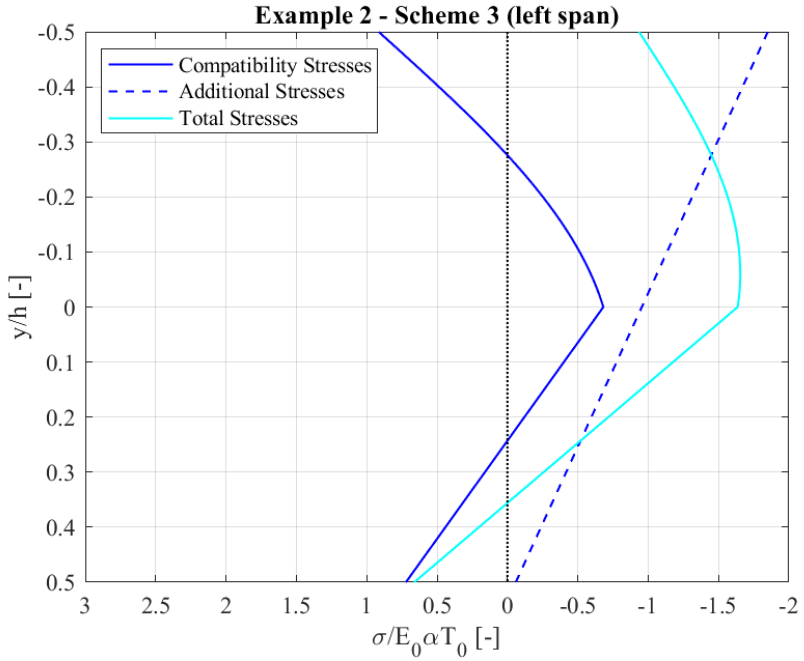

Figure 25 - Total stresses distribution over the depth of the cross section

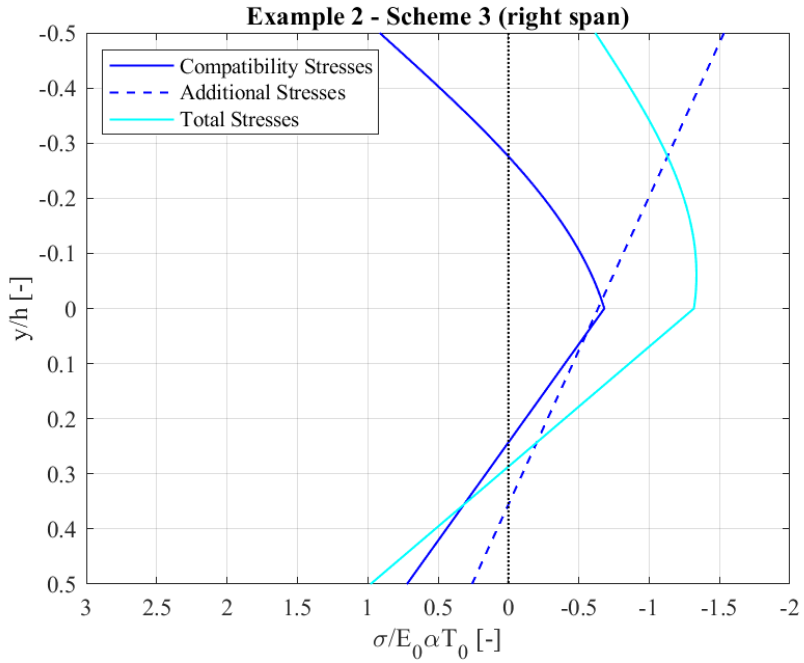

Figure 26 - Total stresses distribution over the depth of the cross section

- Scheme 4

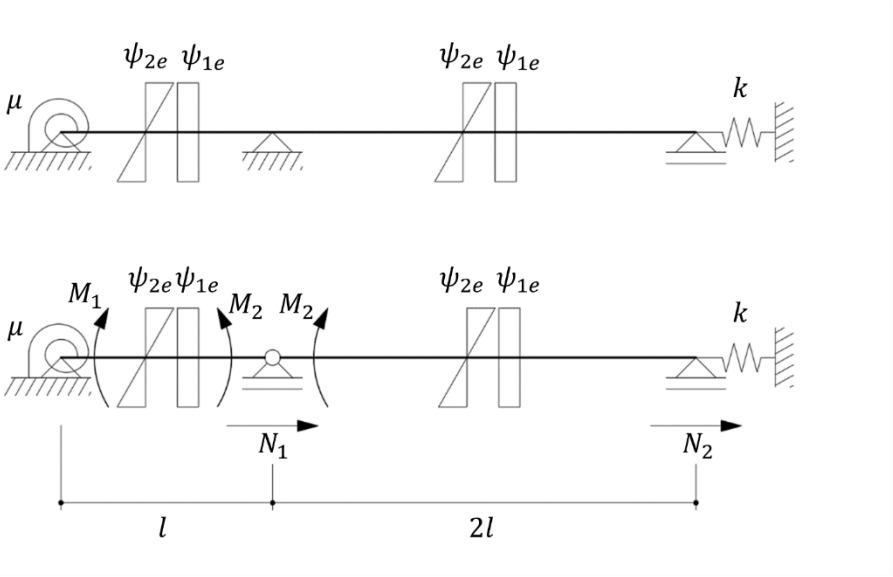

Figure 27 - Four times redundant static scheme with elastic restraints and relative redundant variables

The scheme 4 represented in *Figure 27* is a four times redundant static scheme characterized also by the presence of a rotational and a translational elastic restraint, whose stiffnesses are respectively μ and k.

The compatibility equations, necessary to compute the four redundant variables, are written as follow:

$$\begin{cases} M_1\left(\frac{l}{3E_0I}+\frac{1}{\mu}\right)+M_2\left(\frac{l}{6E_0I}\right)+\psi_{2e}\frac{l}{2}=0 \\ M_1\left(\frac{l}{6E_0I}\right)+M_2\left(\frac{l}{3E_0I}+\frac{2l}{3E_0I}\right)+\psi_{2e}\left(\frac{l}{2}+\frac{2l}{2}\right)=0 \end{cases} \quad (127)$$

$$\begin{cases} N_1\left(\frac{l}{E_0A}+\frac{2l}{E_0A}\right)+N_2\left(-\frac{2l}{E_0A}\right)+\psi_{1e}(l-2l)=0 \\ N_1\left(-\frac{2l}{E_0A}\right)+N_2\left(\frac{2l}{E_0A}+\frac{1}{k}\right)+\psi_{1e}(2l)=0 \end{cases} \quad (128)$$

from which it is obtained:

$$M_1=-\psi_{2e}\frac{9\mu lE_0I}{11\mu l+36E_0I} \quad (129)$$

$$M_2=-\psi_{2e}\frac{15\mu lE_0I+54E_0^2I^2}{11\mu l+36E_0I} \quad (130)$$

$$N_1=\frac{E_0^2A^2-2klE_0A}{2kl+3E_0A}\psi_{1e} \quad (131)$$

$$N_2 = -\frac{4klE_0A}{2kl+3E_0A}\psi_{1e} \quad (132)$$

Similarly to the previously analysed static schemes, the computation of the additional stresses due to the redundant restraints, for the section in correspondence of the central support, is performed as follow. For what concerns the section immediately on the left side of the central support, the additional stresses are given by:

$$\Delta\sigma_{e,left}(y) = \frac{E_0A-6kl}{2kl+3E_0A}E_0\psi_{1e} - \frac{15\mu l+54E_0I}{11\mu l+36E_0I}E_0\psi_{2e}y \quad (133)$$

while for what concerns the section immediately on the right side of the central support, the additional stresses are given by:

$$\Delta\sigma_{e,right}(y) = -\frac{4kl}{2kl+3E_0A}E_0\psi_{1e} - \frac{15\mu l+54E_0I}{11\mu l+36E_0I}E_0\psi_{2e}y \quad (134)$$

In order to provide in *Figure 28* and in *Figure 29* a simple representation of the total stresses at the sectional level, in non-dimensional form, the following values have been considered for the stiffnesses of the elastic restraints:

- $\mu = \frac{3E_0I}{l}$
- $k = \frac{3E_0A}{l}$

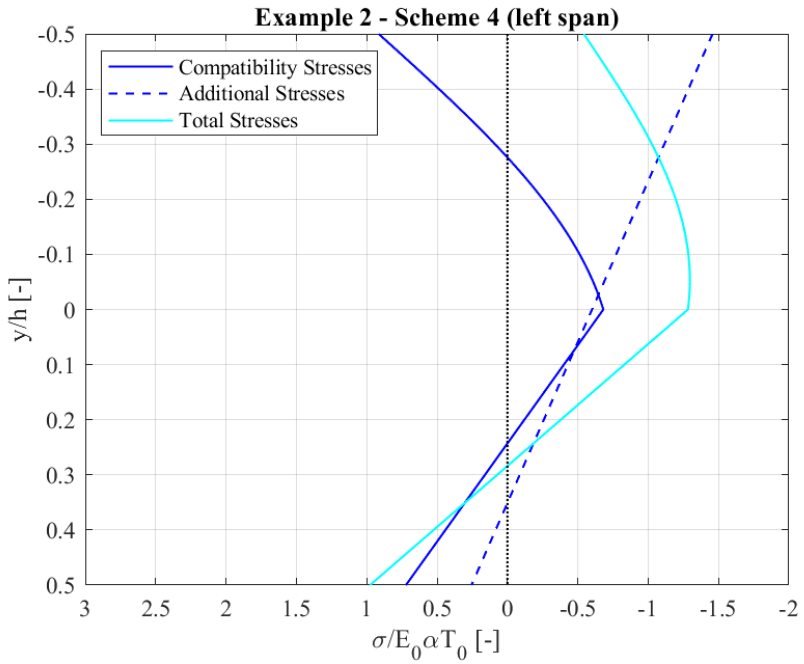

Figure 28 - Total stresses distribution over the depth of the cross section

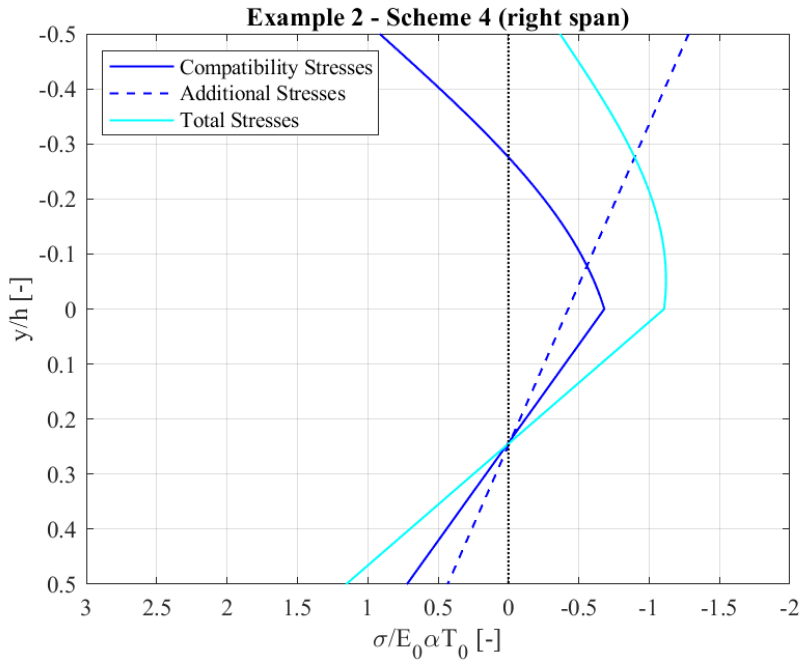

Figure 29 - Total stresses distribution over the depth of the cross section

3.4.3 Example 3

Consider an homogeneous T-shaped cross section subject to an exponential temperature distribution over its depth, whose dimensions are those indicated in *Figure 30*. The aim of this example is to show the application of the method in presence of cross sections characterized by a more complex shape and in particular by a variable width along the y coordinate.

The function of y coordinate considered for the temperature distribution is the following:

$$T(y) = T_0 \cdot e^{-\frac{y}{h}} \qquad (135)$$

Since the origin of the reference system is fixed in correspondence of the centroid of the cross section, the temperature assumes a value equal to T_0 in correspondence of it.

The moment of inertia of the cross section with respect to x axis is:

$I = 28793907{,}4612\ cm^4$

while the area of the section is:

$A = 10750\ cm^2$

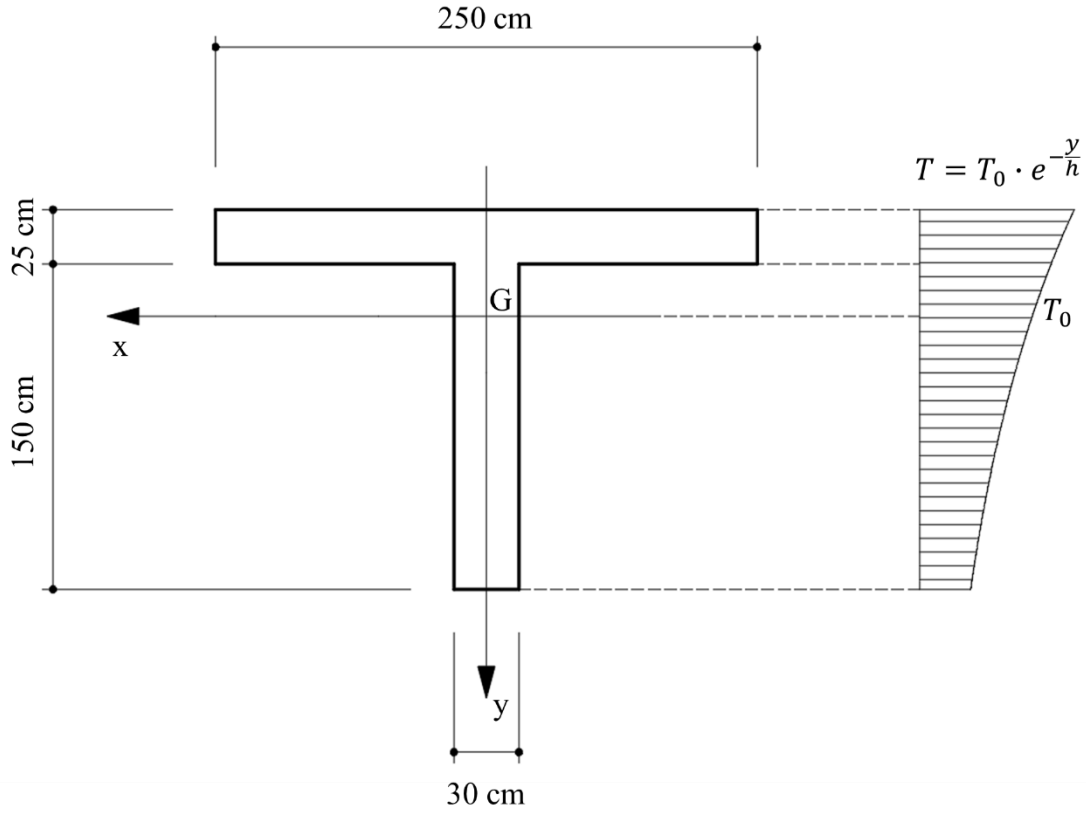

Figure 30 - Homogeneous T-shaped cross section subject to an exponential temperature distribution over its depth

Having computed the area and the moment of inertia with respect to x axis of the cross section, it is possible to apply equations (71) and (72) in order to compute the components of the vector $\underline{\psi}_e$. The integrations are opportunely performed in order to deal with the discontinuity in the width of the section over the y coordinate. Moreover in the following computations the distance of the centroid from the upper fiber of the section, equal to 49,1279 cm, is briefly indicated with y'_g.

$$\psi_{1e} = \frac{\alpha}{A}\int_A T dA = \frac{\alpha}{A}\left\{\int_{-y'_G}^{-y'_G+25} T_0 e^{-\frac{y}{h}} 250 dy + \int_{-y'_G+25}^{175-y'_G} T_0 e^{-\frac{y}{h}} 30 dy\right\} =$$

$$= \frac{T_0\alpha}{A}\left\{\int_{-49,1279}^{-24,1279} e^{-\frac{y}{h}} 250 dy + \int_{-24,1279}^{125,8721} e^{-\frac{y}{h}} 30 dy\right\} =$$

$$= \frac{T_0\alpha}{A}\left\{\left|-he^{-\frac{y}{h}}250\right|_{-49,1279}^{-24,1279} + \left|-he^{-\frac{y}{h}}30\right|_{-24,1279}^{125,8721}\right\} =$$

$$= T_0\alpha \cdot 1{,}04004247\ [-] \qquad (136)$$

$$\psi_{2e} = \frac{\alpha}{\mathrm{I}}\int_A Ty dA = \frac{\alpha}{I}\left\{\int_{-y'_G}^{-y'_G+25} T_0 e^{-\frac{y}{h}}\cdot y\cdot 250dy + \int_{-y'_G+25}^{175-y'_G} T_0 e^{-\frac{y}{h}}\cdot y\cdot 30dy\right\} =$$

$$= \frac{T_0\alpha}{I}\left\{\int_{-49,1279}^{-24,1279} e^{-\frac{y}{h}}\cdot y\cdot 250dy + \int_{-24,1279}^{125,8721} e^{-\frac{y}{h}}\cdot y\cdot 30dy\right\} =$$

$$= \frac{T_0\alpha}{I}\left\{250\cdot\left|-he^{-\frac{y}{h}}y - \left(h^2e^{-\frac{y}{h}}\right)\right|_{-49,1279}^{-24,1279} + 30\cdot\left|\left(-he^{-\frac{y}{h}}\right)(y+h)\right|_{-24,1279}^{125,8721}\right\} =$$

$$= -T_0\alpha\cdot 0{,}005036134\ [1/cm] \qquad (137)$$

The compatibility stresses in the elastic field are computed according to equation (68) as follow:

$$\sigma_e(y) = E_0[\psi_{1e} + \psi_{2e}\cdot y - \alpha\cdot T(y)] \qquad (138)$$

which, by substituting expressions (136), (137) and (135) leads to:

$$\sigma_e(y) = E_0T_0\alpha\left[1{,}04004247 - 0{,}005036134y - e^{-\frac{y}{175}}\right] \qquad (139)$$

The compatibility stresses distribution over the depth of the cross section, normalized with respect to $E_0\alpha T_0$, is reported in *Figure 31* while in *Figure 32* is represented the total deformation of the cross section under the plane section hypothesis, normalized with respect to αT_0.

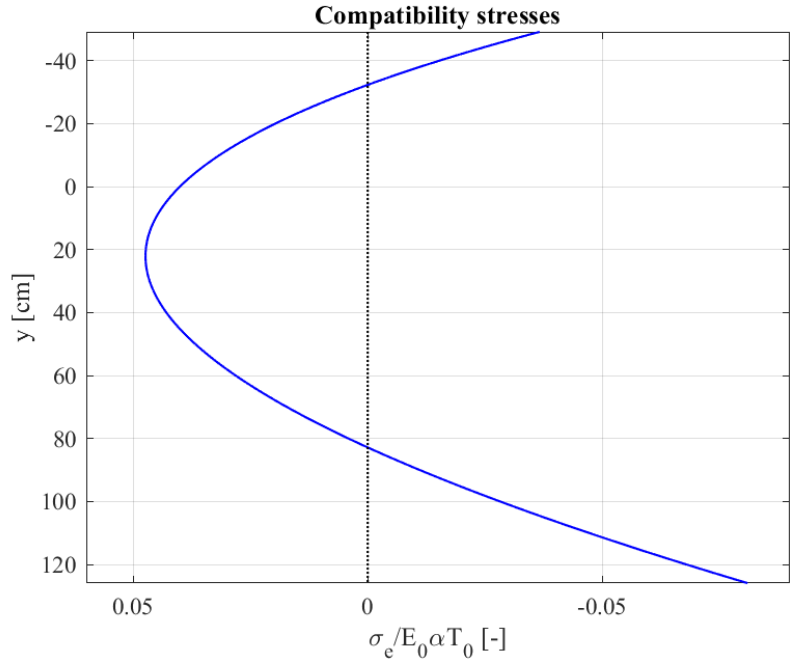

Figure 31 – Compatibility stresses distribution over the depth of the cross section

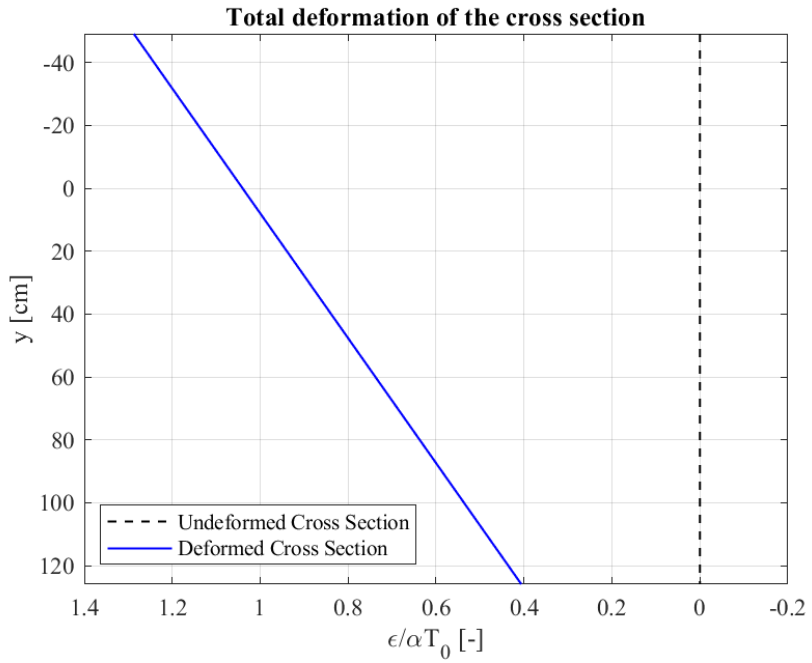

Figure 32 - Total deformation of the cross section

The computations carried out are verified by checking that the equilibrium equations are satisfied:

$$\int_A \underline{\rho}\sigma dA = 0 \qquad (140)$$

which for the example under consideration are:

$$\int_{-y'_G}^{175-y'_G} \sigma_e b dy = E_0 T_0 \alpha \left\{ \int_{-y'_G}^{-y'_G+25} \left(1{,}04004247 - 0{,}005036134y - e^{-\frac{y}{175}}\right) 250 dy + \right.$$

$$\left. + \int_{-y'_G+25}^{175-y'_G} \left(1{,}04004247 - 0{,}005036134y - e^{-\frac{y}{175}}\right) 30 dy \right\} =$$

$$= E_0 T_0 \alpha \left\{ \int_{-49{,}1279}^{-24{,}1279} \left(260{,}0106175 - 1{,}2590335y - 250e^{-\frac{y}{175}}\right) dy + \right.$$

$$\left. + \int_{-24{,}1279}^{125{,}8721} \left(31{,}2012741 - 0{,}15108402y - 30e^{-\frac{y}{175}}\right) dy \right\} =$$

$$= E_0 T_0 \alpha \left\{ \left| 260{,}0106175y - \frac{1{,}2590335}{2} y^2 + 43750e^{-\frac{y}{175}} \right|_{-49{,}1279}^{-24{,}1279} + \right.$$

$$+\left|31{,}2012741y-\frac{0{,}15108402}{2}y^2+5250e^{-\frac{y}{175}}\right|_{-24{,}1279}^{125{,}8721}\Bigg\}=$$

$$=-E_0T_0\alpha\cdot 0{,}000379\ \cong 0 \qquad (141)$$

$$\int_{-y'_G}^{175-y'_G}\sigma_e y b dy=E_0T_0\alpha\left\{\int_{-49{,}1279}^{-24{,}1279}\left(260{,}0106175y-1{,}2590335y^2-250ye^{-\frac{y}{h}}\right)dy+\right.$$

$$\left.+\int_{-24{,}1279}^{125{,}8721}\left(31{,}2012741y-0{,}15108402y^2-30ye^{-\frac{y}{h}}\right)dy\right\}=$$

$$=E_0T_0\alpha\left\{\left|\frac{260{,}0106175}{2}y^2-\frac{1{,}2590335}{3}y^3-250\left(-he^{-\frac{y}{h}}\right)(y+h)\right|_{-49{,}1279}^{-24{,}1279}+\right.$$

$$\left.+\left|\frac{31{,}2012741}{2}y^2-\frac{0{,}15108402}{3}y^3-30\left(-he^{-\frac{y}{h}}\right)(y+h)\right|_{-24{,}1279}^{125{,}8721}\right\}=$$

$$=E_0T_0\alpha\cdot 0{,}09\cong 0 \qquad (142)$$

The equilibrium equations are satisfied therefore, the compatibility stresses computed are correct.

3.4.4 Example 4

Consider the same homogeneous T-shaped cross section analysed in example 3, subject to a discontinuous non-linear temperature distribution over its depth. In particular the temperature distribution is given by a linear function of y coordinate in the top part of the cross section, by a null temperature in the superior portion of the web and by a constant negative temperature in the portion of the web below the centroid, as it can be appreciated in *Figure 33*. The aim of this example is to show the application of the method to the cases characterized by the complexity of a cross section with variable width along y coordinate, as well as by the complexity of a discontinuous non-linear temperature distribution. Both of these aspects will in fact imply the necessity of dividing the various integrations in multiple contributions, as it will be clear from the computations reported in the following.

Having defined as y'_g the distance of the centroid from the upper fiber of the cross section, equal to 49,1279 cm, the linear expression defining the temperature distribution acting on the flange of the T-shaped cross section is determined as follow:

$$T(y)=ay+b \qquad (143)$$

where a and b are found by imposing:

$$\begin{cases} a(-y'_G) + b = T_1 \\ a(-y'_G + 25) + b = 0 \end{cases} \quad (144)$$

which leads to:

$$T(y) = T_1 \left(1 - \frac{y'_G}{25} - \frac{y}{25}\right) \quad (145)$$

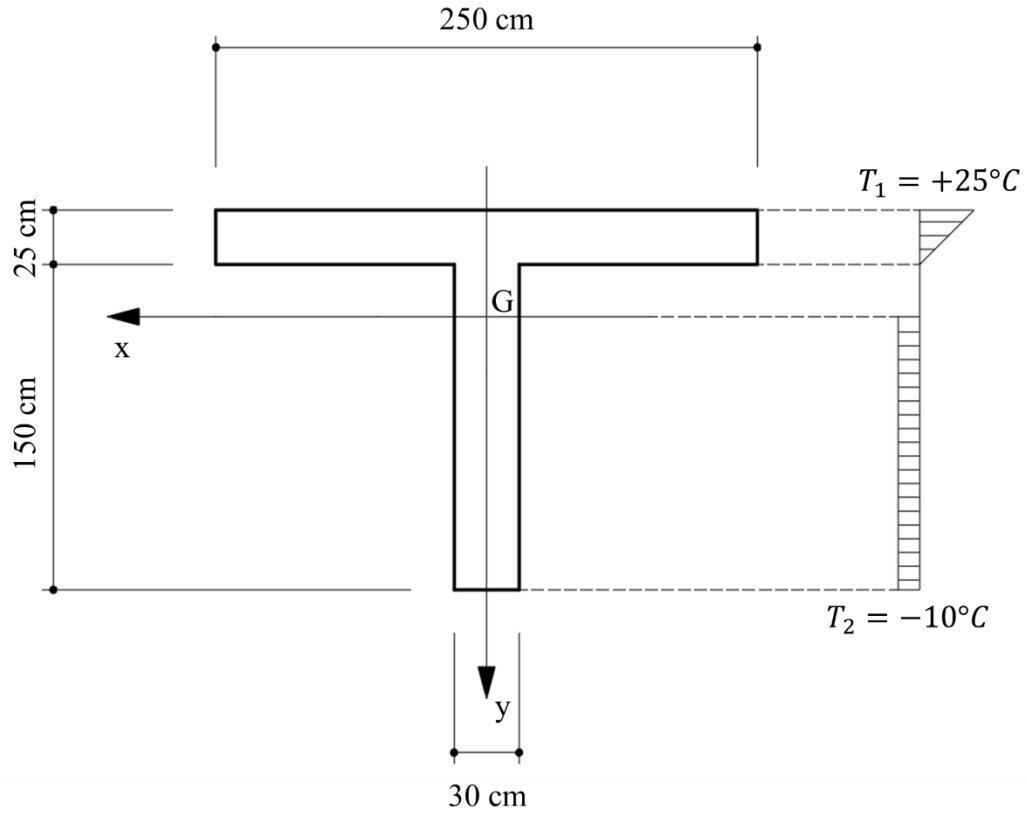

Figure 33 - Homogeneous T-shaped cross section subject to a discontinuous non-linear temperature distribution over its depth

Since the section is the same as the one considered in example 3, the moment of inertia with respect to x axis and the area of the cross section are the same previously reported.

The components of the vector $\underline{\psi_e}$ are computed applying equations (71) and (72) in which the integrals have to be subdivided in two contributions in order to deal with the discontinuity in the width of the section over the y coordinate as well as in the temperature distribution over the depth of the section.

$$\psi_{1e} = \frac{\alpha}{A}\int_A T dA = \frac{\alpha}{A}\left\{\int_{-y'_G}^{-y'_G+25} T_1\left(1 - \frac{y'_G}{25} - \frac{y}{25}\right)250dy + \int_0^{175-y'_G} T_2 30dy\right\} =$$

$$= \frac{\alpha}{A}\left\{\int_{-y'_G}^{-y'_G+25} 6250\left(1 - \frac{y'_G}{25} - \frac{y}{25}\right)dy - \int_0^{175-y'_G} 300dy\right\} =$$

$$= \frac{\alpha}{A}\left\{|6250y - 250y'_G y - 125y^2|_{-y'_G}^{-y'_G+25} - |300y|_0^{175-y'_G}\right\} =$$

$$= \alpha \cdot 3{,}754732093\ [-] \qquad (146)$$

$$\psi_{2e} = \frac{\alpha}{\mathrm{I}}\int_A T y dA = \frac{\alpha}{I}\left\{\int_{-y'_G}^{-y'_G+25} T_1\left(1 - \frac{y'_G}{25} - \frac{y}{25}\right)y250dy + \int_0^{175-y'_G} T_2 y 30dy\right\} =$$

$$= \frac{\alpha}{I}\left\{\int_{-y'_G}^{-y'_G+25} 6250\left(y - \frac{y'_G y}{25} - \frac{y^2}{25}\right)dy - \int_0^{175-y'_G} 300ydy\right\} =$$

$$= \frac{\alpha}{I}\left\{\left|6250\frac{y^2}{2} - 250y'_G\frac{y^2}{2} - 250\frac{y^3}{3}\right|_{-y'_G}^{-y'_G+25} - \left|300\frac{y^2}{2}\right|_0^{175-y'_G}\right\} =$$

$$= -\alpha \cdot 0{,}1932229396\ [1/cm] \qquad (147)$$

The compatibility stresses in the elastic field are computed according to equation (68) which, due to the discontinuity in the temperature distribution, leads to the following expressions:

for $-y'_G \le y \le -y'_G + 25$

$$\sigma_e(y) = E_0\alpha[27{,}88263209 + 0{,}8067770604y] \qquad (148)$$

for $-y'_G + 25 \le y \le 0$

$$\sigma_e(y) = E_0\alpha[3{,}754732093 - 0{,}1932229396y] \qquad (149)$$

for $0 \le y \le 175 - y'_G$

$$\sigma_e(y) = E_0\alpha[13{,}754732093 - 0{,}1932229396y] \qquad (150)$$

The compatibility stresses distribution over the depth of the cross section is reported in *Figure 34* by assuming $E_0 = 35000\ MPa$ and $\alpha = 10^{-5}\ °C^{-1}$ which are values compatible with the ones assumed in the case of a reinforced concrete section. Moreover the total deformation of the cross section under the plane section hypothesis, computed according to equation (74), is represented in *Figure 35* by assuming the same value of α.

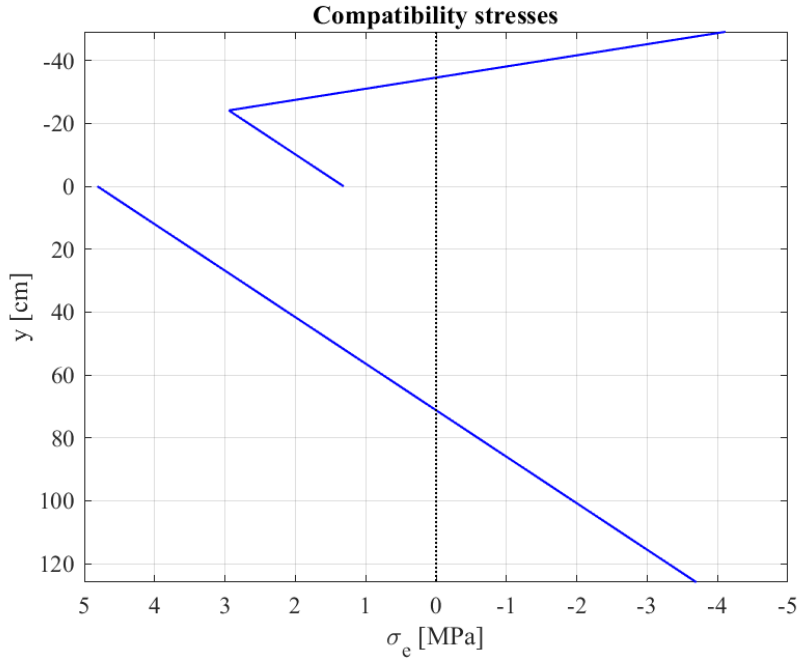

Figure 34 – Compatibility stresses distribution over the depth of the cross section

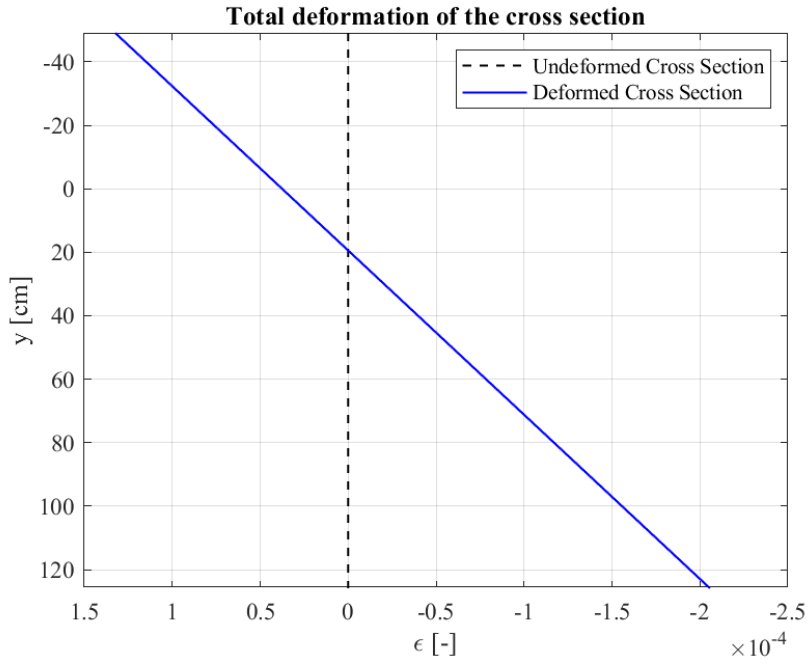

Figure 35 – Total deformation of the cross section

4 VISCOELASTIC FIELD

4.1 Introduction

The analysis in the viscoelastic field of homogeneous structures subject to non-linear temperature distributions over the depth of the cross section is presented in this chapter. As already mentioned in chapter 1, in fact, the aim of the present work is to evaluate the influence of the long-term behaviour of concrete on the stresses which arise in bridges due to thermal actions.

Concrete when subject to sustained stresses, because of its viscoelastic behaviour, shows some delayed deformations which increase in time with decreasing velocity until they stabilize over the years. The dual aspect of this physical phenomenon is the relaxation of concrete, because of which the response of a concrete structure subject to a sustained imposed deformation is characterized by a reduction in time of the initial state of stress. Since, as already discussed, thermal actions on structures are taken into account in structural analysis by means of imposed deformations, this second aspect, related to the time-dependent behaviour of concrete, causes the reduction in time of the stresses which arise in bridges due to temperature and which can be computed according to the procedure presented in chapter 3. The reduction in the stresses will be clearly shown in the present chapter by means of the comparison of the results obtained in the viscoelastic field at 10000 days with the same results previously computed with reference to the elastic field.

The theoretical background necessary to perform the analyses in the viscoelastic field presented in this chapter will be discussed in paragraph 4.2 in the framework of linear viscoelasticity, which holds for moderate stresses, not above 45-50% of the uniaxial concrete compressive strength. In particular, three alternative procedures for the computation of the stresses due to imposed deformations variable in time will be presented: the exact formulation, the algebraic approach and the Fundamental Theorem. According to what has been discussed in chapter 2 with reference to the climatic actions on structures, in order to properly define the temperature variation in time and, on consequence, the variation in time of the imposed deformations due to thermal actions, a sinusoidal time function should be considered. However this aspect leads to several complications in the application of the proposed procedures for the computation of the stresses in the viscoelastic field. These complications will be addressed in detail in chapter 5 while in the present chapter simpler variations in time of the temperature will be considered.

As the exact formulation above mentioned leads to a Volterra Integral Equation, the numerical procedure implemented for its solution is discussed in detail in paragraph 4.3 together with the results obtained with it.

Finally in paragraph 4.4 the application of the Fundamental Theorem, which provides an approximate solution of the problem under discussion, is shown. In particular, the Fundamental Theorem will be applied both to the case of a temperature distribution varying in time as well as

to the case of a temperature distribution constant in time. The application of the theorem in the case of a temperature distribution varying in time will allow to compare the obtained results with those presented in paragraph 4.3 by means of the numerical integration of the Volterra Integral Equation. The application to the case of constant temperature in time is instead motivated by the fact that national and international code prescriptions do not provide temperature gradients varying in time and therefore the same procedure will be applied in chapter 6 for the analysis of two real bridge structures.

4.2 Computation of stresses due to imposed deformations

4.2.1 Exact formulation

The computation in the viscoelastic field of the stress at time t, when the imposed deformations and the history of total deformations are known, is given by the following expression which derives from the application of the McHenry Principle of Superposition [19]:

$$\sigma(t) = \int_0^t d[\varepsilon(t') - \overline{\varepsilon}(t')] \cdot R(t, t') \qquad (151)$$

where the integration from 0 to t represents a Stieltjes integral which allows to integrate also non-continuous functions. The function $R = R(t, t_0)$ is referred as Relaxation Function and represents the stress at time $t > t_0$ generated by a unit deformation applied at $t = t_0$ and sustained in time. Moreover the Relaxation Function is monotonic, growing with t_0 and decreasing with t.

Equation (151) can be specialized for the problem under examination of the computation of stresses due to non-linear temperature distributions over the depth of the cross section as follow:

$$\sigma(y, t) = \int_0^t \left[\underline{\rho}^T d\underline{\psi}(t') - \alpha dT(y, t')\right] \cdot R(t, t') \qquad (152)$$

Imposing the equilibrium:

$$\int_A \underline{\rho} \cdot \sigma \, dA = 0 \qquad (153)$$

and considering equation (152) for the expression of the stress σ, it is found

$$\int_A \int_0^t \left(\underline{\rho}\, \underline{\rho}^t d\underline{\psi}(t') - \alpha dT(y, t')\underline{\rho}\right) \cdot R(t, t') \, dA = 0 \qquad (154)$$

which, according to the definition of the elastic stiffness matrix $\underline{\underline{B_e}}$ and of the vector $\underline{S}(t)$ presented in the previous chapters, can be written as follow:

$$\int_0^t \left(\underline{\underline{B_e}} d\underline{\psi}(t') - d\underline{S}(t')\right) \cdot \frac{R(t, t')}{E_0} = 0 \qquad (155)$$

The previous equation leads to:

$$\int_0^t \left(\underline{\underline{B_e}} d\underline{\psi}(t') - d\underline{S}(t') \right) = 0 \qquad (156)$$

which is equivalent to writing:

$$\underline{\underline{B_e}}\,\underline{\psi}(t) = \underline{S}(t) \qquad (157)$$

from which it is finally found that:

$$\underline{\psi}(t) = \underline{\underline{B_e}}^{-1}\underline{S}(t) = \underline{\psi}_e(t) \qquad (158)$$

It has been demonstrated that the total deformation at time t for the considered problem is the same as the one computed with reference to the elastic field. The vector $\underline{\psi}_e$, known from the elastic solution, can be therefore adopted in the writing of equation (152) as follow:

$$\sigma(y,t) = \int_0^t E_0 \cdot \left(\underline{\rho}^T d\underline{\psi}_e(t') - \alpha dT(y,t') \right) \cdot \frac{R(t,t')}{E_0} = \int_0^t d\sigma_e(y,t') \cdot \frac{R(t,t')}{E_0} \qquad (159)$$

The result just obtained expresses the Second Theorem of Linear Viscoelasticity which in fact holds for homogenous structures subject only to imposed deformations as the ones considered in the present chapter.

In the particular case in which the temperature T is independent from the time variable t, in order to compute the stress $\sigma(y,t)$ it is sufficient to know the Relaxation Function $R(t,t_0)$ for the specific initial time t_0.

$$\sigma(y,t) = \sigma_e(y) \cdot \frac{R(t,t_0)}{E_0} \qquad (160)$$

In the case in which T is instead variable in time, the computation of the stresses $\sigma(y,t)$ is more involved as the function R has to be defined for all the t' necessary to perform the numerical integration of equation (159). The complication in this process is due to the fact that the Relaxation Function has to be determined numerically and it is not provided by design codes. The reason behind this is the fact that the function R cannot be determined experimentally since it would be necessary to perform tests applying a unit deformation constant in time but this is not affordable as concrete is characterized also by the presence of a shrinkage deformation variable in time. The Relaxation Function has therefore to be determined numerically as the solution of the following Volterra Integral Equation, also called Convolution Equation:

$$\int_0^t \frac{\partial R(t',t_0)}{\partial t'} \cdot J(t,t') \cdot dt' = 1 \qquad (161)$$

where the function $J = J(t,t_0)$ is referred as Compliance Function or Creep Function and in a dual way to what happens for the Relaxation Function expresses the total deformation produced at time $t > t_0$ by a unit sustained stress applied at $t = t_0$. Moreover the Creep Function is monotonic,

growing with t and decreasing with t_0. Differently from what happens for the Relaxation Function the Creep Function can be determined experimentally and its analytical expression is found in design codes.

On the basis of these observations, in order to obtain a more immediate procedure for the computation of the stresses $\sigma(y,t)$ it is possible to rearrange equation (159) in the following way:

$$\int_0^t d\sigma(y,t') \cdot J(t,t') = \underline{\rho}^T \underline{\psi}_e(t) - \alpha dT(y,t) \qquad (162)$$

which is written in extended form as follow

$$\int_0^t d\sigma(y,t') \cdot J(t,t') = \psi_{e1}(t) + y \cdot \psi_{e2}(t) - \alpha dT(y,t) \qquad (163)$$

Fixing a value $\bar{y}$ of y coordinate, equation (163) represents a Volterra Integral Equation whose solution provides the stress $\sigma(\bar{y},t)$. Solving the integral equation fixing different values of $\bar{y}$ it is possible to determine, point by point, the function $\sigma(y,t)$ in the interval $y_{sup} \leq y \leq y_{inf}$ where y_{sup} and y_{inf} are respectively the y coordinate of the upper and lower fibers of the cross section.

The numerical technique implemented in a computer code for the solution of the Volterra Integral Equation above mentioned will be discussed in detail in paragraph 4.3.

4.2.2 Algebraic approach

The exact formulation for the computation of the stresses in the viscoelastic field, which is based on the solution of the Volterra Integral Equation, can be substituted by an approximate solution with the aim of eliminating the mathematical complexity connected to the solution of integral equations. In order to do this, in the past various attempts have been done to transform into an algebraic form the Volterra integral form of the constitutive law for a linear viscoelastic material, expressed by:

$$\int_0^t d\sigma(t') \cdot J(t,t') = \varepsilon(t) - \overline{\varepsilon}(t) \qquad (164)$$

which is specialized for the problem under examination according to equation (163). Among these attempts the most refined one is due to Trost (1967) [20], successively manipulated by Bazant (1972) [21], then introduced in the CEB-FIP Model Code 1990 [22] and at present time suggested by various normative codes such as the Eurocode 2 [23].

The basic simplifying hypothesis of the method consists in supposing that the deformation of concrete due to a generic stress history starting at time t_0 can be expressed in the subsequent form:

$$\varepsilon(t) = a + b \cdot \varphi(t,t_0) \qquad (165)$$

where a and b are two arbitrary constants and $\varphi(t,t_0)$ is the creep coefficient which is defined as the ratio between the creep deformation and the initial elastic deformation at time t_0.

Since the creep coefficient can be expressed as follow:

$$\varphi(t,t_0) = E(t_0)\cdot J(t,t_0) - 1 \qquad (166)$$

by substituting this expression in equation (165) it is obtained:

$$\varepsilon(t) = (a-b) + b\cdot E(t_0)\cdot J(t,t_0) \qquad (167)$$

It is therefore immediate to evaluate the stress $\sigma(t)$ associated to the strain $\varepsilon(t)$ by applying the basic concepts of linear viscoelasticity:

$$\sigma(t) = (a-b)\cdot R(t,t_0) + b\cdot E(t_0) \qquad (168)$$

The previous equation, written for $t = t_0$, since $R(t_0,t_0) = E(t_0)$ becomes:

$$\sigma(t_0) = a\cdot E(t_0) \qquad (169)$$

and, as at the initial time the material exhibits an elastic behavior, it follows that:

$$\frac{\sigma(t_0)}{E(t_0)} = a = \varepsilon(t_0) \qquad (170)$$

which, substituted in equation (168) leads to:

$$\sigma(t) = \varepsilon(t_0)\cdot R(t,t_0) + b\cdot [E(t_0) - R(t,t_0)] \qquad (171)$$

From previous equation it is finally found that:

$$b = \frac{[\varepsilon(t)-\varepsilon(t_0)]}{\varphi(t,t_0)} \qquad (172)$$

Combining equation (171) and equation (172) it is obtained:

$$\sigma(t) = \varepsilon(t_0)\cdot R(t,t_0) + \frac{[\varepsilon(t)-\varepsilon(t_0)]}{\varphi(t,t_0)}\cdot [E(t_0) - R(t,t_0)] \qquad (173)$$

which, solved with respect to $\varepsilon(t)$, provides:

$$\varepsilon(t) = \sigma(t)\cdot \frac{\varphi(t,t_0)}{[E(t_0) - R(t,t_0)]} + \varepsilon(t_0)\cdot \left[1 - \frac{R(t,t_0)\cdot\varphi(t,t_0)}{E(t_0) - R(t,t_0)}\right] \qquad (174)$$

Equation (174) represents the algebraic form of the viscoelastic creep law when the simplifying hypothesis expressed by equation (165) is made. Moreover equation (174) can be written in a more concise way by introducing the following equality:

$$\frac{\varphi(t,t_0)}{[E(t_0) - R(t,t_0)]} = \frac{1 + \chi(t,t_0)\cdot\varphi(t,t_0)}{E(t_0)} \qquad (175)$$

in which the function $\chi(t,t_0)$, known as ageing coefficient, is defined as follow:

$$\chi(t,t_0) = \frac{1}{1 - \frac{R(t,t_0)}{E(t_0)}} - \frac{1}{\varphi(t,t_0)} \qquad (176)$$

From equation (175) it is possible to observe that the Relaxation Function $R(t,t_0)$ can be expressed as a function of $\chi(t,t_0)$. Therefore, by performing the inversion of equation (175) it is found:

$$\frac{E(t_0)-R(t,t_0)}{\varphi(t,t_0)}=\frac{E(t_0)}{1+\chi(t,t_0)\cdot\varphi(t,t_0)} \qquad (177)$$

from which derives:

$$\mathrm{R(t,t_0)=E(t_0)\cdot\left[1-\frac{\varphi(t,t_0)}{1+\chi(t,t_0)\cdot\varphi(t,t_0)}\right]} \qquad (178)$$

By inserting equations (175) and (178) in equation (174) it is finally obtained:

$$\mathrm{\varepsilon(t)=\frac{\sigma(t)}{E(t_0)}\cdot[1+\chi(t,t_0)\cdot\varphi(t,t_0)]+\frac{\sigma(t_0)}{E(t_0)}\cdot\varphi(t,t_0)\cdot[1-\chi(t,t_0)]} \qquad (179)$$

Equation (179) is the final form of Trost algebraic approach which can be generalized by adding the imposed deformation $\bar{\varepsilon}(t)$:

$$\mathrm{\varepsilon(t)=\frac{\sigma(t)}{E(t_0)}\cdot[1+\chi(t,t_0)\cdot\varphi(t,t_0)]+\frac{\sigma(t_0)}{E(t_0)}\cdot\varphi(t,t_0)\cdot[1-\chi(t,t_0)]+\bar{\varepsilon}(t)} \qquad (180)$$

For sake of simplicity in the writing of equation (180) it is possible to adopt the following convention:

$$\begin{cases}\varepsilon(t)=\varepsilon\\ \sigma(t)=\sigma\\ \varphi(t,t_0)=\varphi\\ \chi(t,t_0)=\chi\\ E(t_0)=E\\ \sigma(t_0)=\sigma_0\\ \bar{\varepsilon}\,(t)=\bar{\varepsilon}\end{cases} \qquad (181)$$

so it is obtained:

$$\mathrm{\varepsilon=\frac{\sigma}{E}\cdot[1+\chi\cdot\varphi]+\frac{\sigma_0}{E}\cdot\varphi\cdot[1-\chi]+\bar{\varepsilon}} \qquad (182)$$

Equation (182) represents a pseudoelastic form and assuming:

$$\mathrm{E'=\frac{E}{1+\chi\cdot\varphi}} \qquad (183)$$

$$\bar{\bar{\varepsilon}}=\frac{\sigma_0}{E}\cdot\varphi\cdot[1-\chi] \qquad (184)$$

it is possible to write:

$$\varepsilon = \frac{\sigma}{E'} + (\bar{\bar{\varepsilon}} + \bar{\varepsilon}) \qquad (185)$$

This equation is an elastic form referred to the varied modulus E' in which is also introduced the additional imposed deformation $\bar{\bar{\varepsilon}}$ depending on the initial state of strain of concrete.

By solving equation (182) with respect to σ it is finally obtained:

$$\sigma = \frac{E \cdot (\varepsilon - \bar{\varepsilon})}{1 + \chi \cdot \varphi} - \sigma_0 \cdot \frac{\varphi \cdot (1 - \chi)}{1 + \chi \cdot \varphi} \qquad (186)$$

which can be adopted to obtain an approximate solution of the problem under examination of the computation of stresses due to non-linear temperature distributions in the viscoelastic field.

The approach to the long term analysis of viscoelastic structures based on the work of Trost, finalized by Bazant in the so called Age-Adjusted-Effective-Modulus-Method (AAEMM), here presented, allows to obtain results characterized by a good precision for engineering practice. However, even though the AAEMM introduces a strong simplification of the viscoelastic constitutive law, its application to the analysis of complex structures is not immediate as the related algebraic form of the constitutive law contains an additional imposed deformation $\bar{\bar{\varepsilon}}$, proportional to the initial one. This difficulty can be overcome by means of the application of the Fundamental Theorem, which will be discussed in the following paragraph.

4.2.3 Fundamental Theorem

The Fundamental Theorem, demonstrated by Mola [24], shows that the application of the Age-Adjusted-Effective-Modulus-Method can be operated by superposing three elastic solutions avoiding to take into consideration the additional imposed deformation $\bar{\bar{\varepsilon}}$ given by equation (184), as it will be shown in the following. This theorem represents therefore an alternative form of the AAEMM more suitable for the engineering practice maintaining however the same level of accuracy.

Consider the algebraic approach presented in the previous paragraph:

$$\varepsilon = \frac{\sigma}{E} \cdot (1 + \chi \cdot \varphi) + \frac{\sigma_0}{E} \cdot \varphi \cdot (1 - \chi) \qquad (187)$$

or equivalently:

$$\sigma = \frac{E \cdot \varepsilon}{1 + \chi \cdot \varphi} - \sigma_0 \cdot \frac{\varphi \cdot (1 - \chi)}{1 + \chi \cdot \varphi} \qquad (188)$$

Considering equation (188), by virtue of the principle of superposition it is possible to express σ as the sum of two components:

$$\sigma = \sigma_1 + \sigma_2 \qquad (189)$$

with:

$$\sigma_1 = \frac{E \cdot \varepsilon}{1 + \chi \cdot \varphi} \qquad (190)$$

$$\sigma_2 = -\sigma_0 \cdot \frac{\varphi \cdot (1 - \chi)}{1 + \chi \cdot \varphi} \qquad (191)$$

where σ_1 represents the stress produced at time t by the deformation ε, computed assuming the effective modulus E' while σ_0 is the initial stress computed assuming the elastic modulus $E(t_0)$.

To solve equation (191) it is assumed:

$$\sigma_2 = \lambda \frac{\sigma_0}{1 + \chi\varphi} + \mu\sigma_0 \qquad (192)$$

where:

$$\frac{\sigma_0}{(1 + \chi \cdot \varphi)} = \varepsilon_0 \cdot \frac{E}{(1 + \chi \cdot \varphi)} = \sigma_{10} \qquad (193)$$

represents the elastic initial stress generated by the initial deformation ε_0 assuming the effective modulus E' while $\lambda = \lambda(t, t_0)$ and $\mu = \mu(t, t_0)$ are two functions to be determined.

By equating expressions (191) and (192):

$$\frac{\lambda}{1 + \chi\varphi} + \mu = -\frac{\varphi(1 - \chi)}{1 + \chi\varphi} \qquad (194)$$

the polynomial identity requires:

$$\mu = -\frac{1 - \chi}{\chi} \qquad (195)$$

$$\lambda = -\mu \qquad (196)$$

from which the following expression of σ_2 derives:

$$\sigma_2 = \mu(-\sigma_{10} + \sigma_0) \qquad (197)$$

and therefore equation (189) finally becomes:

$$\sigma = \sigma_1 + \mu(\sigma_0 - \sigma_{10}) \qquad (198)$$

Equation (198) is an alternative form of equation (188) and represents the formulation of the Fundamental Theorem which shows that the state of stress in the viscoelastic field can be obtained combining three elastic solutions by means of a special time function depending on the ageing

coefficient χ. The advantage of requiring only elastic computations is what makes this method particularly convenient in the practical applications as it will be shown through the examples provided in paragraph 4.4. regarding the problem of the computation of stresses due to non-linear temperature distributions.

Proceeding in a dual way, starting from equation (187), the Fundamental Theorem can also be formulated as follow:

$$\varepsilon = \varepsilon_1 + \mu(\varepsilon_0 - \varepsilon_{10}) \qquad (199)$$

where ε_1 is the elastic deformation produced by the stress σ acting at time t assuming the effective modulus E', ε_{10} is the initial elastic deformation evaluated assuming the effective modulus E' and finally ε_0 represents the initial deformation computed assuming the elastic modulus $E(t_0)$.

In the particular case in which the applied loads are constant in time it is immediate to observe that

$$\sigma_1(\mathrm{t}) = \sigma_{10} \qquad (200)$$

$$\varepsilon_1(\mathrm{t}) = \varepsilon_{10} \qquad (201)$$

and therefore equations (198) and (199) are simplified as follow:

$$\sigma = \sigma_1 \cdot (1 - \mu) + \mu \cdot \sigma_0 \qquad (202)$$

$$\varepsilon = \varepsilon_1(1 - \mu) + \mu \cdot \varepsilon_0 \qquad (203)$$

It is worth noting that, being an alternative form of the AAEMM, the Fundamental Theorem is also based on the simplifying hypothesis expressed by equation (165) that the deformation $\varepsilon(t)$ is a linear function in the creep coefficient. Therefore in the case of the problem under examination of the computation of stresses due to non-linear temperature distributions in the viscoelastic field, the Fundamental Theorem provides, in general, an approximate solution. The results obtained with the Fundamental Theorem are in fact exact just in the case in which the function expressing the time variation of temperature results to be a linear function of the coefficient $\varphi(t, t_0)$. This particular condition is satisfied by the case of temperature distribution constant in time for which therefore the solution provided by the Fundamental Theorem is exact.

In the framework of the analysis of the stresses which arise in bridges due to non-linear temperature distributions the application of the Fundamental Theorem allows to write:

$$\underline{\psi} = \underline{\psi}_{\mathrm{e}}^{(1)} + \mu \cdot \left(\underline{\psi}_{\mathrm{e}}^{(0)} - \underline{\psi}_{\mathrm{e}}^{(1,0)}\right) \qquad (204)$$

where the quantities with the superscript (1) are computed in the elastic field adopting the effective modulus E' while those characterized by the superscript (1,0) are the analogous ones computed making reference to the external action evaluated at time t_0. Finally the quantities indicated by the superscript (0) are those evaluated in the elastic field at initial time.

Considering the analyses performed in the elastic field, which are described in chapter 3, it is possible to observe that the expressions of the two components of the vector $\underline{\psi}_e$ are independent from the elastic modulus of concrete:

$$\psi_{1e} = \frac{\alpha}{A} \int_A T dA \tag{205}$$

$$\psi_{2e} = \frac{\alpha}{\mathrm{I}} \int_A T y dA \tag{206}$$

therefore it is possible to write:

$$\underline{\psi}_{\mathrm{e}}^{(1)} = \underline{\psi}_e \tag{207}$$

$$\underline{\psi}_{\mathrm{e}}^{(1,0)} = \underline{\psi}_e^{(0)} \tag{208}$$

from which it follows:

$$\underline{\psi} = \underline{\psi}_e \tag{209}$$

As already discussed in paragraph 4.2.1 this result is in agreement with the Second Theorem of Linear Viscoelasticity which in fact holds for homogenous structures subject only to imposed deformations as the ones considered in the present chapter.

Moreover, considering again the analyses performed in the viscoelastic field, it is possible to write:

$$\sigma_e^{(1)} = \frac{\sigma_e}{1 + \chi \cdot \varphi} \tag{210}$$

$$\sigma_e^{(1,0)} = \frac{\sigma_e^{(0)}}{1 + \chi \cdot \varphi} \tag{211}$$

and introducing the following quantity:

$$\lambda(t) = \frac{T(y,t)}{T(y,t_0)} \tag{212}$$

equation (210) can be written as follow:

$$\sigma_e^{(1)} = \lambda \cdot \frac{\sigma_e^{(0)}}{1 + \chi \cdot \varphi} \tag{213}$$

Substituting equation (211) and (213)in equation (198) it is obtained:

$$\sigma = \sigma_{\mathrm{e}}^{(0)} \cdot \left[\frac{\lambda}{1 + \chi \cdot \varphi} + \mu \cdot \left(1 - \frac{1}{1 + \chi \cdot \varphi} \right) \right] \tag{214}$$

which after some simple manipulations, introducing the expression previously found for μ, is written as follow:

$$\sigma = \sigma_e^{(0)} \cdot \left[\frac{\lambda + \chi \cdot \varphi}{1 + \chi \cdot \varphi} - \frac{\varphi}{1 + \chi \cdot \varphi}\right] \quad (215)$$

Since, as already discussed, the Fundamental Theorem provides an approximate solution for the problem under examination, equation (215) represents the approximate form of equation(159).

4.3 Numerical solution of the Volterra Integral Equation

4.3.1 Algorithm for the computation of the stresses

In order to solve the Volterra Integral equation (163) found with reference to the exact formulation, it has been implemented a MATLAB code which allows to perform its numerical integration. The numerical procedure implemented is the one proposed in the CEB Bulletin 142-142bis [25] and consists in the step-by-step solution of the Volterra Integral Equation for the determination of the stress response to a given strain history by approximating the Stieltjes hereditary integrals with finite sums. In particular, two different numerical approximations can be considered: the first one is based on the rectangular rule while the second one is based on the trapezoidal rule. In both cases, as it is well known, the accuracy of the numerical solution increases with the reduction of the amplitude of the considered time steps. For practical applications the CEB Bulletin suggests the second kind of approximation, considering a time step definition as the one described in the following paragraph.

The trapezoidal rule is written as follow:

$$\varepsilon_{tot}(t_k) - \varepsilon_n(t_k) = \sum_{i=1}^{k} \frac{1}{2}[J(t_k, t_i) + J(t_k, t_{i-1})]\Delta\sigma(t_i) \quad (216)$$

and from it derives the following recurrent algebraic formula which has been implemented in a MATLAB code:

for $k = 1$

$$\Delta\sigma(t_1) = 2\frac{\varepsilon_{tot}(t_1) - \varepsilon_n(t_1)}{J(t_1, t_1) + J(t_1, t_0)} \quad (217)$$

for $k > 1$

$$\Delta\sigma(t_k) = \\ = 2\frac{\Delta\varepsilon_{tot}(t_k) - \Delta\varepsilon_n(t_k) - \sum_{i=1}^{k-1}\frac{\Delta\sigma(t_i)}{2}[J(t_k, t_i) + J(t_k, t_{i-1}) - J(t_{k-1}, t_i) - J(t_{k-1}, t_{i-1})]}{J(t_k, t_k) + J(t_k, t_{k-1})}$$

where:

ε_{tot} = total deformation

ε_n= imposed deformation

and the stress at time $t = t_k$ is finally obtained as follow:

$$\sigma(t_k) = \sum_{i=1}^{k} \Delta\sigma(t_i) \quad (218)$$

It is important to point out that the implemented MATLAB code has been conceived for strain histories characterized by an instantaneous variation at $t = t_1 \equiv t_0$. This choice implies the necessity to impose that t_0 is equal to t_1 in the algorithm given by equation (217).

For what concerns the definition of the Creep Function $J(t, t_0)$ adopted in the procedure, it is given by the following expression:

$$J(t, t_0) = \frac{1}{E(t_0)} \cdot [1 + \varphi(t, t_0)] \quad (219)$$

where the creep coefficient $\varphi(t, t_0)$ has been computed according to the formulation suggested by the CEB-FIP Model Code 1990 [22]:

$$\varphi(t, t_0) = \varphi_0 \cdot \beta_c(t - t_0) \quad (220)$$

where:

- φ_0 is the notional creep coefficient - eq. (221)
- β_c is the coefficient describing the development of creep with time after loading - eq. (225)
- t is the age of concrete in days at the considered moment
- t_0 is the age of concrete in days at loading

The notional creep coefficient may be estimated from:

$$\varphi_0 = \varphi_{RH} \cdot \beta(f_{cm}) \cdot \beta(t_0) \quad (221)$$

with:

$$\varphi_{RH} = 1 + \frac{1 - RH/RH_0}{0{,}46 \cdot (h/h_0)^{1/3}} \quad (222)$$

$$\beta(f_{cm}) = \frac{5{,}3}{(f_{cm}/f_{cm0})^{0{,}5}} \quad (223)$$

$$\beta(t_0) = \frac{1}{0{,}1 + (t_0/t_1)^{0{,}2}} \tag{224}$$

where:

- h=$2A_c/u$ is the notional size of the member [mm], where A_c is the cross section area and u is the perimeter of the member in contact with the atmosphere
- f_{cm} is the mean compressive strength of concrete at the age of 28 days [MPa]
- f_{cm0}= 10 MPa
- RH is the relative humidity of the ambient environment [%]
- RH_0=100%
- h_0=100 mm
- t_1=1day

The development of creep with time is given by:

$$\beta_c(t - t_0) = \left[\frac{(t - t_0)/t_1}{\beta_H + (t - t_0)/t_1}\right]^{0{,}3} \tag{225}$$

with:

$$\beta_H = 150 \cdot \left\{1 + \left(1{,}2\frac{RH}{RH_0}\right)^{18}\right\}\frac{h}{h_0} + 250 \ \leq 1500 \tag{226}$$

It is interesting to observe that the implemented algorithm, in the particular case of a constant prescribed unit strain, allows to determine the Relaxation Function $R(t, t_0)$ which is in fact given by the solution of the Volterra Integral Equation (161). An important benchmark to test if the implemented MATLAB code provides correct results has been therefore the possibility to determine the Relaxation Function from the Creep Function.

In order to do this the following parameters, necessary to compute the Creep Function $J(t, t_0)$, have been assumed:

- $C40/50$ concrete
- h = 200 mm
- RH = 0,7
- t_0 = 28 days

The values assumed by the Creep Function computed according to equation (219) on the basis of these parameters are plotted in non-dimensional form in *Figure 36*.

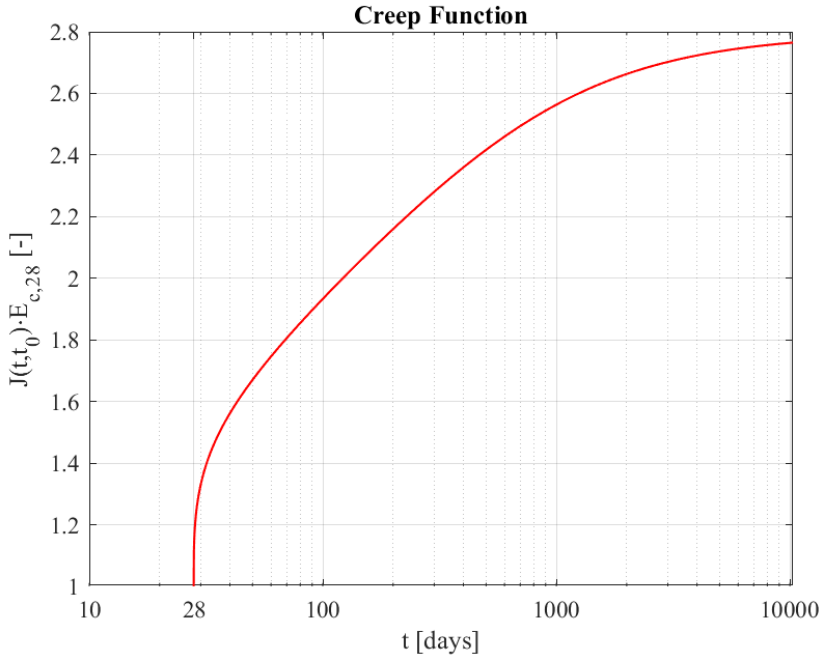

Figure 36 – Creep Function $J(t, t_0)$

Adopting the Creep Function obtained in this way, the algorithm implemented in the MATLAB code has been applied considering a constant prescribed unit strain:

$$\begin{cases} for\ t \leq t_0\colon\ \varepsilon_{tot}(t) - \varepsilon_n(t) = 0 \\ for\ t \geq t_1\colon\ \varepsilon_{tot}(t) - \varepsilon_n(t) = 1 \end{cases} \quad (227)$$

with $t_0 \equiv t_1$

and thus:

$$\begin{cases} \varepsilon_{tot}(t_1) - \varepsilon_n(t_1) = \Delta\varepsilon_{tot}(t_1) = 1 \\ \Delta\varepsilon_{tot}(t_k) - \Delta\varepsilon_n(t_k) = 0 \quad per\ k > 1 \end{cases} \quad (228)$$

In this case the stress response is, by definition, $\sigma(t_k) = R(t_k, t_0)$ and therefore the algorithm provides the Relaxation Function whose plot is reported in *Figure 37*. The obtained result is satisfactory as the curve representing the Relaxation Function has the expected shape; moreover it is worth noting that the function value for $t = t_0$, normalized with respect to the value of the elastic modulus of concrete at 28 days, is exactly equal to 1. This result is in agreement with the fact that the assumed value of t_0 was 28 days and therefore $R(t_0, t_0) = E(t_0) = E_{c,28}$.

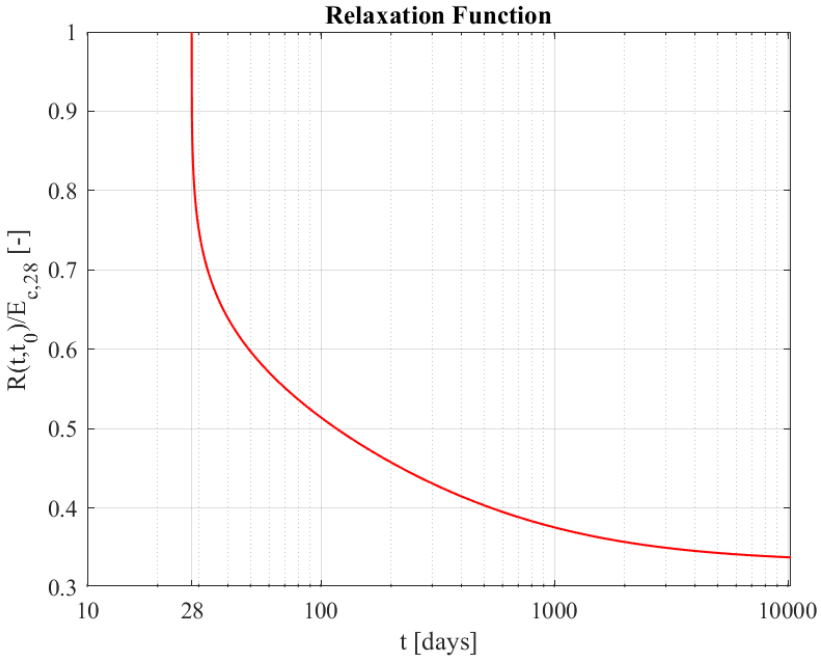

Figure 37– Relaxation Function $R(t, t_0)$

4.3.2 Time step definition

For what concerns the time step definition, for practical computations, the CEB Bulletin suggests to adopt increasing time steps which leads to an adequate level of accuracy associated with a minimum of computation time for usual strain histories.

In particular, it is possible to determine the time step $(t_k - t_0)$ according to a geometric progression. This translates into the following relation:

$$\frac{(t_k - t_0)}{(t_{k-1} - t_0)} = constant = q \qquad (229)$$

and putting:

$$(t_k - t_0) = 10^{\frac{1}{m}}(t_{k-1} - t_0) \qquad (230)$$

it is possible to determine the expression for the computation of the generic time step Δt_k:

$$\Delta t_k = 10^{\frac{1}{m}} \cdot \sum_{i=2}^{k-1} \Delta t_i - \sum_{i=2}^{k-1} \Delta t_i \qquad (231)$$

It is worth noting that the index of the summations in the above expression start from $i = 2$. This choice is justified by the fact that, as already mentioned, the implemented algorithm is conceived for strain histories characterized by an instantaneous variation at $t = t_1 \equiv t_0$.

Moreover the values adopted for Δt_2 and for m, are the ones suggested by the CEB Bulletin when computing the Relaxation Function associated to a Creep Function of the type of the CEB 1978 creep model:

$$\Delta t_2 = t_2 - t_1 = 0{,}05\ day$$

$$m = 16 \quad (\text{i.e. } q \cong 1{,}15)$$

By making this choice, the number of steps required to cover a time span of about 30 years is equal to $80 \div 90$, as it has been confirmed by the analyses performed with the MATLAB code implemented.

The amplitude of the time step in days with respect to the number of the considered step is reported in the following graph, which is obtained considering a time span for the integration equal to 10000 days (i.e. $\cong$ 30 years):

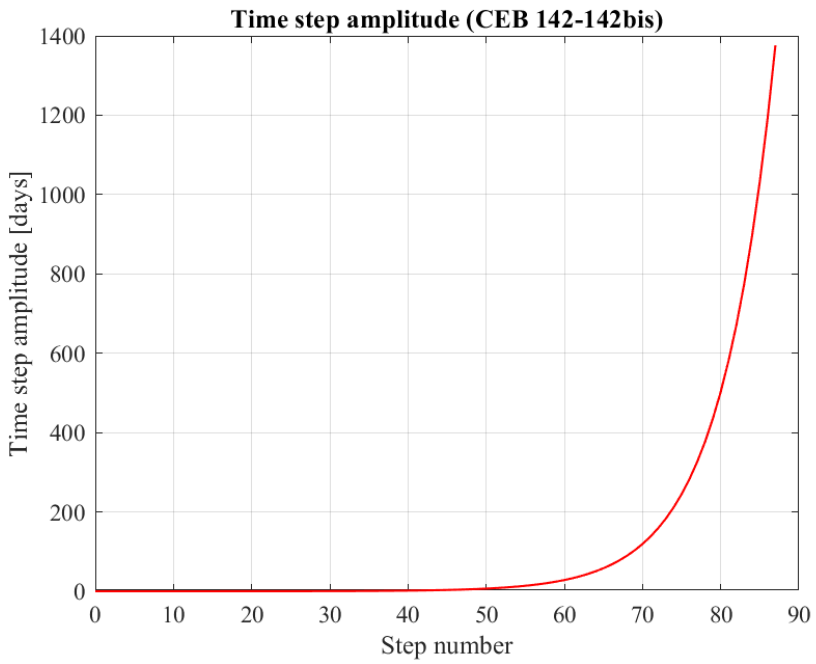

Figure 38 – Time step amplitude according to CEB bulletin 142-142bis

The graph reported in *Figure 38* clearly shows the increase in the time step amplitudes, which is strongly evident starting from the time step number 50, reaching time step amplitudes of more than 1300 days. It is important to highlight the fact that time step amplitudes of this magnitude are not

suitable for the integration of the Volterra Integral Equation when complex strain histories are considered. In fact the values of the time step amplitudes here reported have been obtained in the framework of the procedure suggested by the CEB Bulletin for usual strain histories and a specific discussion in order to integrate more complex strain histories, such as the ones associated to the periodic time variation of temperature distributions, will be provided in chapter 5.

4.3.3 Example of application

An example of application of the MATLAB code implemented in order to solve the Volterra Integral Equation (163) is here provided. In particular it is considered the problem presented in paragraph 3.4.1 with reference to the elastic field. The same cross section and the same static schemes have been analysed in the viscoelastic field according to the exact formulation presented in paragraph 4.2.1, allowing to obtain the compatibility stresses and the additional stresses due to the redundant restraints at 10000 days. These stresses distributions over the depth of the cross section are found by performing several numerical integrations of the Volterra Integral Equation (13) by means of the implemented algorithm, each time fixing a different value $\bar{y}$ of y coordinate, allowing to determine, point by point, the function $\sigma(y,t)$.

The various data assumed for the present example are the following:

- $C40/50$ concrete
- h = 200 mm (notional size of the member)
- RH = 0,7
- t_0 = 28 days
- $\alpha = 10^{-5}\ °C^{-1}$

where it has been assumed for the value of the notional size of the member an admissible, even though arbitrary, value as the cross section dimensions have been generically defined as b and h.

For what concerns the non-linear temperature distribution along the y coordinate it is given by:

$$T(y) = T_0\left(-2\frac{y^2}{h^2} + 3\frac{y}{h} + 1\right) \qquad (232)$$

but in order to perform the analysis in the viscoelastic field it is also necessary to know its variability in time. As already discussed in the introduction of the present chapter, the formulation here adopted is valid only for simple variations in time of the temperature while specific considerations will be done in chapter 5 in order to extend the formulation to the case of the periodic time variation of temperature distributions. Because of this, in order to express the time variation of $T(y)$ for the present example, it has been considered a parameter T_0 in equation(232) which varies in time according to an exponential decreasing law:

$$T_0(t) = 20 \cdot e^{-\frac{t-t_0}{t}}\ [°C] \qquad (233)$$

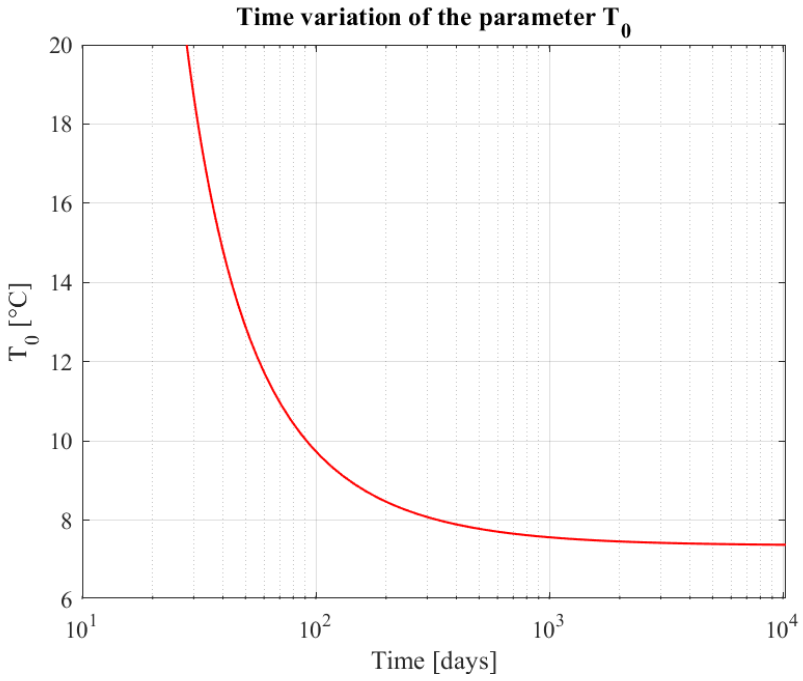

Figure 39 – Time variation of the parameter T_0

According to the Second Theorem of Linear Viscoelasticity the total deformation at time t is the same as the one computed with reference to the elastic field. The components of the vector $\underline{\psi}$ are therefore the same as the ones of the vector $\underline{\psi_e}$ previously computed:

$$\psi_1(t) = \psi_{1e}(t) = \frac{5}{6}\alpha T_0(t) \tag{234}$$

$$\psi_2(t) = \psi_{2e}(t) = 3\frac{\alpha T_0(t)}{h} \tag{235}$$

The total deformation, which has to be provided as an input value to the implemented MATLAB code, is computed as follow:

$$\varepsilon_{tot}(t) = \psi_1(t) + \psi_2(t) \cdot y \tag{236}$$

while the imposed deformation is given by:

$$\varepsilon_n(t) = \alpha T(t) \tag{237}$$

The distribution of compatibility stresses over the depth of the cross section computed at 10000 days by means of the implemented algorithm (σ_{10000}) is reported in *Figure 40* in comparison with the same distribution computed with reference to the elastic field (σ_0).

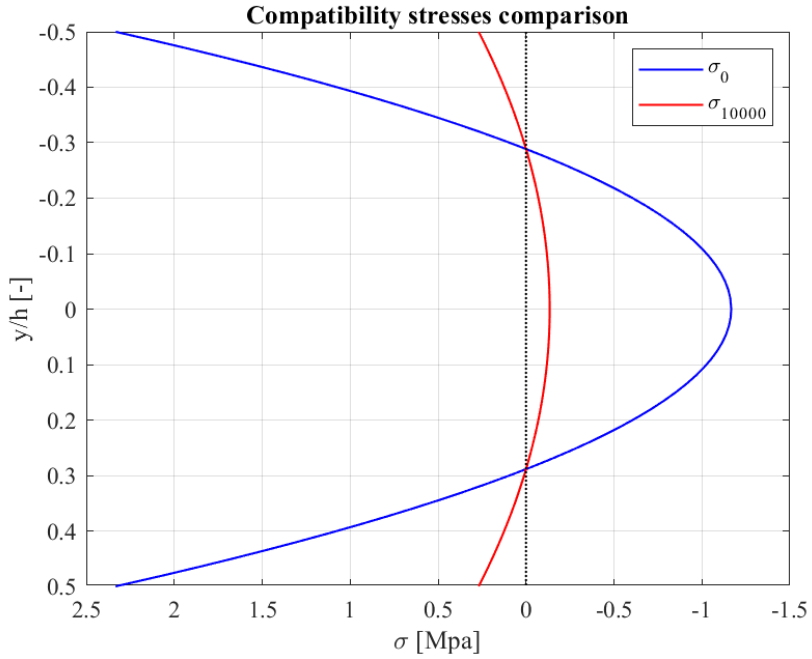

Figure 40 – Compatibility stresses comparison

In order to obtain the total stresses distribution over the depth of the cross section at 10000 days it is necessary to compute also the additional stresses distribution at the same time. The expressions of the additional stresses computed in the elastic field with reference to the two different static schemes considered for the example under analysis are given by:

$$\Delta\sigma_{scheme\ 1}(y,t) = -E_0\psi_{1e}(t) - E_0\psi_{2e}(t)\cdot y = E_0\alpha T_0(t)\cdot\left(-\frac{5}{6} - 3\frac{y}{h}\right) \quad (238)$$

$$\Delta\sigma_{scheme\ 2}(y,t) = -\frac{3}{2}E_0\psi_{2e}(t)\cdot y = E_0\alpha T_0(t)\cdot\left(-\frac{9}{2}\frac{y}{h}\right) \quad (239)$$

from which it is possible to obtain the total deformations to be provided as an input to the implemented algorithm:

$$\varepsilon_{tot,scheme\ 1}(t) = -\psi_{1e}(t) - \psi_{2e}(t)\cdot y = \alpha\cdot T_0(t)\cdot\left(-\frac{5}{6} - 3\frac{y}{h}\right) \quad (240)$$

$$\varepsilon_{tot,scheme\ 2}(t) = -\frac{3}{2}\psi_{2e}(t)\cdot y = \alpha\cdot T_0(t)\cdot\left(-\frac{9}{2}\frac{y}{h}\right) \quad (241)$$

The imposed deformations to be provided as an input to the implemented algorithm are instead null in both cases.

By operating in this way the implemented MATLAB code allows to compute the additional stresses distributions at 10000 days for the two considered static schemes. These distributions are then added to the one of the compatibility stresses, obtaining therefore the total stresses

distributions ($\sigma_{tot,10000}$) represented in *Figure 41* and in *Figure 42*, where they are compared with the same results obtained in the elastic field ($\sigma_{tot,0}$).

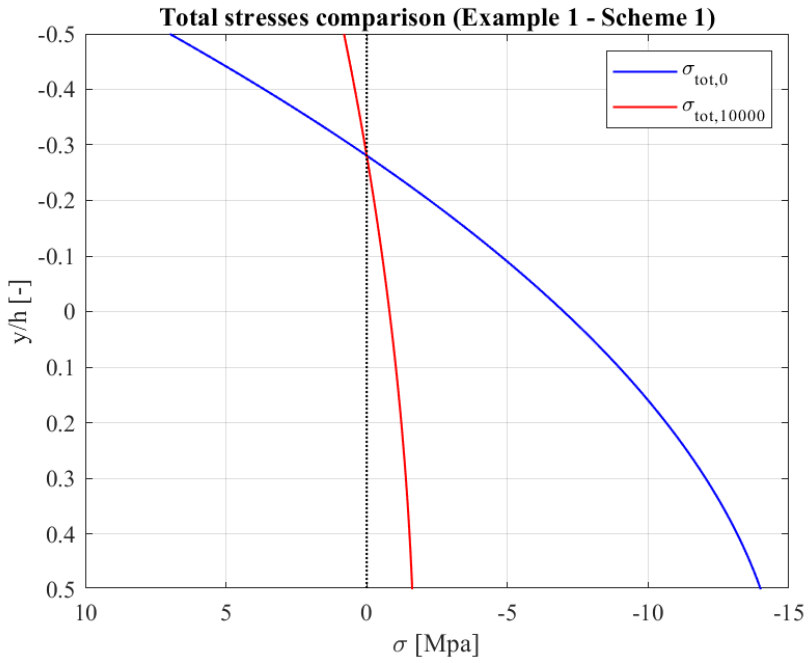

Figure 41 – Total stresses comparison (Static scheme 1)

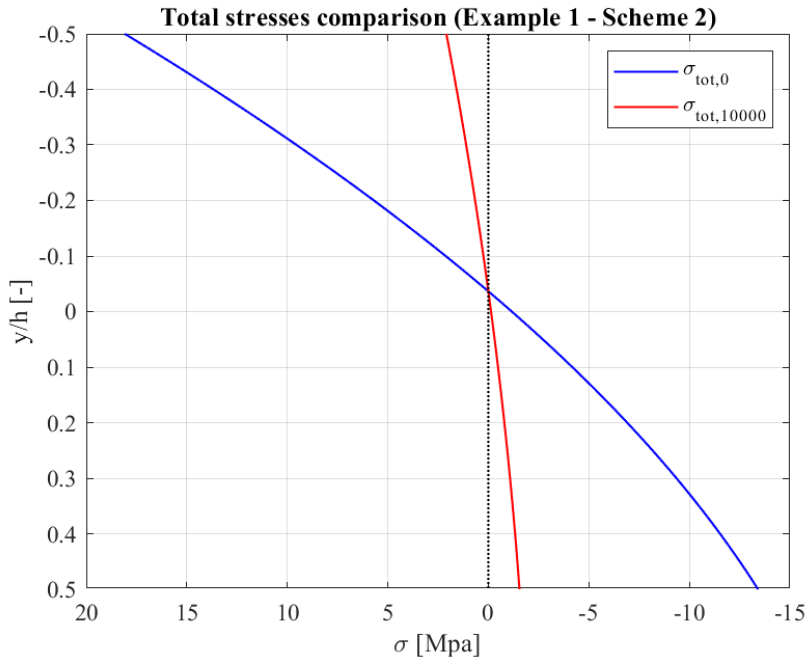

Figure 42 - Total stresses comparison (Static scheme 2)

In conclusion it is worth mentioning that the obtained results in the viscoelastic field correctly show a reduction of the stresses previously computed in the elastic field. In fact, due to the phenomenon of relaxation of concrete, the response of a concrete structure subject to a sustained imposed deformation is characterized by a reduction in time of the initial state of stress.

4.4 Application of the Fundamental Theorem

4.4.1 Example of application with temperature distributions variable in time

An example of application of the Fundamental Theorem in the case of a temperature distribution varying in time is here presented. In particular the same problem analysed in paragraph 4.3.3 by means of the exact formulation is considered, allowing to compare the approximate solution provided by the Fundamental Theorem with the exact one represented by the numerical integration of the Volterra Integral Equation.

The Fundamental Theorem has been applied in the form expressed by equation (215) in order to compute the compatibility stresses and the additional stresses due to the redundant restraints at 10000 days. The application of equation (215), specifically obtained in the framework of the computation of the stresses which arise in bridges due to non-linear temperature distributions, can be performed quite easily, simply starting from the knowledge of the solution in the elastic field at initial time $\sigma_e^{(0)}$.

Considering as $\sigma_e^{(0)}$ in equation (215) the expression of the compatibility stresses previously computed in chapter 3 with reference to the elastic field and given by:

$$\sigma_e(y,t_0) = E_0 \alpha T_0\,(t_0)\left(2\frac{y^2}{h^2} - \frac{1}{6}\right) \qquad (242)$$

it is obtained the compatibility stresses distribution at $t = 10000$ days as follow:

$$\sigma_e(y,t) = E_0 \alpha T_0\,(t_0)\left(2\frac{y^2}{h^2} - \frac{1}{6}\right)\cdot\left[\frac{\lambda+\chi\cdot\varphi}{1+\chi\cdot\varphi} - \frac{\varphi}{1+\chi\cdot\varphi}\right] \qquad (243)$$

Proceeding in an analogous way, for what concerns the additional stresses due to the redundant restraints, it is obtained:

$$\Delta\sigma_{scheme\,1}(y,t) = E_0 \alpha T_0(t_0)\left(-\frac{5}{6} - 3\frac{y}{h}\right)\cdot\left[\frac{\lambda+\chi\cdot\varphi}{1+\chi\cdot\varphi} - \frac{\varphi}{1+\chi\cdot\varphi}\right] \qquad (244)$$

$$\Delta\sigma_{scheme\,2}(y,t) = E_0 \alpha T_0(t_0)\left(-\frac{9}{2}\frac{y}{h}\right)\cdot\left[\frac{\lambda+\chi\cdot\varphi}{1+\chi\cdot\varphi} - \frac{\varphi}{1+\chi\cdot\varphi}\right] \qquad (245)$$

The results obtained in terms of compatibility stresses by means of the Fundamental Theorem are compared in *Figure 43* with the same results obtained by means of the exact formulation.

Furthermore the two solutions in the viscoelastic field are compared in *Figure 44* with the same stresses previously computed in the elastic field.

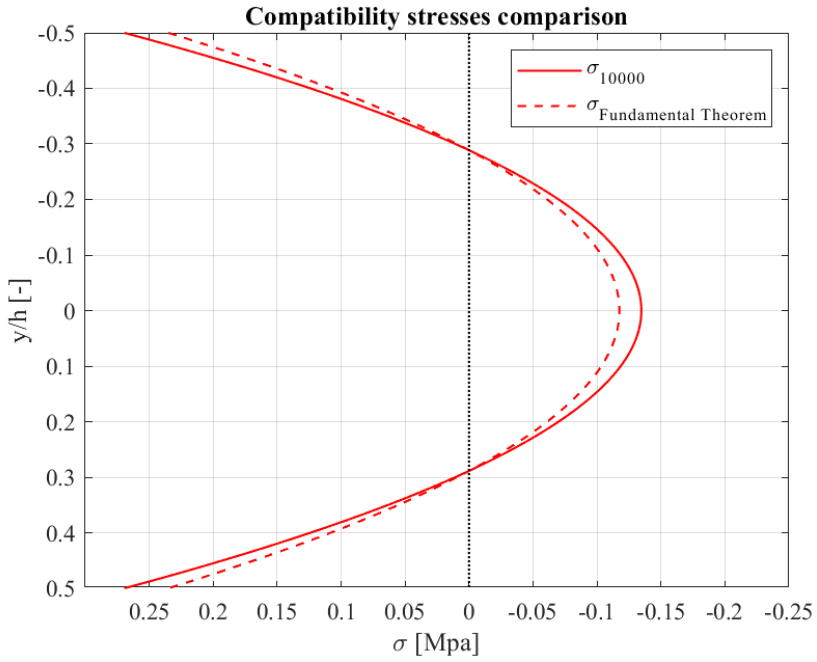

Figure 43 – Comparison of the solutions in the viscoelastic field

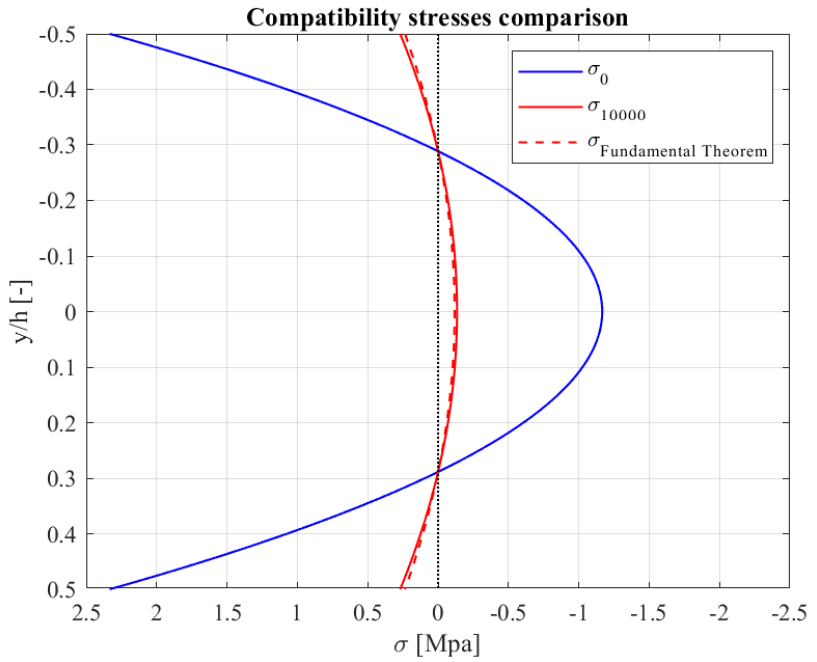

Figure 44 – Compatibility stresses comparison

The same comparisons are reported in *Figure 45* and in *Figure 46* for what concerns the total stresses computed for the problem under examination when the static scheme 1 is considered.

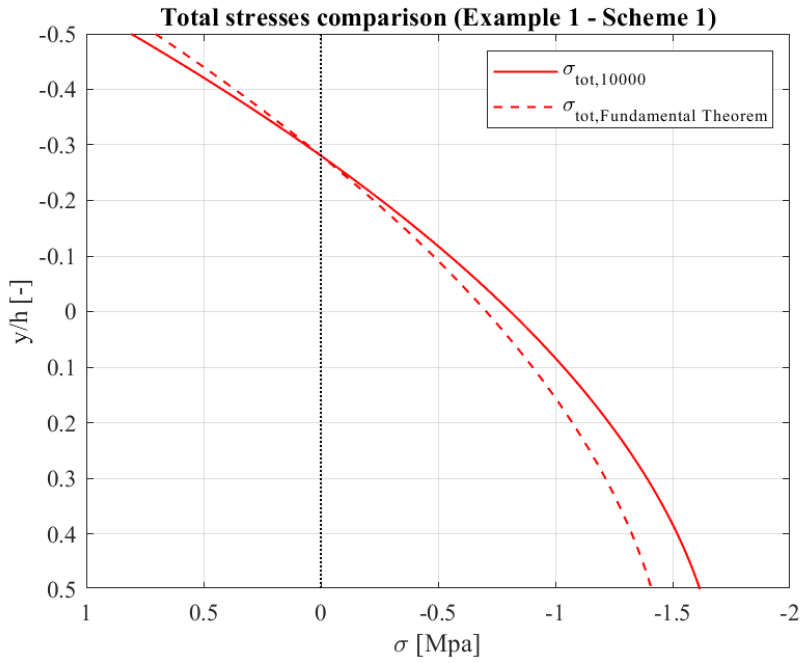

Figure 45 - Comparison of the solutions in the viscoelastic field

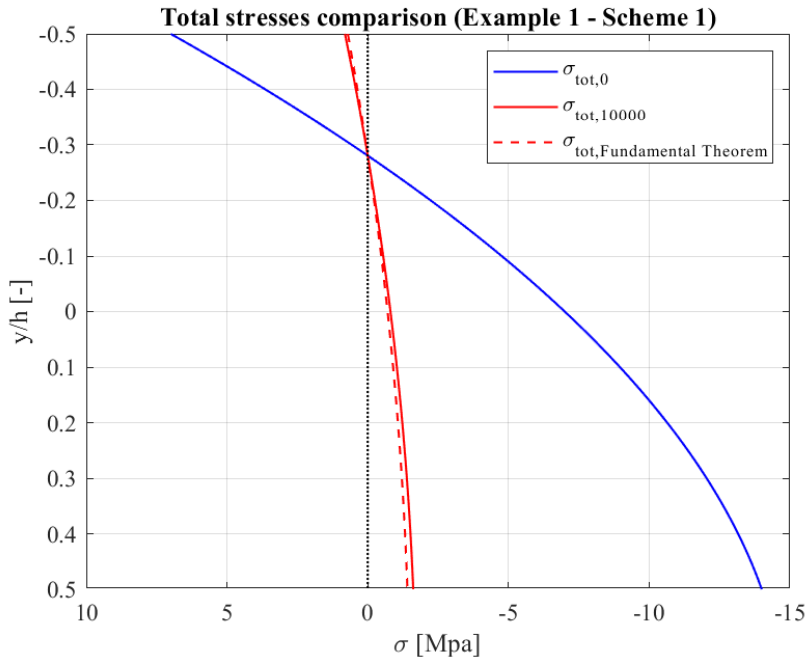

Figure 46 – Total stresses comparison (Static scheme 1)

Finally the same comparisons are also reported in *Figure 47* and in *Figure 48* for what concerns the total stresses computed for the problem under examination when the static scheme 2 is considered.

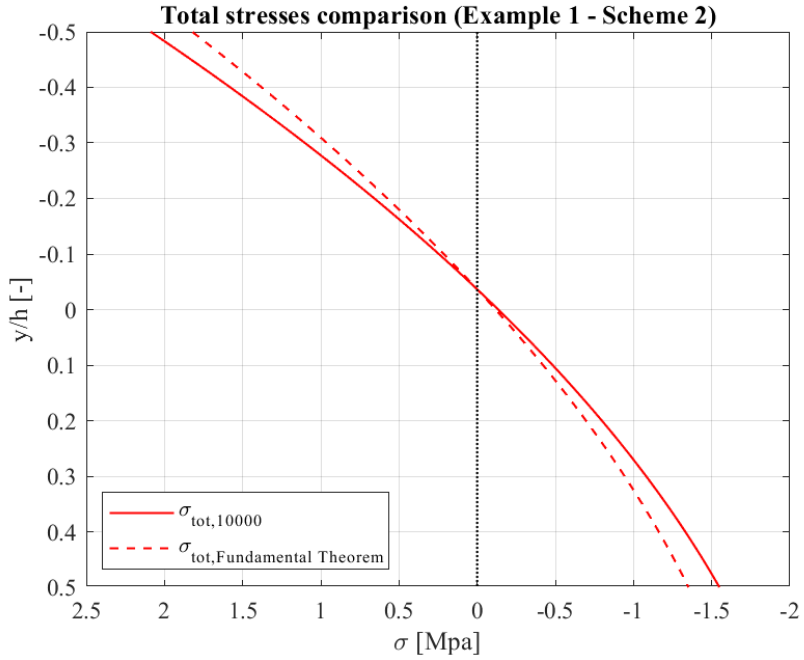

Figure 47 - Comparison of the solutions in the viscoelastic field

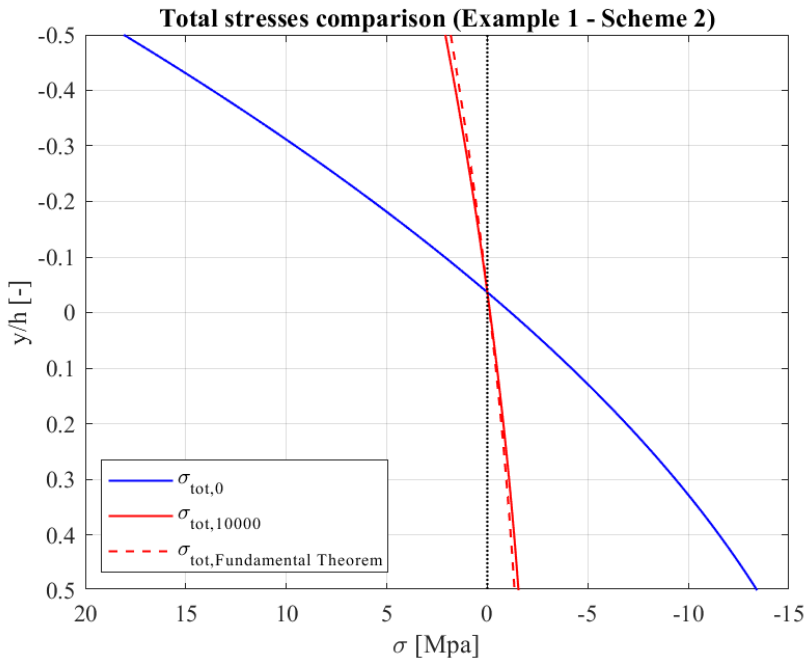

Figure 48 – Total stresses comparison (Static scheme 2)

From the previous figures it is evident the excellent level of approximation provided by the Fundamental Theorem. This aspect together with the simplicity of application of this procedure makes the Fundamental Theorem a particularly convenient tool for the engineering practice.

However it is important to point out that the procedure here presented is valid in the case of homogeneous structures. When dealing instead with structures which are characterized by the presence of elastic restraints, such as the case of the static scheme 4 presented with reference to example 2 in the elastic field, particular care has to be adopted in the analysis. For what concerns the procedure for the computation of the additional stresses $\Delta\sigma$, in fact, it is necessary to compute the redundant restraints reactions according to the following equation:

$$\underline{X} = \underline{X}_1 + \mu(\underline{X}_0 - \underline{X}_{10}) \qquad (246)$$

where $\underline{X}$ is the column vector of the restraints reactions, $\underline{X}_1$ is the elastic solution associated to the external actions applied at time t assuming for concrete the effective modulus E', $\underline{X}_{10}$ is the elastic solution associated to the external actions applied at time t_0 assuming for concrete the effective modulus E' and $\underline{X}_0$ is the initial solution assuming for concrete the elastic modulus $E(t_0)$.

4.4.2 Example of application with temperature distributions constant in time

An example of application of the Fundamental Theorem in the case of a temperature distribution constant in time is here presented. As already pointed out in paragraph 4.2, the application of the Fundamental Theorem in this case provides the exact solution for the considered problem of the computation of stresses due to non-linear temperature distributions in the viscoelastic field. However the solution becomes approximate when for sake of simplicity $\chi = 0{,}8$ is assumed. This choice, in practical applications, is motivated by the fact that the variation in time of the function χ can be in many cases neglected by adopting this value.

The problem considered for this application is the same one analysed in paragraphs 4.4.1 and 4.3.3. The same temperature distribution over the y coordinate is considered even though in this case it is assumed constant in time.

For sake of simplicity the computations reported in the following are performed by considering a value of the creep coefficient equal to 2,5. Having adopted $\chi = 0{,}8$ and $\varphi = 2{,}5$ the effective modulus E' is given by:

$$E' = \frac{E(t_0)}{1 + \chi\varphi} = \frac{E(t_0)}{3} \qquad (247)$$

Since the temperature distribution is constant in time, the Fundamental Theorem is applied according to the simplified expression (202) in order to compute the compatibility stresses and the additional stresses due to the redundant restraints in the viscoelastic field.

In particular, applying equation (202) for the computation of the compatibility stresses, the stresses σ_0 have been considered equal to the compatibility stresses previously computed with reference to the elastic field in chapter 3:

$$\sigma_0 = E_0 \alpha T_0 \left(2\frac{y^2}{h^2} - \frac{1}{6} \right) \quad (248)$$

while the stresses σ_1 are given by the same stresses computed adopting the effective modulus E':

$$\sigma_1 = E' \alpha T_0 \left(2\frac{y^2}{h^2} - \frac{1}{6} \right) \quad (249)$$

Proceeding in an analogous way, for the computation of the additional stresses due to redundant restraints in the viscoelastic field it is considered:

$$\Delta\sigma_{0,scheme\ 1} = E_0 \alpha T_0 \left(-\frac{5}{6} - 3\frac{y}{h} \right) \quad (250)$$

$$\Delta\sigma_{0,scheme\ 2} = E_0 \alpha T_0(t_0) \left(-\frac{9}{2}\frac{y}{h} \right) \quad (251)$$

$$\Delta\sigma_{1,scheme\ 1} = E' \alpha T_0 \left(-\frac{5}{6} - 3\frac{y}{h} \right) \quad (252)$$

$$\Delta\sigma_{1,scheme\ 2} = E' \alpha T_0(t_0) \left(-\frac{9}{2}\frac{y}{h} \right) \quad (253)$$

The compatibility stresses computed in the viscoelastic field by means of the procedure here described, are compared with the same stresses computed in the elastic field in *Figure 49* where the stresses are normalized with respect to $E_0 \alpha T_0$ and the y coordinate is normalized with respect to the depth h of the cross section.

The total stresses computed in the viscoelastic field by means of the procedure here described, are also represented in non-dimensional form in *Figure 50* and in *Figure 51* in which they are compared with the same stresses computed in the elastic field.

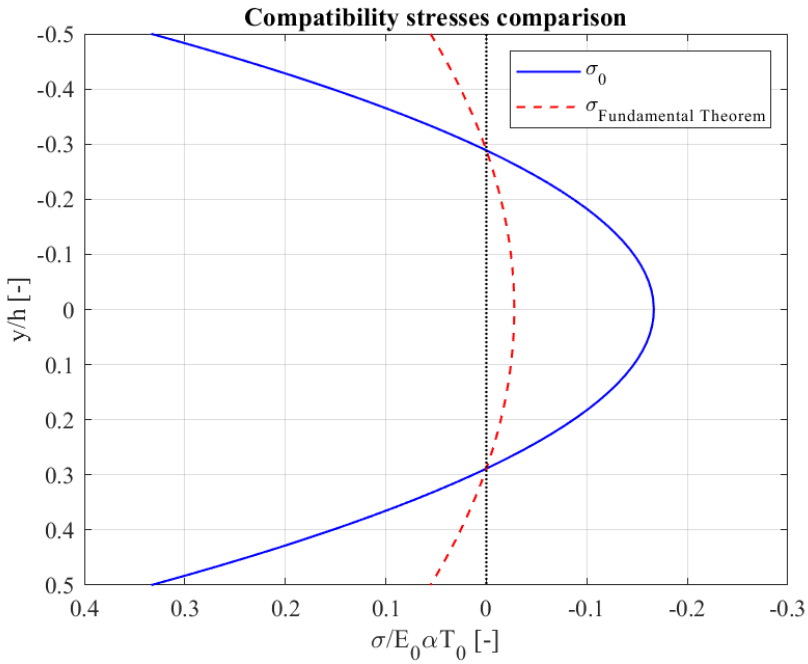

Figure 49 - Compatibility stresses comparison

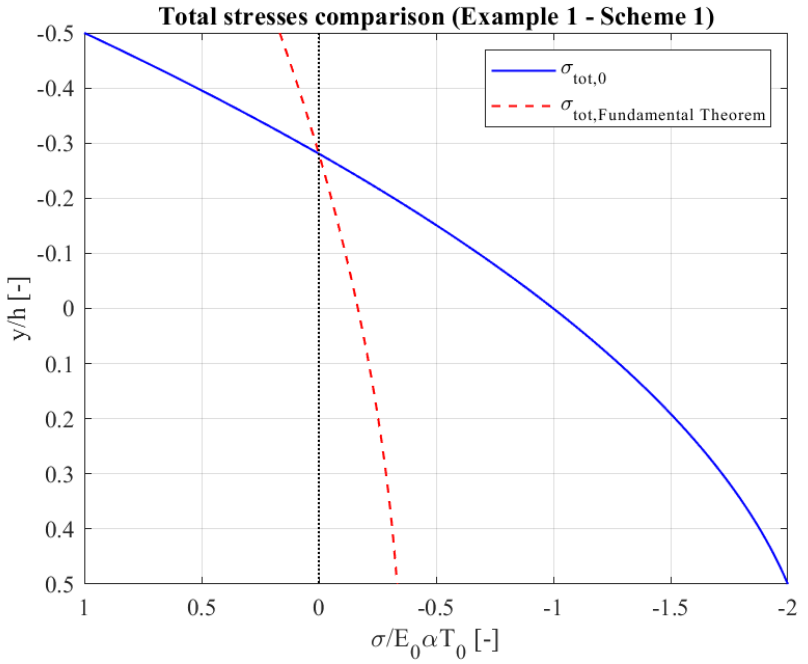

Figure 50 – Total stresses comparison (Static scheme 1)

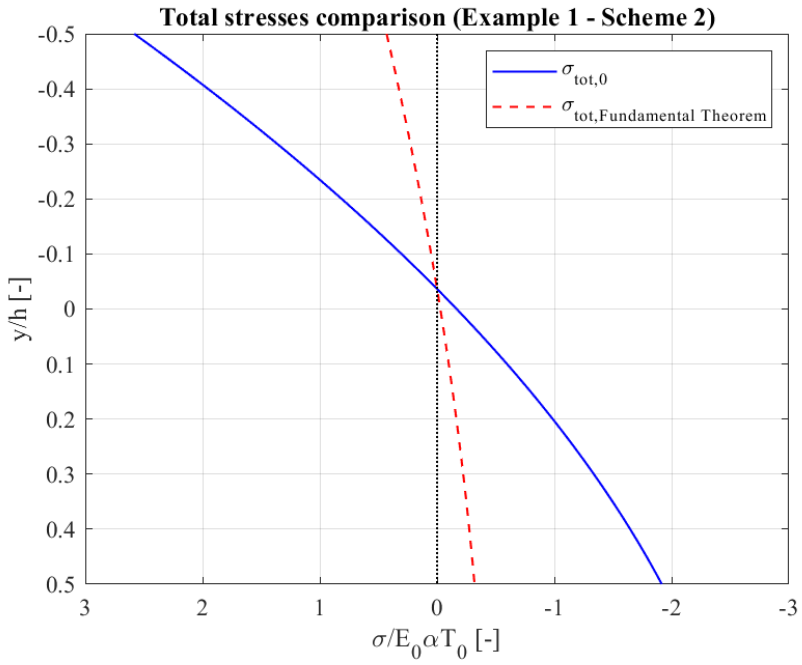

Figure 51 - Total stresses comparison (Static scheme 2)

5 VISCOELASTIC FIELD AND SINUSOIDAL TEMPERATURE VARIATIONS

5.1 Introduction

Since the long term analysis requires the presence of permanent or quasi-permanent actions, in defining the time variation of the temperature function it is considered an average annual variation as the daily fluctuations do not produce significative delayed phenomena. On the basis of what has been discussed in chapter 2 with reference to the thermal actions on structures, in order to do this, it is possible to consider a sinusoidal time function which reproduces with sufficient precision the seasonal variation of climatic actions.

The description of the different sinusoidal temperature variations which can be considered, depending on the season in which the casting of the structure takes place, is provided in paragraph 5.2.

Since, as discussed in chapter 4, the Fundamental Theorem is based on the simplifying hypothesis that the deformation is a linear function in the creep coefficient $\varphi(t, t_0)$ it cannot be applied when sinusoidal time functions of the temperature are considered. In fact, because of the sinusoidal variation in time of the temperature, imposed deformations due to thermal actions strongly differ from a linear function in $\varphi(t, t_0)$. Therefore, for the considered problem of the long-term analysis of the stresses arising in bridge structures due to non linear temperature variations, only the exact formulation should be adopted. However also for what concerns the numerical solution of the Volterra Integral Equation associated to the exact formulation, the fact of dealing with sinusoidal time functions introduces some complications which will be addressed in paragraph 5.3 in order to extend the formulation to the solution of the considered problems.

Finally in paragraph 5.4 the procedure discussed in paragraph 5.3 will be applied in order to show the variation in time of the stresses arising in presence of non-linear temperature distributions characterized by a sinusoidal variation in time.

5.2 Sinusoidal temperature variations

The sinusoidal function which can be used to describe the temperature variations associated to the different climatic conditions over the year has been determined on the basis of the work done by Mola [26] and is given by the following expression:

$$T(t) = (-1)^h \cdot \Delta T \cdot \left\{ K + sin\left[2\pi \cdot \left(\frac{(t - t_0)}{T_a} + \phi \right) \right] \right\} \qquad (254)$$

where:

- ΔT = semi-amplitude of the sinusoidal function $[°C]$
- K = constant defining the position on the ordinate axis
- ϕ = phase constant
- T_a = period (assumed equal to one year)
- t_0 = initial time
- $h = 0\,;1$ = sign constant

Making reference to equation (254) it is possible to consider four different scenarios for the period of the year in which the casting of the structure takes place: Spring, Summer, Autumn and Winter.

In particular, for the case of casting in Spring, the parameters of equation (254) assume the following values:

- $h = 0$
- $K = 0$
- $\phi = 0$

therefore equation (254) becomes:

$$T(t) = \Delta T \cdot \ sin\left[2\pi \cdot \frac{(t - t_0)}{T_a}\right] \qquad (\ 255\ )$$

whose graph, assuming $\Delta T = 20°C$ and $t_0 = 28$ days, is reported in *Figure 52* over a time span of 2000 days and in *Figure 53* over the period of one year.

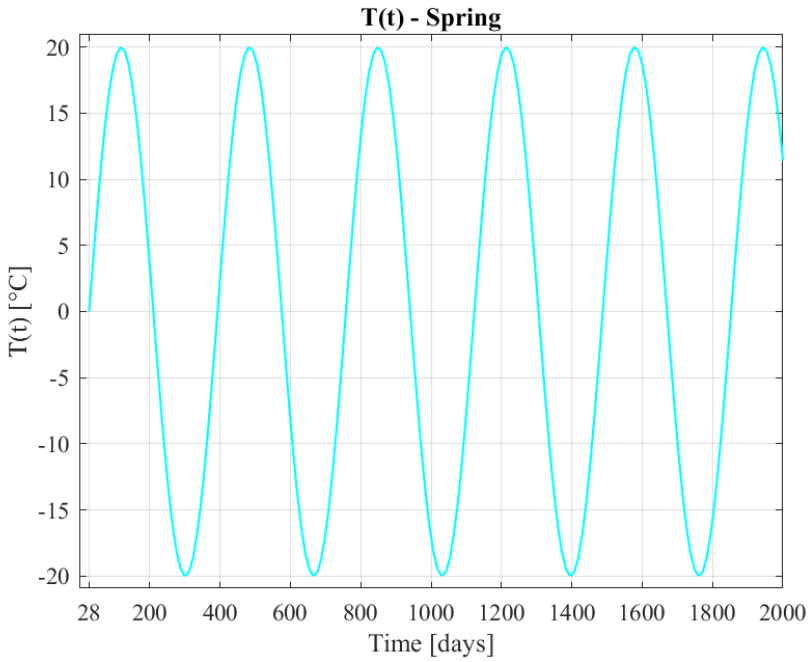

Figure 52 – Temperature function (casting of the structure in Spring)

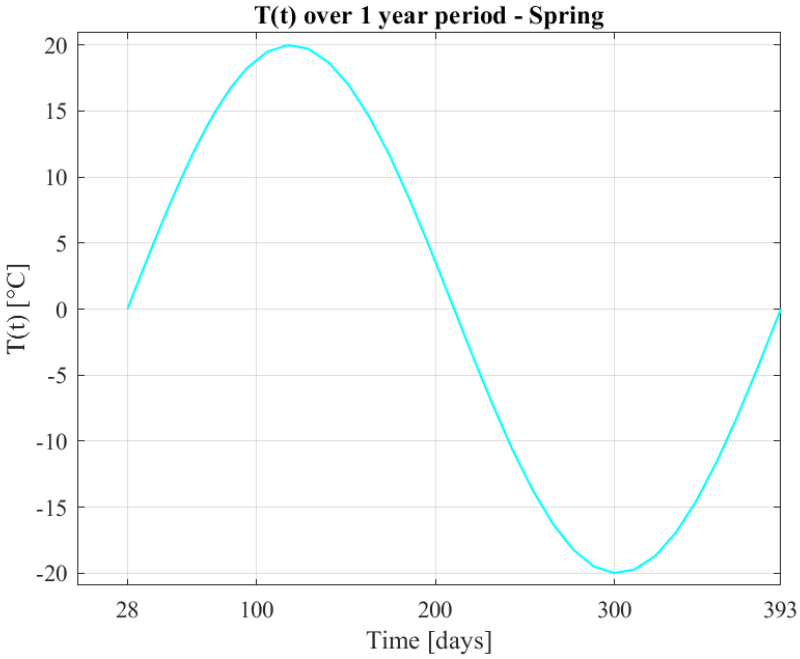

Figure 53 - Temperature function over the period of 1 year (casting of the structure in Spring)

For the case of casting in Autumn the parameters of equation (254) assume the following values:

- $h = 1$
- $K = 0$
- $\phi = 0$

therefore equation (254) becomes:

$$T(t) = -\Delta T \cdot \ sin\left[2\pi \cdot \frac{(t - t_0)}{T_a}\right] \qquad (256)$$

Comparing equation (256) and equation (255) it is evident that the temperature function in Autumn has the same values as the one in Spring but with opposite sign. This aspect leads to the arising of stress states which are identical but opposite in sign in these two situations as it will be clearly shown in the example of paragraph 5.4.

The graph of $T(t)$ for the case of casting in Autumn, assuming $\Delta T = 20°C$ and $t_0 = 28$ days, is reported in *Figure 54* over a time span of 2000 days and in *Figure 55* over the period of one year.

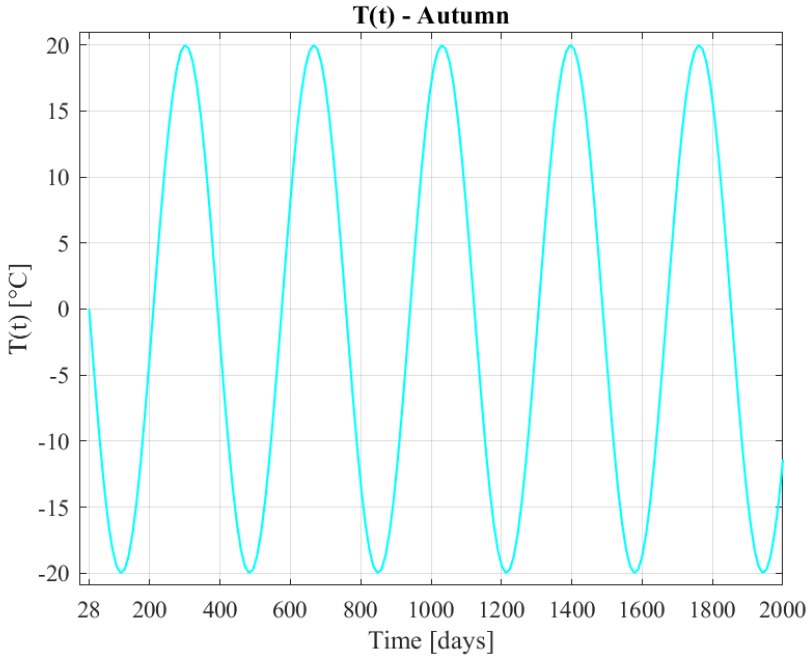

Figure 54 – Temperature function (casting of the structure in Autumn)

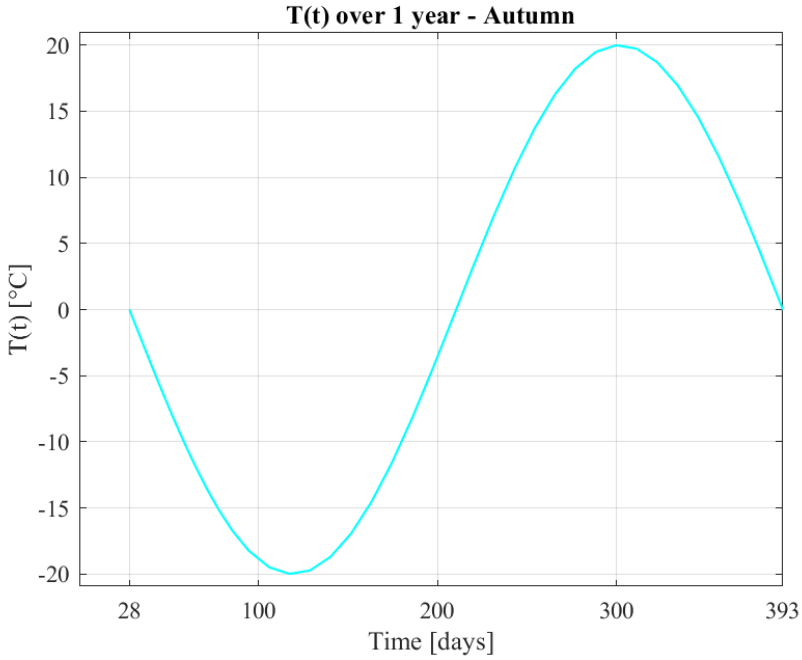

Figure 55 - Temperature function over the period of 1 year (casting of the structure in Autumn)

For the case of casting in Winter the parameters of the equation (254) assume the following values:

- $h = 0$
- $K = 1$
- $\phi = -0{,}25$

therefore equation (254) becomes:

$$T(t) = \Delta T \cdot \left\{1 + sin\left[2\pi \cdot \left(\frac{(t - t_0)}{T_a} - \frac{1}{4}\right)\right]\right\} \qquad (257)$$

whose graph, assuming $\Delta T = 20°C$ and $t_0 = 28$ days, is reported in *Figure 56* over a time span of 2000 days and in *Figure 57* over the period of one year. From these figures it is possible to appreciate that the temperature function assumes only values grater or equal to zero, differently from what happens in the case of casting in Spring or Autumn when the temperature function oscillates assuming values which are both positive and negative.

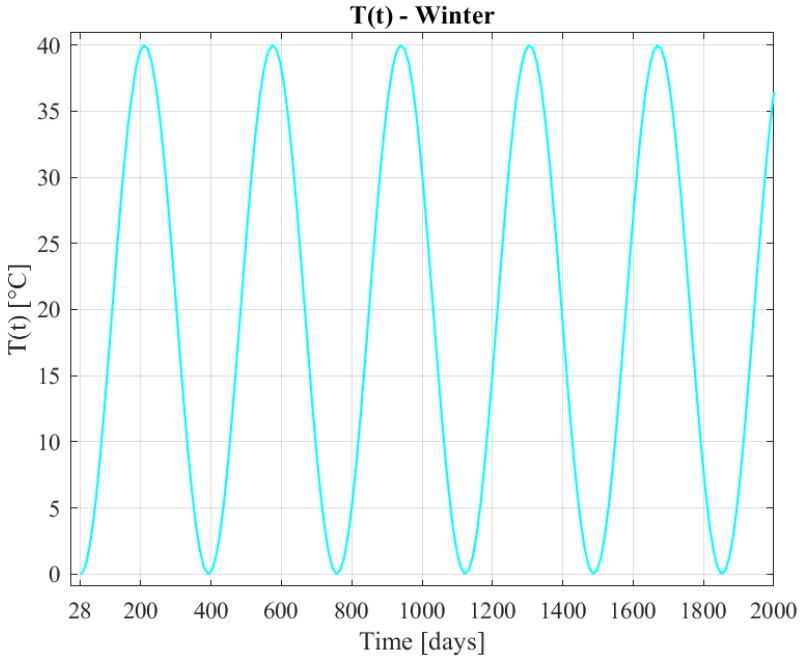

Figure 56 – Temperature function (casting of the structure in Winter)

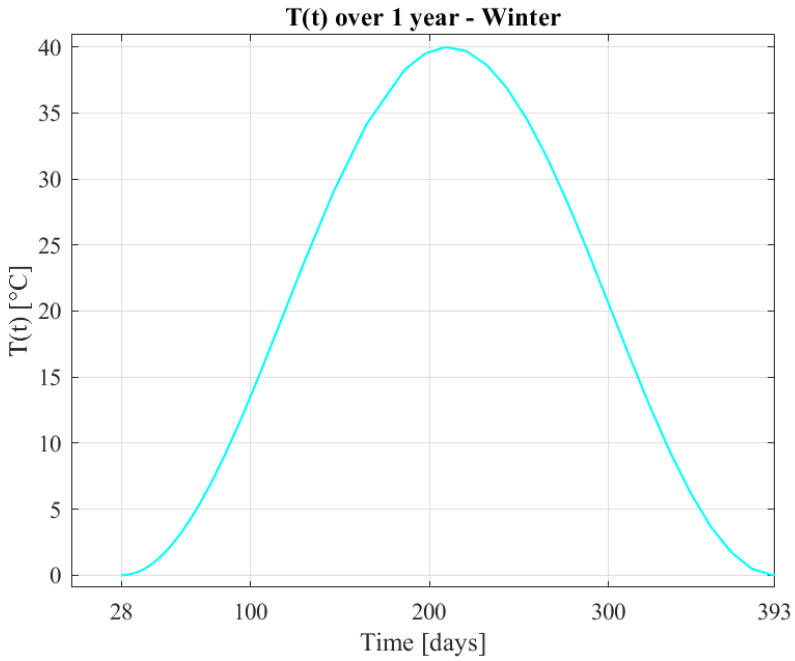

Figure 57 - Temperature function over the period of 1 year (casting of the structure in Winter)

Finally, for the case of casting in Summer the parameters of the equation (254) assume the following values:

- $h = 1$
- $K = 1$
- $\phi = -0{,}25$

therefore equation (254) becomes:

$$T(t) = -\Delta T \cdot \left\{1 + sin\left[2\pi \cdot \left(\frac{(t - t_0)}{T_a} - \frac{1}{4}\right)\right]\right\} \qquad (\ 258\ )$$

Comparing equation (258) and equation (257) it is evident that the temperature function in Summer has the same values as the one in Winter but with opposite sign. Also in this case, as happens for the case of Spring and Autumn, this aspect leads to the arising of stress states which are identical but opposite in sign.

The graph of $T(t)$ for the case of casting in Summer, assuming $\Delta T = 20°C$ and $t_0 = 28$ days, is reported in *Figure 58* over a time span of 2000 days and in *Figure 59* over the period of one year.

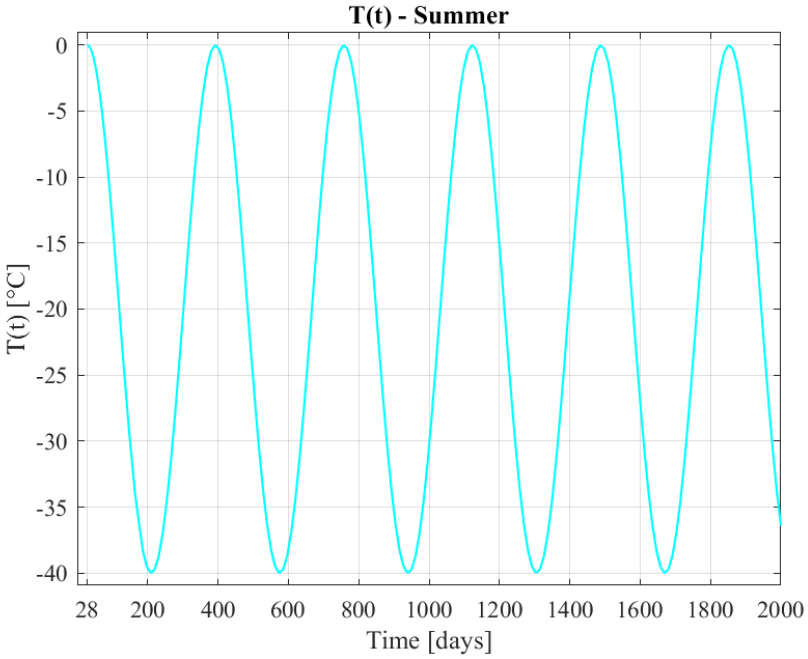

Figure 58 – Temperature function (casting of the structure in Summer)

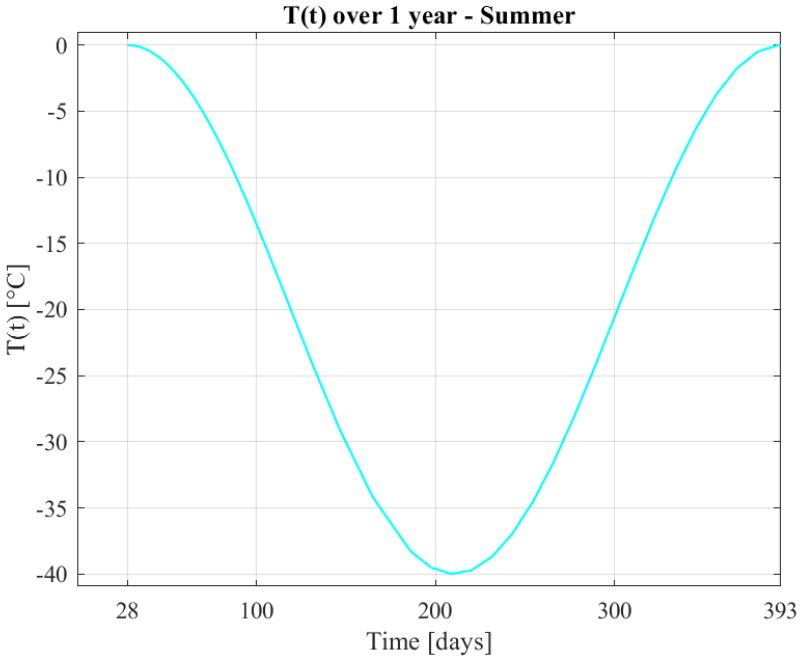

Figure 59 - Temperature function over the period of 1 year (casting of the structure in Summer)

5.3 Numerical solution of the Volterra Integral Equation

In chapter 4 the procedure for the numerical solution of the Volterra Integral Equation has been discussed on the basis of the suggestions provided by the CEB Bulletin 142-142bis [25] when usual strain histories are considered. In that case, the adoption of increasing time steps leads to an adequate level of accuracy associated with a minimum of computation time but, as already pointed out, the magnitude of the time step amplitudes so obtained is not suitable for the integration procedure when dealing with the strain histories associated to the periodic time variation of temperature distributions. It is in fact important to observe that, due to the sinusoidal temperature variation, the time step discretization can be assumed to be of logarithmic type, as the one suggested by the CEB Bulletin, just with reference to the first half-period or to the first quarter of period (depending on the season in which the casting of the structure takes place) when the temperature is monotonically increasing or decreasing. After that time interval, the time steps should be properly defined in order to describe with sufficient accuracy the cyclic variation in time of the temperature. This goal can be achieved by means of a constant time step which has produced reliable results.

On the basis of the considerations above reported, the implemented MATLAB code for the numerical solution of the Volterra Integral Equation has been properly modified adopting the following scheme for the time step definition:

- Casting of the structure in Spring or Autumn

  For $t_0 \leq t \leq T_a/4$ the time step is defined according to the CEB Bulletin:

  $$\frac{(t_k - t_0)}{(t_{k-1} - t_0)} = 1{,}15$$

  $$\Delta t_2 = t_2 - t_1 = 0{,}05\ days \qquad (259)$$

  For $t \geq T_a/4$ the time step is assumed constant:

  $$\Delta t = \frac{T_a}{32}$$

  The amplitude of the time step in days with respect to the number of the considered step is reported in *Figure 60*, which is obtained considering a time span for the integration equal to 2000 days. From this figure it is well evident the constancy in the amplitude of the time steps which are adopted after the first quarter of period.

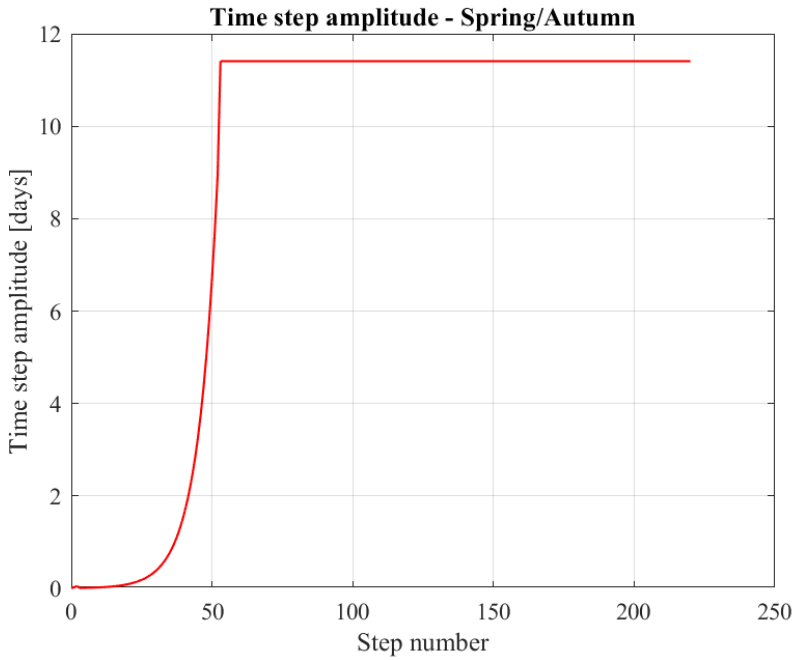

Figure 60 – Time step amplitude (casting of the structure in Spring or Autumn)

- Casting of the structure in Summer or Winter

For $t_0 \leq t \leq T_a/2$

$$\frac{(t_k - t_0)}{(t_{k-1} - t_0)} = 1.15$$

$$\Delta t_2 = t_2 - t_1 = 0.05\ days \tag{260}$$

For $t \geq T_a/2$

$$\Delta t = \frac{T_a}{32}$$

The amplitude of the time step in days with respect to the number of the considered step is reported in *Figure 61*, which is obtained considering a time span for the integration equal to 2000 days. From this figure it is well evident the constancy in the amplitude of the time steps which are adopted after the first half-period.

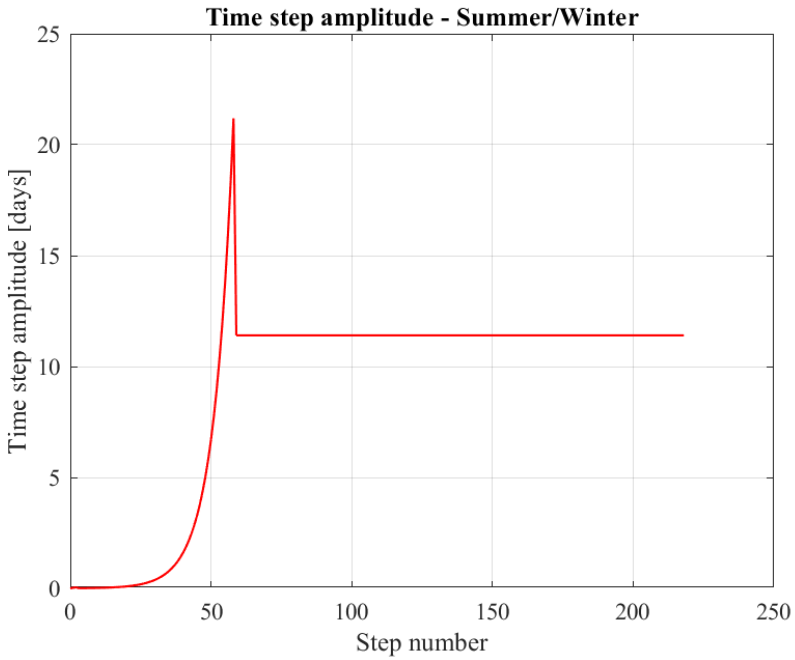

Figure 61 – Time step amplitude (casting of the structure in Summer or Winter)

5.4 Example of application

An example of application of the MATLAB code, opportunely modified according to what has been presented in the previous paragraph is here provided. In particular the problem presented in paragraph 3.4.1 with reference to the elastic field, then analysed in chapter 4 in the viscoelastic field considering simple temperature variations in time, is here presented in the case of sinusoidal temperature variations.

Since the compatibility stresses distribution as well as the additional stresses distribution due to the redundant restraints, which arise in bridge structures due to non-linear temperature variations, have been deeply studied in chapter 3 and their reduction due to the long-term behaviour of concrete has been shown in chapter 4, in the present chapter the results of the performed analysis will be provided trying to highlight the evolution in time of those stresses distributions when sinusoidal temperature variations are considered. With this aim, rather than showing the stresses distributions diagrams over the depth of the section, the time variation of the stres at the level of a specific fiber of the cross section will be shown. In particular it will be considered just the variation in time of the compatibility stres at the level of the bottom fiber of the section. This is justified by the fact that for what concerns the additional stresses due to the redundant restraints or the total stresses the only difference would be in their entity as they are affected by the same kind of variability in time.

The function defining the temperature distribution over the depth of the cross section for the considered problem is given by:

$$T(y) = T_0\left(-2\frac{y^2}{h^2} + 3\frac{y}{h} + 1\right) \qquad (261)$$

In order to consider the variability in time of this distribution, it has been assumed a parameter T_0 which varies in time according to the various expressions found in paragraph 5.2 for the different scenarios associated to the period of the year in which the casting of the structure takes place, assuming $\Delta T = 20°C$.

Moreover for what concerns the data assumed for the present example, it has been considered:

- $C40/50$ concrete
- h = 200 mm (notional size of the member)
- RH = 0,7
- t_0 = 28 days
- $\alpha = 10^{-5}\ °C^{-1}$

where it has been assumed for the value of the notional size of the member an admissible, even though arbitrary, value as the cross section dimensions have been generically defined as b and h.

The results obtained in terms of compatibility stresses at the level of the bottom fiber of the section, considering the four scenarios previously presented, are shown in the following figures.

In particular for each of the four seasons in which the casting of the structure can take place, the variability in time of the stress computed by means of the implemented MATLAB code in the viscoelastic field is reported in a first graph and then it is compared in a second graph with the elastic solution, computed taking into account the variability in time of the elastic modulus. For what concerns the variability in time of the elastic modulus of concrete, it has been considered the formulation provided by the CEB-FIP Model Code 1990 [22].

The first situation analysed is the one associated to the casting in Spring and the relative results are represented in *Figure 62* and in *Figure 63.* In the first graph it is evident the decreasing in time of the peak values assumed by the stresses. Moreover by comparing the viscoelastic solution with the elastic one in the second graph, it is clear the reduction of the stresses computed in the viscoelastic field with respect to the ones computed in the elastic field. Considering *Figure 63* it is also possible to appreciate the effect of the variability of the elastic modulus of concrete which leads to a moderate increase in time of the peak values of the elastic solution.

By comparing the results associated to the casting in Spring with the ones of *Figure 64* and *Figure 65,* relative to the casting in Autumn, it is evident that the stresses which arise in these two situations are identical but opposite in sign.

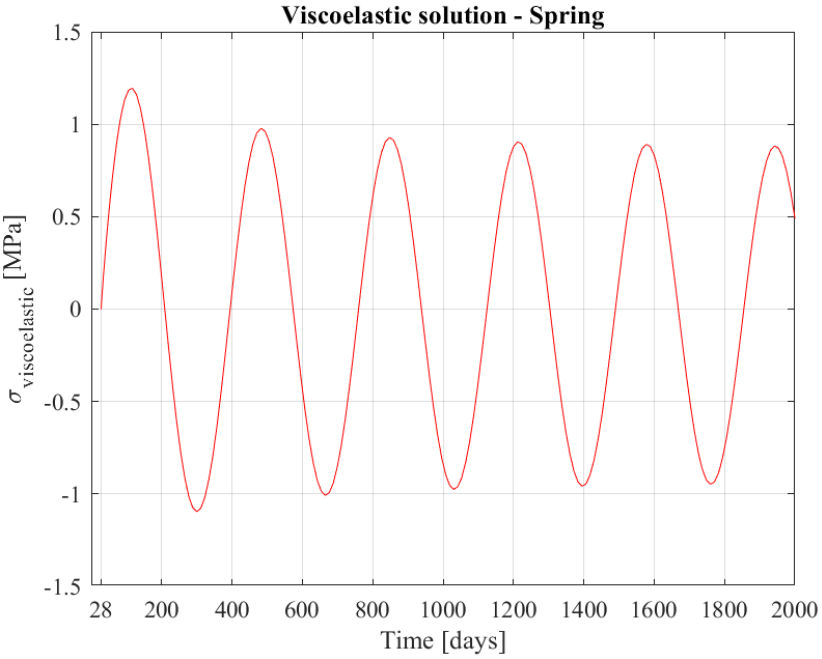

Figure 62 - Variation in time of the compatibility stress
(casting of the structure in Spring)

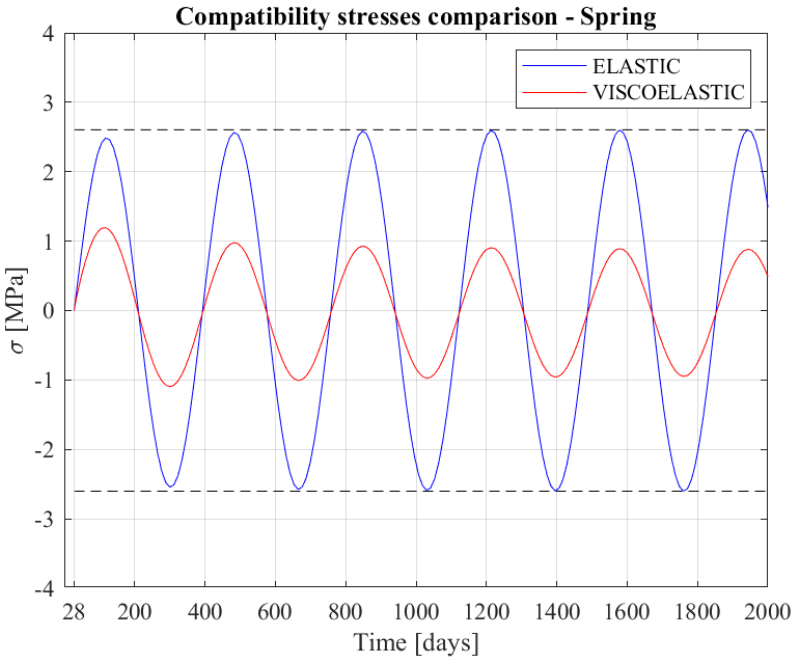

Figure 63 - Comparison of elastic and viscoelastic solutions
(casting of the structure in Spring)

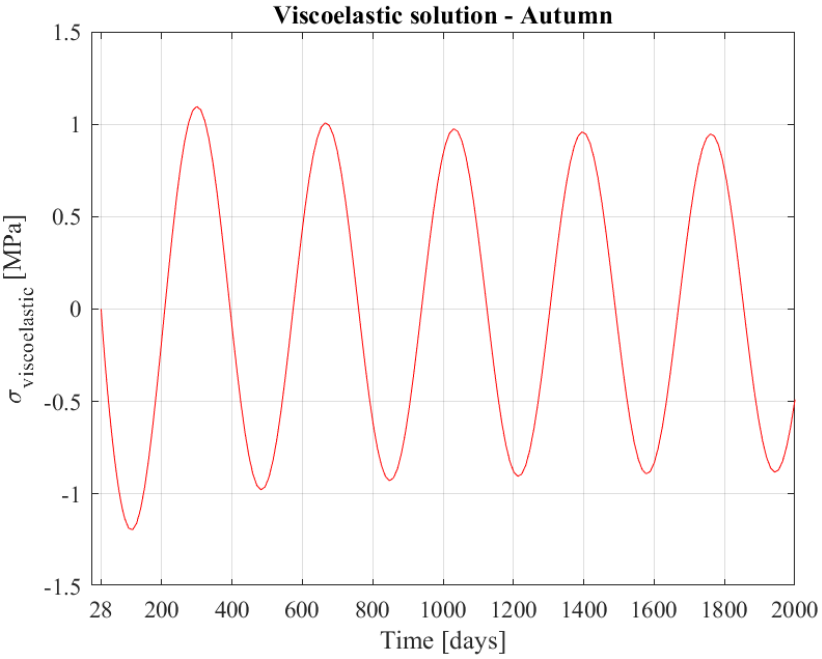

Figure 64 - Variation in time of the compatibility stress (casting of the structure in Autumn)

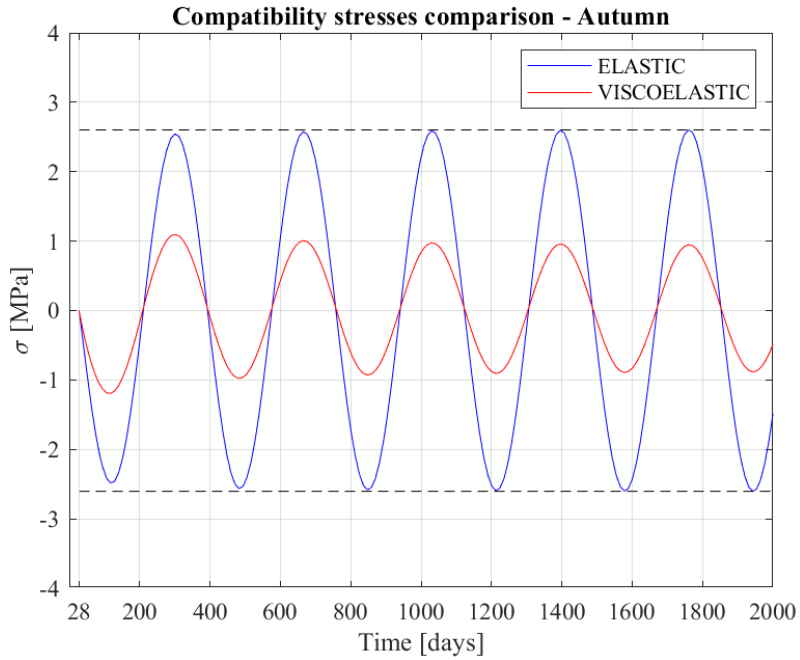

Figure 65 - Comparison of elastic and viscoelastic solutions (casting of the structure in Autumn)

The results obtained considering the case of casting of the structure in Winter are represented in *Figure 66* and *Figure 67*.

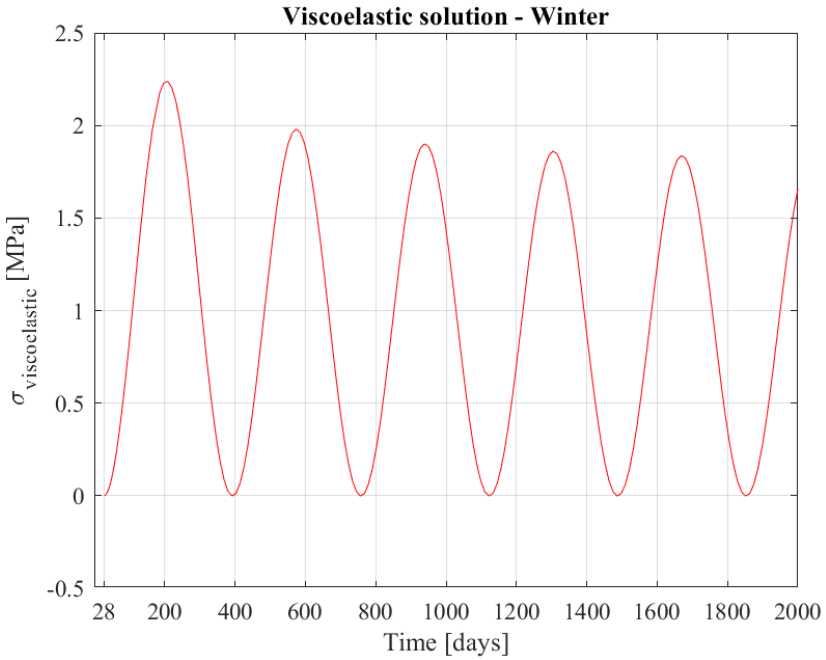

Figure 66 - Variation in time of the compatibility stress (casting of the structure in Winter)

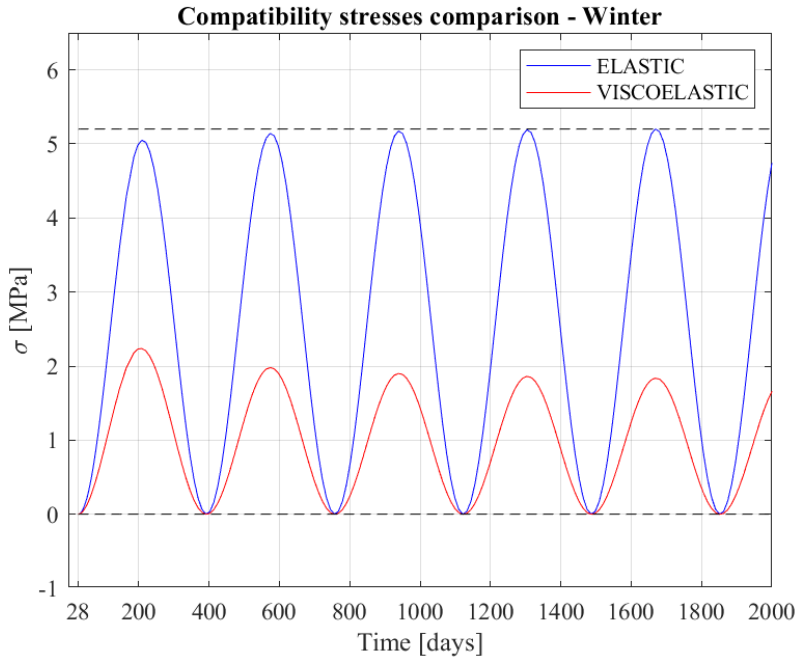

Figure 67 - Comparison of elastic and viscoelastic solutions (casting of the structure in Winter)

The results obtained considering the case of casting of the structure in Summer are represented in *Figure 68* and *Figure 69*.

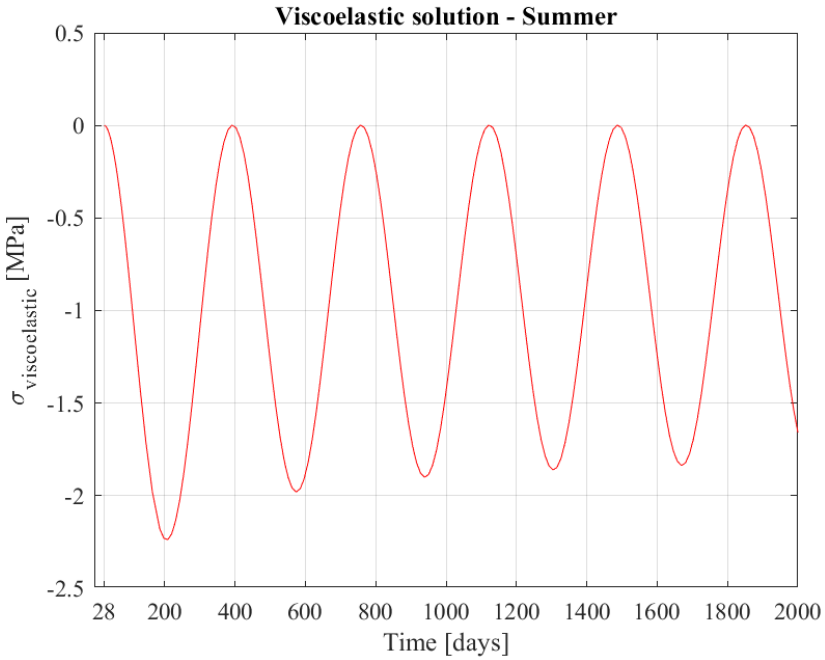

Figure 68 - Variation in time of the compatibility stress (casting of the structure in Summer)

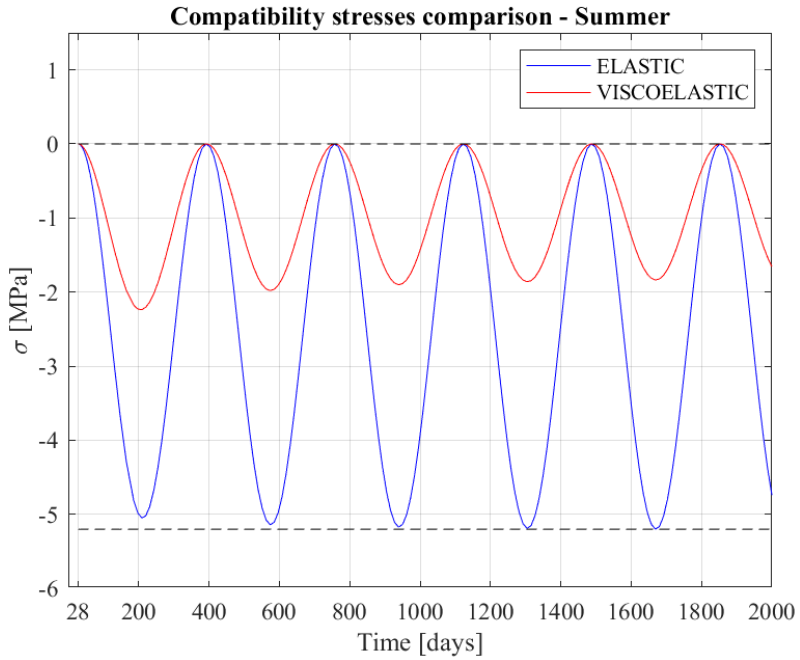

Figure 69 - Comparison of elastic and viscoelastic solutions (casting of the structure in Summer)

Analogous observations to the ones made about the results obtained for the cases of casting in Spring and in Autumn can be made with reference to the results associated to Winter and Summer. Moreover, as already anticipated, since the temperature function in Summer has the same values as the ones in Winter but with opposite sign, also the stresses which arise in these two situations are identical but opposite in sign.

Finally it is possible to observe that the stresses associated to the extreme seasons are almost the double the ones associated to the middle seasons.

6 CASE STUDIES

6.1 Introduction

In the present chapter two case studies regarding the evaluation of the long-term response of two real bridge structures subject to thermal actions are presented. Even though the rigorous analysis in the viscoelastic field of this kind of structures should be performed considering sinusoidal temperature variations, as discussed in chapter 5, national and international code prescriptions do not provide temperature gradients varying in time. For the case studies here presented non-linear temperature distributions constant in time are therefore considered. In this framework the Fundamental Theorem can be applied and it has been adopted for the analyses of the case studies as a very convenient tool to be used in the engineering practice to which is associate an excellent level of approximation, as demonstrated by the results presented in chapter 4. As a matter of fact, as already discussed, when constant temperature distributions are considered the Fundamental Theorem provides the exact solution for the problem of the computation of stresses due to non-linear temperature distributions in the viscoelastic field. However, in order to make the procedure immediately feasible for practical applications, the solution becomes approximate when for sake of simplicity the time variation of $\chi(t, t_0)$ is neglected assuming the constant value $\chi(t, t_0) = 0{,}8$.

The first case study, presented in paragraph 6.2, consists in a multi-span continuous box girder bridge which has been analysed in presence of the non-linear temperature distribution suggested by the Eurocode 1 [11] in the framework of the complex approach described in paragraph 2.5. Since the considered bridge is a redundant structure, it has been necessary to consider the compatibility stresses due to non-linear temperature distributions as well as the additional stresses due to the redundant restraints, allowing to highlight both of these aspects of the problem with reference to a real bridge structure.

Moreover, a second case study, presented in paragraph 6.3, consists in a bridge characterized by a composite deck and by a simply supported static scheme. The analysis of this structure has the aim of showing the extension of the concepts previously presented, in particular in chapter 4, to the case of non-homogeneous structures with reference to a real bridge structure.

6.2 Case study 1: Multi-span continuous box girder bridge

6.2.1 Description of the structure

The structure analysed is represented in *Figure 70* and consists in a multi-span continuous box girder bridge. The shape and the dimensions (in cm) of the cross section are reported in *Figure 71*.

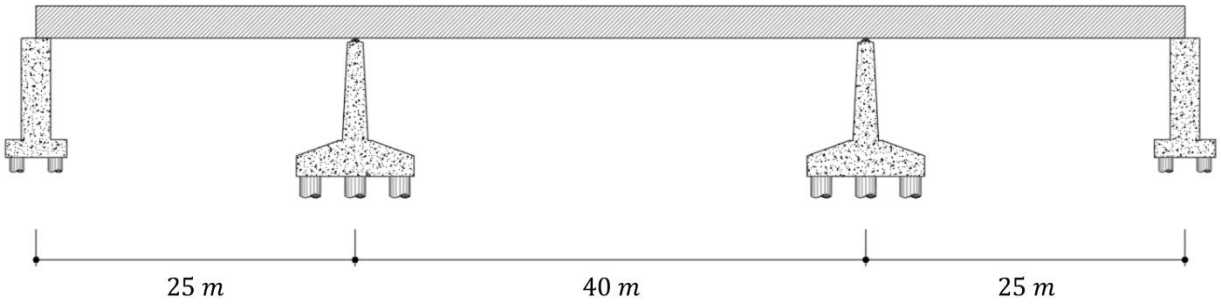

Figure 70 – Case study 1: Multi-span continuous box girder bridge

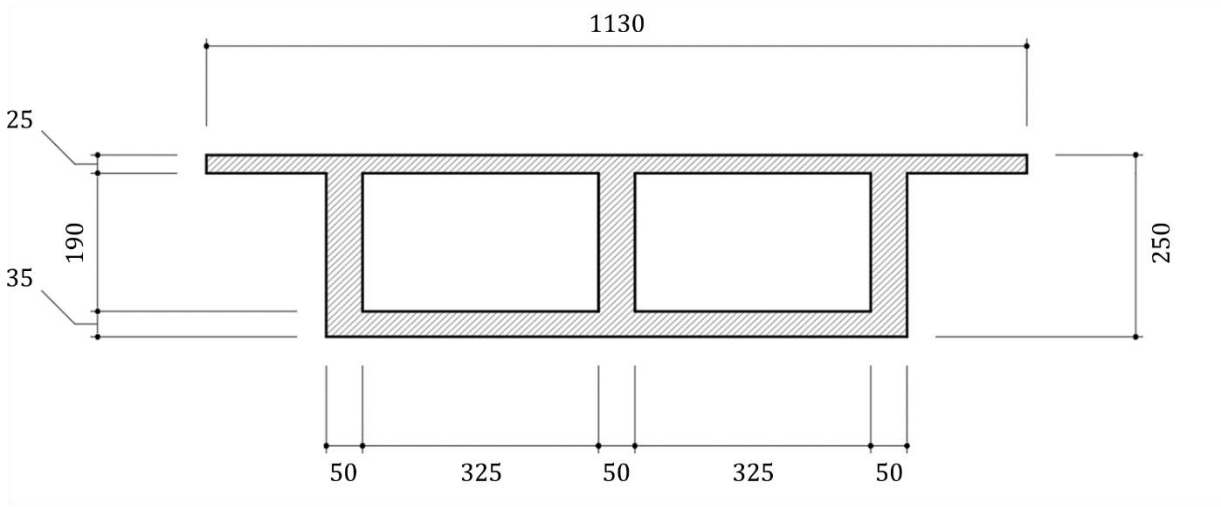

Figure 71 – Cross section shape and dimensions (in cm)

For what concerns the characteristics of the material for the bridge deck a C40/50 concrete is adopted, which is endowed with a characteristic cylindrical strength of 40 MPa and with an elastic modulus at 28 days E_0 of 35000 MPa.

Moreover it is important to point out that the cross section can be considered homogeneous since the quantity of reinforcing steel is very small if compared with the amount of concrete constituting the section itself. In addition to this, the coefficient of thermal expansion α for concrete, equal to

$10^{-5}\ °C^{-1}$, is of the same order of magnitude as the one associated to steel and therefore the cross section can be considered homogeneous also from this point of view.

The non-linear temperature distribution which has been considered for the analysis of the structure is the one suggested for the case of heating by Eurocode 1 [11] in the framework of the complex approach described in paragraph 2.5, which is based on the method of the British regulations. In particular the diagram of the temperature distribution is the one reported in the following figure:

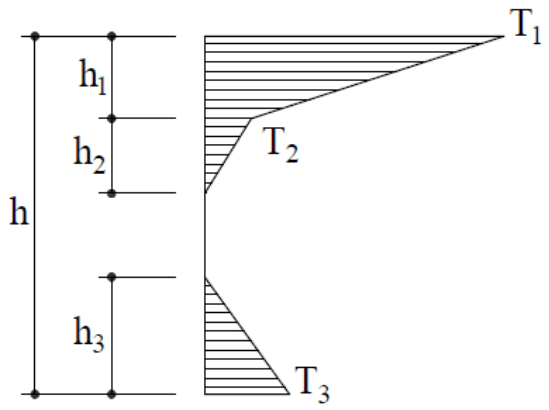

Figure 72 – Eurocode 1 non-linear temperature distribution (heating)

where:

- h is the depth of the cross section
- $h_1 = 0{,}3h$ but $\leq 0{,}15$ m
- $h_2 = 0{,}3h$ but $\geq 0{,}10$ m and $\leq 0{,}25$ m
- $h_3 = 0{,}3h$ but $\leq (0{,}10\ \text{m} + \text{surfacing depth in meters})$

For the present case study the surfacing depth has been considered equal to 100 mm and, since $h = 2{,}5$ m, the values of h_1,h_2 and h_3 to be considered are:

- $h_1 = 0{,}15$ m
- $h_2 = 0{,}25$ m
- $h_3 = 0{,}20$ m

Moreover the values provided by the Eurocode for T_1,T_2 and T_3 depend on the depth h of the cross section and in this case, since $h \geq 0{,}8$ m, it is considered:

- $T_1 = 13°C$
- $T_2 = 3°C$
- $T_3 = 2{,}5°C$

6.2.2 Analysis of the structure in the elastic field

In order to correctly apply the procedure presented in chapter 3 for the analysis of the structure subject to a non-linear temperature distribution over the depth of the cross section, it is necessary to fix the origin of the principal reference system in the centroid of the section itself. The first step to be performed is therefore the computation of the position of the centroid which, for the cross section of the present case study, is located in correspondence of the vertical symmetry line of the cross section itself, at a distance $y_g = 121{,}3348\ cm$ from the extrados of the girder.

The moment of inertia with respect to the x axis is:

$$I_x = 770755249{,}8\ cm^4$$

while the area of the cross section is:

$$A = 84750\ cm^2$$

The function of the y coordinate, whose origin is fixed in the centroid of the cross section, describing the non-linear temperature distribution over the depth of the section, is determined on the basis of the values reported in paragraph 6.2.1 and is given by:

For $-y_g \leq y \leq -y_g + h_1$

$$T(y) = -67{,}8899 - 2/3\ y \qquad (262)$$

For $-y_g + h_1 \leq y \leq -y_g + h_1 + h_2$

$$T(y) = -9{,}760176 - 0{,}12 \cdot y \qquad (263)$$

For $-y_g + h_1 + h_2 \leq y \leq -y_g + h - h_3$

$$T(y) = 0 \qquad (264)$$

For $-y_g + h - h_3 \leq y \leq -y_g + h$

$$T(y) = -13{,}58315 + 0{,}125 \cdot y \qquad (265)$$

The two components of the vector $\underline{\psi}_e$ can be computed according to equations (71) and (72) presented in chapter 3:

$$\psi_{1e} = \frac{\alpha}{A}\int_A T dA =$$

$$= \frac{\alpha}{A}\left\{\int_{-121{,}3348}^{-106{,}3348}\left(-67{,}8899 - \frac{2}{3}y\right)\cdot 1130 dy + \int_{-106{,}3348}^{-96{,}3348}(-9{,}760176 - 0{,}12 \cdot y)\cdot 1130 dy +\right.$$

$$+\int_{-96,3348}^{-81,3348}(-9{,}760176-0{,}12\cdot y)\cdot 3\cdot 50dy+$$

$$+\int_{108,6652}^{128,6652}(-13{,}58315+0{,}125\cdot y)\cdot 800dy\Big\}=$$

$$=\frac{10^{-5}}{84750}\{135599{,}435+27120+2025+20000\}=2{,}179875339\cdot 10^{-5}\quad[-]\qquad(266)$$

$$\psi_{2e}=\frac{\alpha}{I_x}\int_A T\cdot ydA=$$

$$=\frac{\alpha}{I_x}\Big\{\int_{-121,3348}^{-106,3348}\left(-67{,}8899-\frac{2}{3}y\right)\cdot 1130\cdot ydy+$$

$$+\int_{-106,3348}^{-96,3348}(-9{,}760176-0{,}12\cdot y)\cdot 1130\cdot ydy+$$

$$+\int_{-96,3348}^{-81,3348}(-9{,}760176-0{,}12\cdot y)\cdot 3\cdot 50\cdot ydy+$$

$$+\int_{108,6652}^{128,6652}(-13{,}58315+0{,}125\cdot y)\cdot 800\cdot ydy\Big\}=$$

$$=\frac{10^{-5}}{770755249{,}8}\{-15647809{,}56-2759499{,}776-184952{,}97+2439970{,}667\}=$$

$$=-2{,}095644713\cdot 10^{-7}\quad[1/cm]\qquad(267)$$

Knowing the temperature function over the depth of the section and having computed ψ_{1e} and ψ_{2e}, the compatibility stresses in the elastic field are determined according to equation (68):

$$\sigma_e(y)=E_0[\psi_{1e}+\psi_{2e}\cdot y-\alpha\cdot T(y)]\qquad(268)$$

The compatibility stresses distribution over the depth of the section, obtained in this way, is reported in *Figure 73* while the total deformation of the cross section under the plane section hypothesis is represented in *Figure 74*.

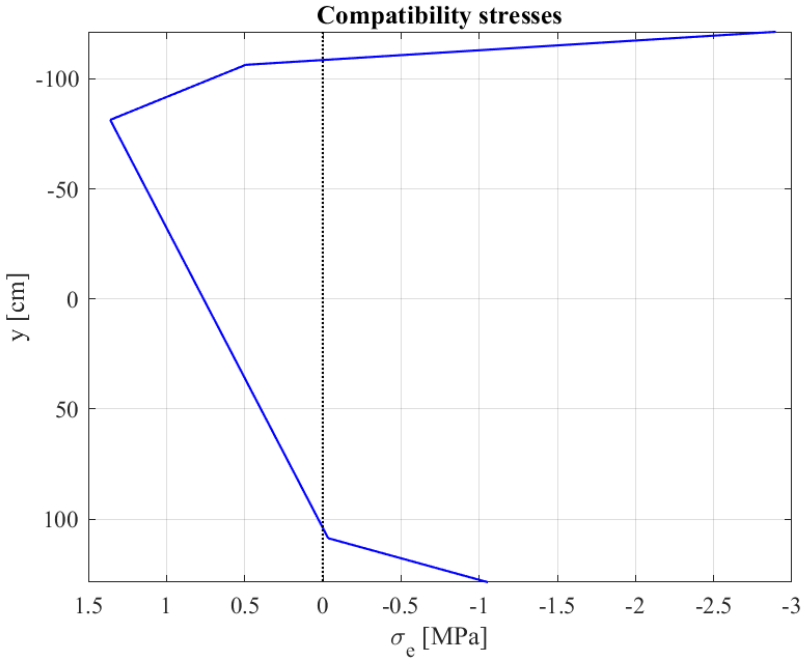

Figure 73 – Compatibility stresses distribution over the depth of the cross section

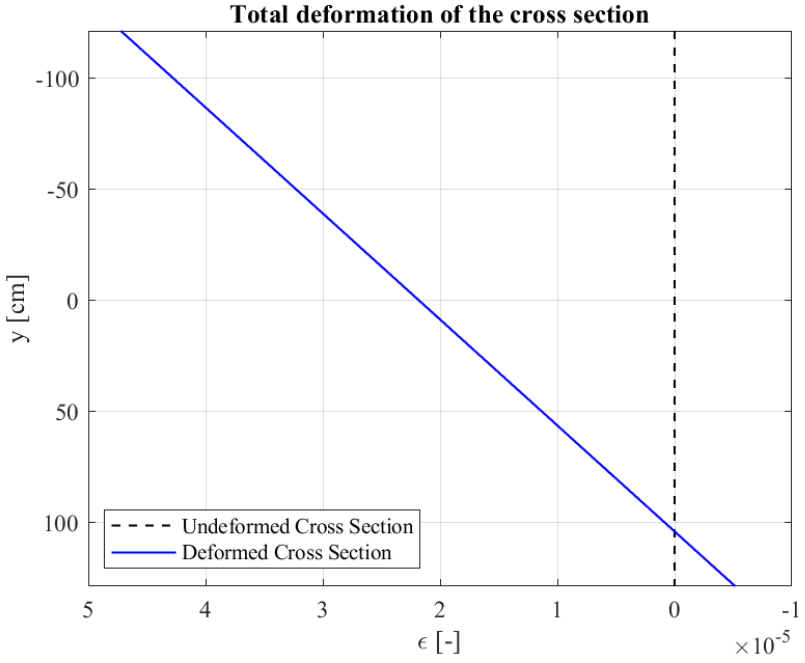

Figure 74 – Total deformation of the cross section

The computations carried out are verified by checking that the equilibrium equations are satisfied:

$$\int_A \underline{\rho}\sigma dA = 0 \qquad (269)$$

which for the case under consideration are written as follow:

$$E_0\left\{\int_{-121.3348}^{-106,3348}\left[2{,}179875339\cdot 10^{-5} - 2{,}095644713\cdot 10^{-7}\cdot y - 10^{-5}\cdot\left(-67{,}8899 - \frac{2}{3}y\right)\right]\cdot\right.$$

$$\cdot 1130dy + \int_{-106,3348}^{-96,3348}[2{,}179875339\cdot 10^{-5} - 2{,}095644713\cdot 10^{-7}\cdot y - 10^{-5}\cdot$$

$$\cdot(-9{,}760176 - 0{,}12\cdot y)]\cdot 1130dy +$$

$$+\int_{-96,3348}^{-81,3348}[2{,}179875339\cdot 10^{-5} - 2{,}095644713\cdot 10^{-7}\cdot y - 10^{-5}\cdot$$

$$\cdot(-9{,}760176 - 0{,}12\cdot y)]\cdot 3\cdot 50dy +$$

$$+\int_{-81,3348}^{93,6652}[2{,}179875339\cdot 10^{-5} - 2{,}095644713\cdot 10^{-7}\cdot y]\cdot 3\cdot\ 50dy +$$

$$+\int_{93,6652}^{108,6652}[2{,}179875339\cdot 10^{-5} - 2{,}095644713\cdot 10^{-7}\cdot y]\cdot 800dy +$$

$$+\int_{108,6652}^{128,6652}[2{,}179875339\cdot 10^{-5} - 2{,}095644713\cdot 10^{-7}\cdot y - 10^{-5}\cdot(-13{,}58315 +$$

$$\left.+0{,}125\cdot y)]\cdot 800dy\right\} = E_0\cdot(-1{,}46954\cdot 10^{-7}) \cong 0 \qquad (270)$$

$$E_0\left\{\int_{-121.3348}^{-106,3348}\left[2{,}179875339\cdot 10^{-5} - 2{,}095644713\cdot 10^{-7}\cdot y - 10^{-5}\cdot\left(-67{,}8899 - \frac{2}{3}y\right)\right]\cdot\right.$$

$$\cdot 1130\cdot ydy + \int_{-106,3348}^{-96,3348}[2{,}179875339\cdot 10^{-5} - 2{,}095644713\cdot 10^{-7}\cdot y - 10^{-5}\cdot$$

$$\cdot(-9{,}760176 - 0{,}12\cdot y)]\cdot 1130\cdot ydy +$$

$$+\int_{-96,3348}^{-81,3348}[2{,}179875339\cdot 10^{-5} - 2{,}095644713\cdot 10^{-7}\cdot y - 10^{-5}\cdot$$

$$\cdot(-9{,}760176 - 0{,}12\cdot y)]\cdot 3\cdot 50\cdot ydy +$$

$$+\int_{-81,3348}^{93,6652}[2{,}179875339\cdot10^{-5}-2{,}095644713\cdot10^{-7}\cdot y]\cdot 3\cdot\ 50\cdot ydy+$$

$$+\int_{93,6652}^{108,6652}[2{,}179875339\cdot10^{-5}-2{,}095644713\cdot10^{-7}\cdot y]\cdot 800\cdot ydy+$$

$$+\int_{108,6652}^{128,6652}[2{,}179875339\cdot10^{-5}-2{,}095644713\cdot10^{-7}\cdot y-10^{-5}\cdot(-13{,}58315+$$

$$+0{,}125\cdot y)]\cdot 800\cdot ydy\}=E_0\cdot(-6{,}125\cdot10^{-5})\cong 0 \qquad (271)$$

The equilibrium equations are both satisfied, therefore the compatibility stresses computed are correct.

Finally, since the bridge under examination is characterized by a redundant static scheme, in order to conclude the analysis in the elastic field, it is necessary to compute the additional stresses due to the redundant restraints. In particular the static scheme to be considered is the following:

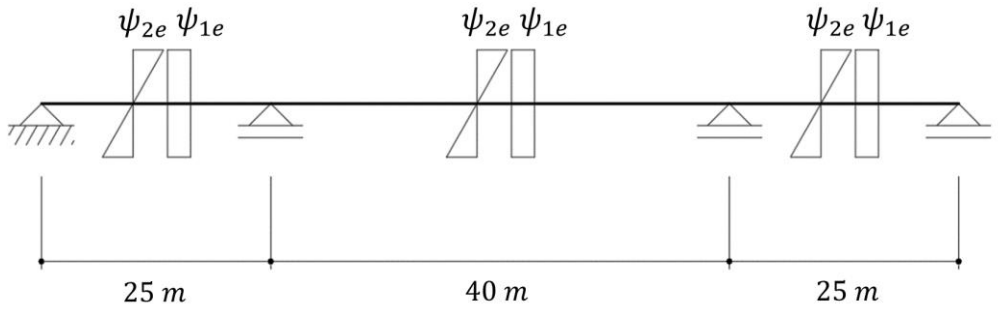

Figure 75 – Static scheme of the multi-span bridge

The structural scheme is analysed in presence of the geometrical actions ψ_{1e} and ψ_{2e} previously determined at the sectional level. The two redundant variables M_1 and M_2 have been highlighted in *Figure 76*, however it is possible to observe that, due to the symmetry in the geometry of the structure as well as in the disposition of the geometrical actions on it, it must be $M_1 = M_2$. Moreover it is worth mentioning that, since no redundant axial variables are present, the geometrical action ψ_{1e} does not appear in the compatibility equations and therefore does not influence the additional stresses distribution.

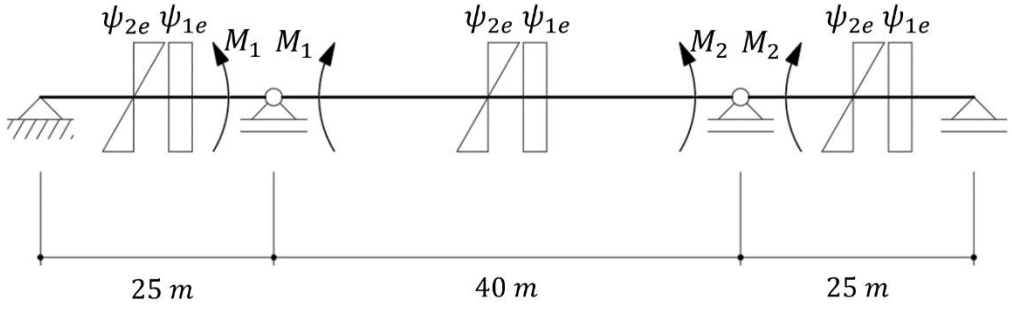

Figure 76 - Static scheme of the multi-span bridge and relative redundant variables

The compatibility equations, necessary to compute the redundant variables, are written as follow:

$$\begin{cases} M_1\left(\frac{l_1}{3E_0I}+\frac{l_2}{3E_0I}\right)+M_2\left(\frac{l_2}{6E_0I}\right)+\psi_{2e}\frac{l_1}{2}+\psi_{2e}\frac{l_2}{2}=0 \\ M_1\left(\frac{l_2}{6E_0I}\right)+M_2\left(\frac{l_1}{3E_0I}+\frac{l_2}{3E_0I}\right)+\psi_{2e}\frac{l_1}{2}+\psi_{2e}\frac{l_2}{2}=0 \end{cases} \quad (272)$$

where:

- $l_1 = 2500\ cm$
- $l_2 = 4000\ cm$
- $E_0 = 35000\ MPa$
- $I = 770755249{,}8\ cm^4$

from which it is obtained:

$$M_1 = M_2 = M = -648467002{,}7\ N \cdot cm \quad (273)$$

The additional stresses distribution for the sections in correspondence of the two central supports is therefore computed as follow:

$$\Delta\sigma_e(y) = E_0 \cdot \left(\frac{M}{E_0I}\cdot y\right) = \frac{M}{I}\cdot y \quad (274)$$

The total stresses at the sectional level, given by the sum of the compatibility stresses $\sigma_e(y)$ and of the additional stresses $\Delta\sigma_e(y)$ are represented in *Figure 77*.

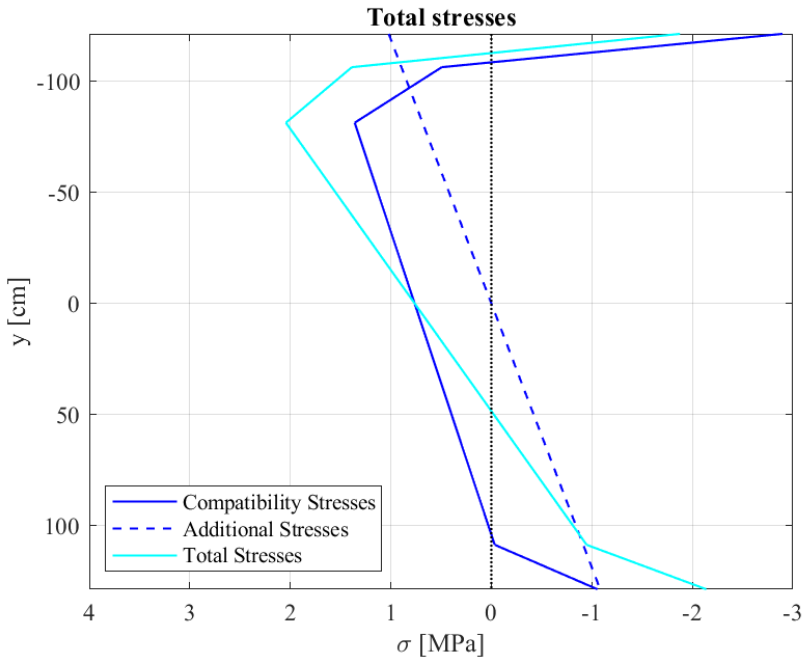

Figure 77 – Total stresses distribution over the depth of the cross section

6.2.3 Analysis of the structure in the viscoelastic field

The analysis in the viscoelastic field in order to compute the compatibility stresses and the additional stresses due to the redundant restraints at 10000 days has been performed by applying the Fundamental Theorem. Moreover, as already discussed, in order to make the procedure immediately feasible for practical applications it is possible to consider the constant value $\chi(t, t_0) = 0{,}8$ to which corresponds $\mu(t, t_0) = -0{,}25$.

Since the temperature distribution provided by the Eurocode and adopted for the present case study is constant in time, the Fundamental Theorem can be written according to the simplified expression given by:

$$\sigma(y,t) = \sigma_1(y,t)\big(1 - \mu(t,t_0)\big) + \mu(t,t_0)\sigma(y,t_0) \qquad (275)$$

In particular, applying equation (275) for the computation of the compatibility stresses, $\sigma(y, t_0)$ is given by the compatibility stresses previously computed with reference to the elastic field:

$$\sigma(y,t_0) = \sigma_e(y) = E_0[\psi_{1e} + \psi_{2e} \cdot y - \alpha \cdot T(y)] \qquad (276)$$

while the stresses $\sigma_1(y,t)$ are given by the same stresses computed adopting the effective modulus E' as follow:

$$\sigma_1(y,t) = E'[\psi_{1e} + \psi_{2e} \cdot y - \alpha \cdot T(y)] \quad (277)$$

where the effective modulus E' is given by:

$$E' = \frac{E_0}{1 + \chi(t,t_0) \cdot \varphi(t,t_0)} = 15625\ MPa \quad (278)$$

with:

- $\chi(t,t_0) = 0{,}8$
- $\varphi(t,t_0) = 1{,}55$

The value of the creep coefficient $\varphi(t,t_0)$ has been determined according to the formulation presented in the CEB-FIP Model Code 1990 [22] assuming $t = 10000$ days, $t_0 = 28$ days, a relative humidity of 70% and a notional size of the member $h = 614\ mm$.

Proceeding in an analogous way, for the computation of the additional stresses due to the redundant restraints at 10000 days, equation (275) is applied assuming:

$$\Delta\sigma(y,t_0) = \Delta\sigma_e(y) = \frac{M}{I} \cdot y \quad (279)$$

and

$$\Delta\sigma_1(y,t) = E'\Delta\sigma(y,t_0) \quad (280)$$

It is important to mention that the Fundamental Theorem can be applied according to the procedure here presented for the computation of the additional stresses due to the redundant restraint because the considered structure is homogeneous and it is not interacting with elastic restraints. In fact, in this case, the Second Theorem of Linear Viscoelasticity holds and because of it the geometrical action ψ_{2e} remains the same as the one computed with reference to the elastic field. As a consequence, when re-writing the compatibility equations in order to compute the redundant variable M which finally provides $\Delta\sigma_1(y,t)$, the known term remains the same one of the elastic field while the stiffness matrix is computed considering the effective modulus E'. This will lead to a different value in the redundant variable from which $\Delta\sigma_1(y,t)$ is computed. However, by performing the computations, it finally results that $\Delta\sigma_1(y,t)$ is given by equation (280).

The compatibility stresses distribution over the depth of the cross section computed at 10000 days is reported in *Figure 78*, while the total stresses distribution at the same time is represented in *Figure 79*.

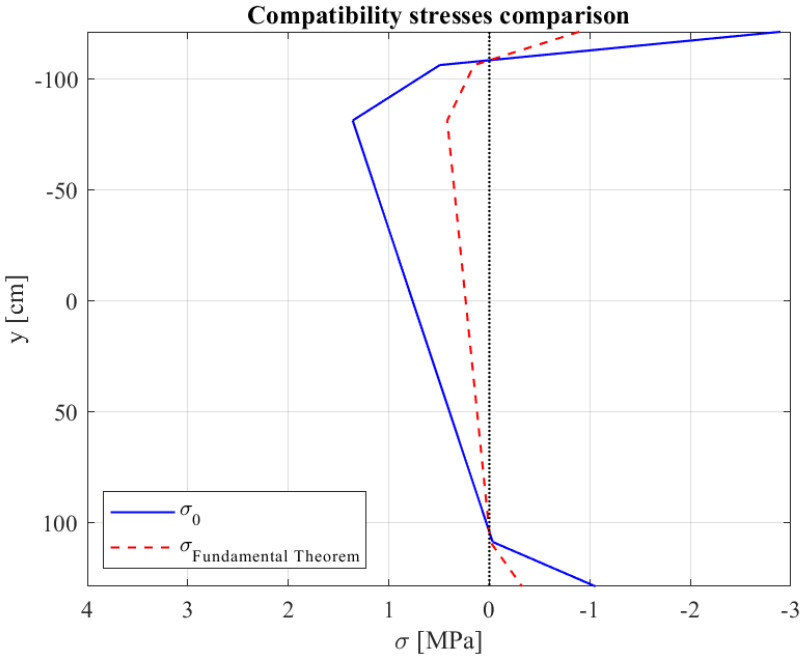

Figure 78 – Compatibility stresses comparison

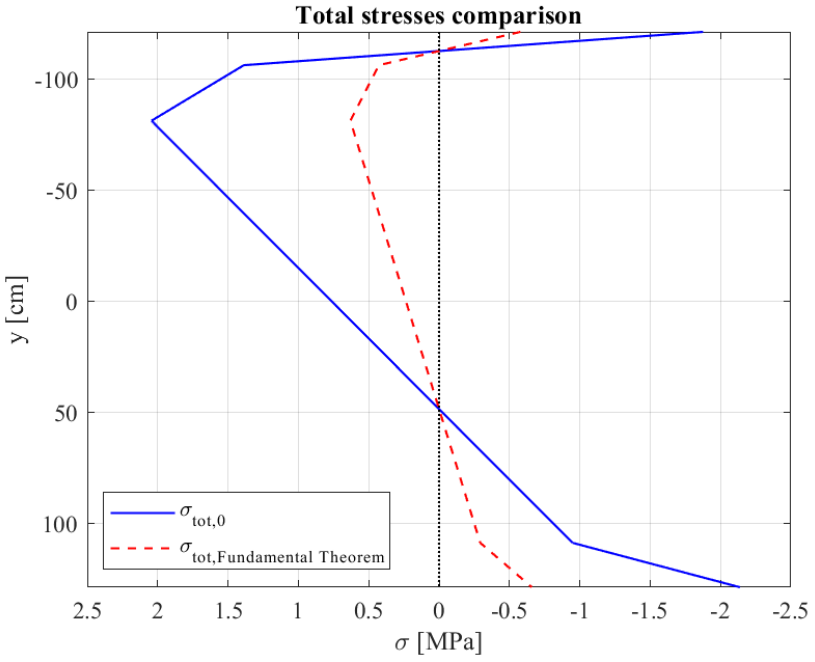

Figure 79 – Total stresses comparison

6.3 Case study 2: Simply supported bridge with composite deck

6.3.1 Description of the structure

The structure analysed consists in a bridge characterized by a composite deck and by a simply supported static scheme. The cross section of the composite deck is represented in *Figure 80* and is made by three I-shaped steel beams and by a reinforced concrete slab.

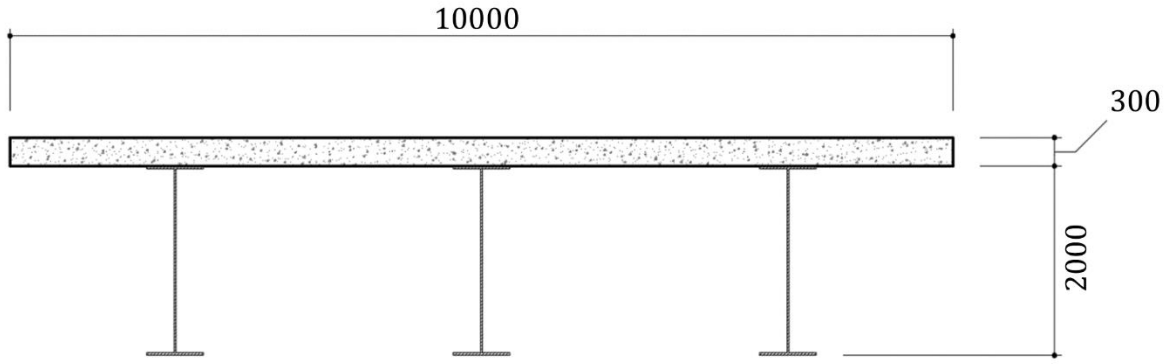

Figure 80 – Cross section of the composite deck (dimensions in mm)

The I-shaped steel beams consists in a 20 mm thick web and two flanges characterized by a thickness of 30 mm and a width of 600 mm. A detail of the I-shaped cross section is reported in *Figure 81*.

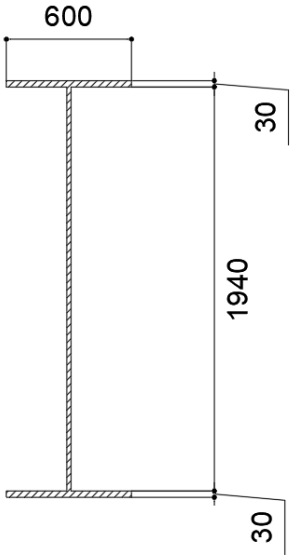

Figure 81 - I-shaped steel beam (dimensions in mm)

For what concerns the characteristics of the materials, for the concrete slab it is adopted a C40/50 concrete, which is endowed with a characteristic cylindrical strength of 40 MPa and with an elastic modulus at 28 days E_0 of 35000 MPa. The modulus of elasticity E_s of the steel beams is instead equal to 210000 MPa.

The coefficient of thermal expansion α_c for concrete is equal to $10^{-5}\ °C^{-1}$ while the one adopted for the steel beams, indicated as α_s, is equal to $1{,}2 \cdot 10^{-5}\ °C^{-1}$.

Since the aim of the present case study is to show the extension of the concepts previously presented to the case of non-homogeneous structures, for sake of simplicity, a simple temperature distribution has been considered: a positive constant temperature ΔT acting only on the steel beams of the composite deck.

6.3.2 Analysis of the structure in the elastic field

In order to extend to the case of non-homogeneous structures the procedure previously presented for the computation of the compatibility stresses due to non-linear temperature distributions, it is important to fix the origin of the principal reference system in the centroid of the homogenized cross section.

The homogenization coefficient α_e is computed as follow:

$$\alpha_e = \frac{E_s}{E_0} = \frac{210000}{35000} = 6 \qquad (281)$$

The position of the centroid of the homogenized cross section is therefore computed with respect to the top fiber of the concrete slab as follow:

$$y_{g,homogenized} = \frac{A_c \cdot y_{g,c} + \alpha_e \cdot A_s \cdot y_{g,s}}{(A_c + \alpha_e \cdot A_s)} = 506{,}2396466\ mm \qquad (282)$$

where:

- $A_c = 3000000\ mm^2$ is the area of the concrete slab cross section
- $A_s = 3 \cdot 74800 = 224400\ mm^2$ is the total area of the steel portion of the cross section
- $y_{g,c} = 150\ mm$ is the position of the centroid of the concrete area with respect to the top fiber of the concrete slab
- $y_{g,s} = 1300$ mm is the position of the centroid of the total steel area with respect to the top fiber of the concrete slab

After having fixed the origin of the principal reference system in the centroid of the homogenized cross section just computed, analogously to what is done in the procedure for the homogeneous cross section, the equilibrium is imposed.

The equilibrium equations are:

$$\int_{A_c} \underline{\rho}\, \sigma_c dA_c + \int_{A_s} \underline{\rho}\, \sigma_s dA_s = 0 \qquad (283)$$

which can be written in extended form as:

$$E_0 \int_{A_c} \left(\underline{\rho}\, \underline{\rho}^T \underline{\psi}_e - \underline{\rho}\, \alpha_c T\right) dA_c + E_s \int_{A_s} \left(\underline{\rho}\, \underline{\rho}^T \underline{\psi}_e - \underline{\rho}\, \alpha_s T\right) dA_s = 0 \qquad (284)$$

Having defined the y coordinate, contained in the vector $\underline{\rho}$, with respect to the centroid of the homogenized cross section, it is possible to write a system of two decoupled equilibrium equations which are:

$$E_0(A_c + \alpha_e A_s) \cdot \psi_{1e} = E_0 \alpha_c \int_{A_c} T(y) dA_c + E_s \alpha_s \int_{A_s} T(y) dA_s = S_{c1} + S_{s1} \qquad (285)$$

$$E_0\left(I_{x,c} + \alpha_e I_{x,s}\right) \cdot \psi_{2e} = E_0 \alpha_c \int_{A_c} T(y) \cdot y dA_c + E_s \alpha_s \int_{A_s} T(y) \cdot y dA_s = S_{c2} + S_{s2} \qquad (286)$$

where:

- $(A_c + \alpha_e A_s)$ is the area of the homogenized cross section
- $\left(I_{x,c} + \alpha_e I_{x,s}\right)$ is the moment of inertia of the homogenized cross section

For the case study under examination the area of the homogenized cross section is:

$(A_c + \alpha_e A_s) = 4346400\ mm^2$

while the moment of inertia of the homogenized cross section is:

$\left(I_{x,c} + \alpha_e I_{x,s}\right) = 2{,}099322701 \cdot 10^{12}\ mm^4$

It is possible to observe that in equation (285) and in equation (286) the quantities S_{c1} and S_{c2} assume null value due to the fact that the temperature distribution over the depth of the cross section is null in correspondence of the concrete slab.

In order to compute the two components of the vector $\underline{\psi}_e$, the quantities S_{s1} and S_{s2} are determined. For what concerns S_{s1} it is interesting to observe that in the present case, due to the fact that the temperature distribution over the area of the steel portion is constant, its expression simply reduces to:

$$S_{s1} = E_s \alpha_s \int_{A_s} T(y) dA_s = E_s \alpha_s \int_{A_s} \Delta T\, dA_s = E_s \alpha_s \Delta T \cdot A_s \qquad (287)$$

For what concerns S_{s2} instead, for the same reason, its expression simply reduces to:

$$S_{s2} = E_s\alpha_s \int_{A_s} T(y) \cdot y dA_s = E_s\alpha_s \int_{A_s} \Delta T \cdot y dA_s = E_s\alpha_s \Delta T \cdot S_{y_g} \quad (288)$$

where $S_{y_g}$is the first order moment of the area of steel.

From equation (285) it is therefore obtained ψ_{1e} as follow:

$$E_0(A_c + \alpha_e A_s) \cdot \psi_{1e} = E_s\alpha_s \Delta T \cdot A_s \quad (289)$$

$$E_0(A_c + \alpha_e A_s) \cdot \psi_{1e} = E_0 \cdot \alpha_e \cdot \alpha_s \Delta T \cdot A_s \quad (290)$$

$$4346400 \cdot \psi_{1e} = \alpha_s \Delta T \cdot 1346400 \quad (291)$$

$$\psi_{1e} = \alpha_s \Delta T \cdot 0{,}3097736057\ [-] \quad (292)$$

while from equation (286) it is obtained ψ_{2e} as follow:

$$E_0\left(I_{x,c} + \alpha_e I_{x,s}\right) \cdot \psi_{2e} = E_s\alpha_s \Delta T \cdot S_{y_g} \quad (293)$$

$$E_0\left(I_{x,c} + \alpha_e I_{x,s}\right) \cdot \psi_{2e} = E_0 \cdot \alpha_e \cdot \alpha_s \Delta T \cdot S_{y_g} \quad (294)$$

$$2{,}099322701 \cdot 10^{12} \cdot \psi_{2e} = \alpha_s \Delta T \cdot 1068718939 \quad (295)$$

$$\psi_{2e} = \alpha_s \Delta T \cdot 5{,}0907797 \cdot 10^{-4}\ [1/mm] \quad (296)$$

Having computed ψ_{1e} and ψ_{2e} and knowing the temperature distribution over the depth of the cross section, the compatibility stresses in the concrete portion are obtained as follow:

$$\sigma_{e,c}(y) = E_0[\psi_{1e} + \psi_{2e} \cdot y - \alpha_c T(y)] \quad (297)$$

while the compatibility stresses in the steel portion are obtained as:

$$\sigma_{e,s}(y) = E_s[\psi_{1e} + \psi_{2e} \cdot y - \alpha_s T(y)] \quad (298)$$

The compatibility stresses distribution over the depth of the section, obtained in this way, is reported in *Figure 82* while the total deformation of the cross section under the plane section hypothesis is represented in *Figure 83*.

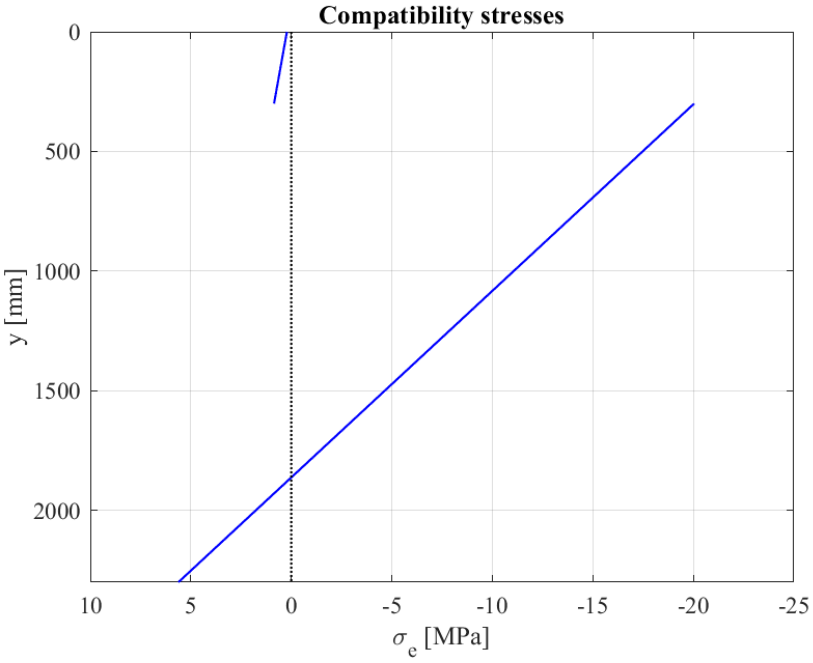

Figure 82 – Compatibility stresses distribution over the depth of the cross section

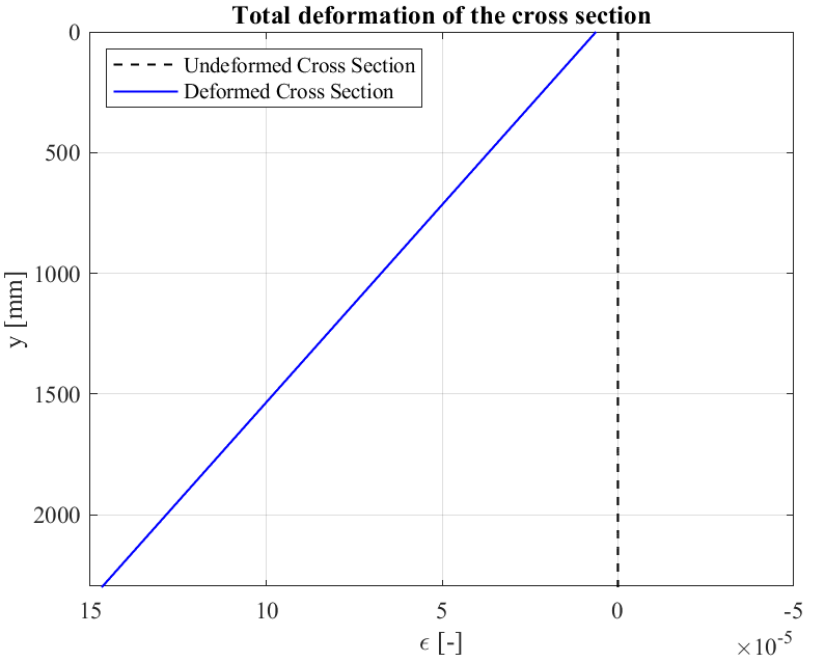

Figure 83 – Total deformation of the cross section

The computations carried out are verified by checking that the equilibrium equations are satisfied:

$$\int_{A_c} \underline{\rho}\, \sigma_c dA_c + \int_{A_s} \underline{\rho}\, \sigma_s dA_s = 0 \qquad (299)$$

which for the case under consideration are written as follow:

$$\int_{A_c} E_0[\psi_{1e} + \psi_{2e} \cdot y] dA_c + \int_{A_s} E_s[\psi_{1e} + \psi_{2e} \cdot y - \alpha_s \Delta T] dA_s =$$

$$= E_0 \left\{ \int_{A_c} [\psi_{1e} + \psi_{2e} \cdot y] dA_c + \alpha_e \cdot \int_{A_s} [\psi_{1e} + \psi_{2e} \cdot y - \alpha_s \Delta T] dA_s \right\} =$$

$$= E_0 \alpha_s \Delta T \left\{ \int_{-506,2396466}^{-206,2396466} [0{,}3097736057 + 5{,}0907797 \cdot 10^{-4} \cdot y] \cdot 10000 dy + \right.$$

$$+6 \cdot \int_{-206,2396466}^{-176,2396466} [0{,}3097736057 + 5{,}0907797 \cdot 10^{-4} \cdot y - 1] \cdot 3 \cdot 600 dy +$$

$$+6 \cdot \int_{-176,2396466}^{1763,760353} [0{,}3097736057 + 5{,}0907797 \cdot 10^{-4} \cdot y - 1] \cdot 3 \cdot 20 dy +$$

$$\left. +6 \cdot \int_{1763,760353}^{1793,760353} [0{,}3097736057 + 5{,}0907797 \cdot 10^{-4} \cdot y - 1] \cdot 3 \cdot 600 dy \right\} =$$

$$= E_0 \alpha_s \Delta T \{-3{,}4 \cdot 10^{-4}\} = -1{,}428 \cdot 10^{-4} \cdot \Delta T \cong 0 \qquad (300)$$

$$\int_{A_c} E_0[\psi_{1e} + \psi_{2e} \cdot y] \cdot y dA_c + \int_{A_s} E_s[\psi_{1e} + \psi_{2e} \cdot y - \alpha_s \Delta T] \cdot y dA_s =$$

$$= E_0 \left\{ \int_{A_c} [\psi_{1e} + \psi_{2e} \cdot y] \cdot y dA_c + \alpha_e \cdot \int_{A_s} [\psi_{1e} + \psi_{2e} \cdot y - \alpha_s \Delta T] \cdot y dA_s \right\} =$$

$$= E_0 \alpha_s \Delta T \left\{ \int_{-506,2396466}^{-206,2396466} [0{,}3097736057 + 5{,}0907797 \cdot 10^{-4} \cdot y] \cdot 10000 \cdot y dy + \right.$$

$$+6 \cdot \int_{-206,2396466}^{-176,2396466} [0{,}3097736057 + 5{,}0907797 \cdot 10^{-4} \cdot y - 1] \cdot 3 \cdot 600 \cdot y dy +$$

$$+6 \cdot \int_{-176,2396466}^{1763,760353} [0{,}3097736057 + 5{,}0907797 \cdot 10^{-4} \cdot y - 1] \cdot 3 \cdot 20 \cdot y dy +$$

$$+6 \cdot \int_{1763,760353}^{1793,760353} [0{,}3097736057 + 5{,}0907797 \cdot 10^{-4} \cdot y - 1] \cdot 3 \cdot 600 \cdot y dy \Big\} =$$

$$= E_0 \alpha_s \Delta T\{-1{,}19\} = -0{,}4998 \cdot \Delta T \cong 0 \qquad (301)$$

The equilibrium equations are both satisfied, therefore the compatibility stresses computed are correct.

6.3.3 Analysis of the structure in the viscoelastic field

In order to perform the analysis in the viscoelastic field it is important to highlight the fact that, since the structure is non-homogeneous, the Second Theorem of Linear Viscoelasticity does not hold. Therefore, differently from what happens in the case of homogeneous cross sections, the total deformation at time t is not the same as the one computed with reference to the elastic field.

Consequently the components of the vector $\underline{\psi}$ have to be re-computed according to an analogous procedure to the one discussed in paragraph 6.3.2 with reference to the elastic field. The only difference is that here the cross section has to be homogenized considering a different value of α_e.

In particular for the computation of the homogenization coefficient α_e it considered the ratio between the modulus of elasticity E_s and the effective modulus E':

$$\alpha'_e = \frac{E_s}{E'} = \frac{210000}{14982{,}877} = 14{,}02 \qquad (302)$$

where the effective modulus E' has been computed as follow:

$$E' = \frac{E_0}{1 + \chi(t, t_0) \cdot \varphi(t, t_0)} = 14982{,}877\ MPa \qquad (303)$$

with:

- $\chi(t, t_0) = 0{,}8$
- $\varphi(t, t_0) = 1{,}67$

The value of the creep coefficient $\varphi(t, t_0)$ has been determined according to the formulation presented in the CEB-FIP Model Code 1990 [22] assuming $t = 10000$ days, $t_0 = 28$ days, a relative humidity of 70% and a notional size of the member $h = 319\ mm$.

The position of the centroid of the homogenized cross section is therefore computed with respect to the top fiber of the concrete slab as follow:

$$y'_{g,homogenized} = \frac{A_c \cdot y_{g,c} + \alpha'_e \cdot A_s \cdot y_{g,s}}{(A_c + \alpha'_e \cdot A_s)} = 738{,}6673279\ mm \qquad (304)$$

where:

- $A_c = 3000000\ mm^2$ is the area of the concrete slab cross section
- $A_s = 3 \cdot 74800 = 224400\ mm^2$ is the total area of the steel portion of the cross section
- $y_{g,c} = 150\ mm$ is the position of the centroid of the concrete area with respect to the top fiber of the concrete slab
- $y_{g,s} = 1300$ mm is the position of the centroid of the total steel area with respect to the top fiber of the concrete slab

After having fixed the origin of the principal reference system in the centroid of the homogenized cross section just computed, analogously to what is done in the procedure described for the elastic field, the equilibrium is imposed considering the effective modulus E' and the homogenization coefficient α'_e. Proceeding in this way the two components of the vector $\underline{\psi}$ are computed and are given by:

$$\psi_1 = \alpha_s \Delta T \cdot 0{,}511884633 \quad [-] \tag{305}$$

$$\psi_2 = \alpha_s \Delta T \cdot 4{,}377339322 \cdot 10^{-4} \quad [1/mm] \tag{306}$$

The obtained results can be verified by checking that the equilibrium equations are satisfied:

$$\int_{A_c} \underline{\rho}\, \sigma_c dA_c + \int_{A_s} \underline{\rho}\, \sigma_s dA_s = 0 \tag{307}$$

which for the case under consideration are written as follow:

$$\int_{A_c} E'[\psi_1 + \psi_2 \cdot y] dA_c + \int_{A_s} E_s[\psi_1 + \psi_2 \cdot y - \alpha_s \Delta T] dA_s =$$

$$= E' \left\{ \int_{A_c} [\psi_1 + \psi_2 \cdot y] dA_c + \alpha'_e \cdot \int_{A_s} [\psi_1 + \psi_2 \cdot y - \alpha_s \Delta T] dA_s \right\} =$$

$$= E' \alpha_s \Delta T \left\{ \int_{-738,6673279}^{-438,6673279} [0{,}511884633 + 4{,}377339322 \cdot 10^{-4} \cdot y] \cdot 10000 dy + \right.$$

$$+14{,}02 \cdot \int_{-438,6673279}^{-408,6673279} [0{,}511884633 + 4{,}377339322 \cdot 10^{-4} \cdot y - 1] \cdot 3 \cdot 600 dy +$$

$$+14{,}02 \cdot \int_{-408,6673279}^{1531,332672} [0{,}511884633 + 4{,}377339322 \cdot 10^{-4} \cdot y - 1] \cdot 3 \cdot 20 dy +$$

$$\left. +14{,}02 \cdot \int_{1531,332672}^{1561,332672} [0{,}511884633 + 4{,}377339322 \cdot 10^{-4} \cdot y - 1] \cdot 3 \cdot 600 dy \right\} =$$

$$= E'\alpha_s \Delta T\{3 \cdot 10^{-4}\} = 5{,}39383572 \cdot 10^{-5} \cdot \Delta T \cong 0 \quad (308)$$

$$\int_{A_c} E'[\psi_1 + \psi_2 \cdot y] \cdot y dA_c + \int_{A_s} E_s[\psi_1 + \psi_2 \cdot y - \alpha_s \Delta T] \cdot y dA_s =$$

$$= E'\left\{\int_{A_c} [\psi_1 + \psi_2 \cdot y] \cdot y dA_c + \alpha'_e \cdot \int_{A_s} [\psi_1 + \psi_2 \cdot y - \alpha_s \Delta T] \cdot y dA_s\right\} =$$

$$= E'\alpha_s \Delta T \left\{\int_{-738{,}6673279}^{-438{,}6673279} [0{,}511884633 + 4{,}377339322 \cdot 10^{-4} \cdot y] \cdot 10000 \cdot y dy + \right.$$

$$+14{,}02 \cdot \int_{-438{,}6673279}^{-408{,}6673279} [0{,}511884633 + 4{,}377339322 \cdot 10^{-4} \cdot y - 1] \cdot 3 \cdot 600 \cdot y dy +$$

$$+14{,}02 \cdot \int_{-408{,}6673279}^{1531{,}332672} [0{,}511884633 + 4{,}377339322 \cdot 10^{-4} \cdot y - 1] \cdot 3 \cdot 20 \cdot y dy +$$

$$\left. +14{,}02 \cdot \int_{1531{,}332672}^{1561{,}332672} [0{,}511884633 + 4{,}377339322 \cdot 10^{-4} \cdot y - 1] \cdot 3 \cdot 600 \cdot y dy \right\} =$$

$$= E'\alpha_s \Delta T\{0{,}801\} = 0{,}1440154137 \cdot \Delta T \cong 0 \quad (309)$$

The equilibrium equations are both satisfied, therefore the obtained results are correct.

Since the temperature distribution adopted for the present case study is constant in time, the Fundamental Theorem can be written according to the simplified expressions given by:

$$\sigma_c(y,t) = \sigma_{1,c}(y,t)\big(1 - \mu(t,t_0)\big) + \mu(t,t_0)\sigma_c(y,t_0) \quad (310)$$

$$\sigma_s(y,t) = \sigma_{1,s}(y,t)\big(1 - \mu(t,t_0)\big) + \mu(t,t_0)\sigma_s(y,t_0) \quad (311)$$

$$\varepsilon(y,t) = \varepsilon_1(y,t)\big(1 - \mu(t,t_0)\big) + \mu(t,t_0)\varepsilon(y,t_0) \quad (312)$$

where, for the case study under examination:

- $\sigma_c(y,t_0)$ are the stresses in concrete previously computed in the elastic field
- $\sigma_s(y,t_0)$ are the stresses in steel previously computed in the elastic field
- $\varepsilon(y,t_0)$ is the total deformation previously computed in the elastic field
- $\sigma_{1,c}(y,t) = E'[\psi_1 + \psi_2 \cdot y]$
- $\sigma_{1,s}(y,t) = E_s[\psi_1 + \psi_2 \cdot y - \alpha_s \Delta T]$
- $\varepsilon_1(y,t) = \psi_1 + \psi_2 \cdot y$

A very important aspect to be considered in applying the Fundamental Theorem as reported above, is the fact that the stresses $\sigma_c(y,t_0)$ and $\sigma_s(y,t_0)$ as well as the total deformation $\varepsilon(y,t_0)$ have been computed in the elastic field considering a y coordinate whose origin was fixed in the centroid of the cross section homogenized adopting a factor $\alpha_e = 6$ while $\sigma_{1,c}(y,t)$, $\sigma_{1,s}(y,t)$, $\varepsilon_1(y,t)$ have been computed considering a y coordinate whose origin was fixed in the centroid of the cross section homogenized adopting a factor $\alpha'_e = 14{,}02$. The correct application of the Fundamental Theorem implies therefore the necessity to refer all the previously cited quantities to the same coordinate y, in order to perform in equations (310),(311) and (312) the summations of stresses and deformations at the level of the same fiber of the cross section.

The comparison in terms of compatibility stresses between the results obtained in the elastic field and the ones obtained in the viscoelastic field at 10000 days is reported in *Figure 84.*

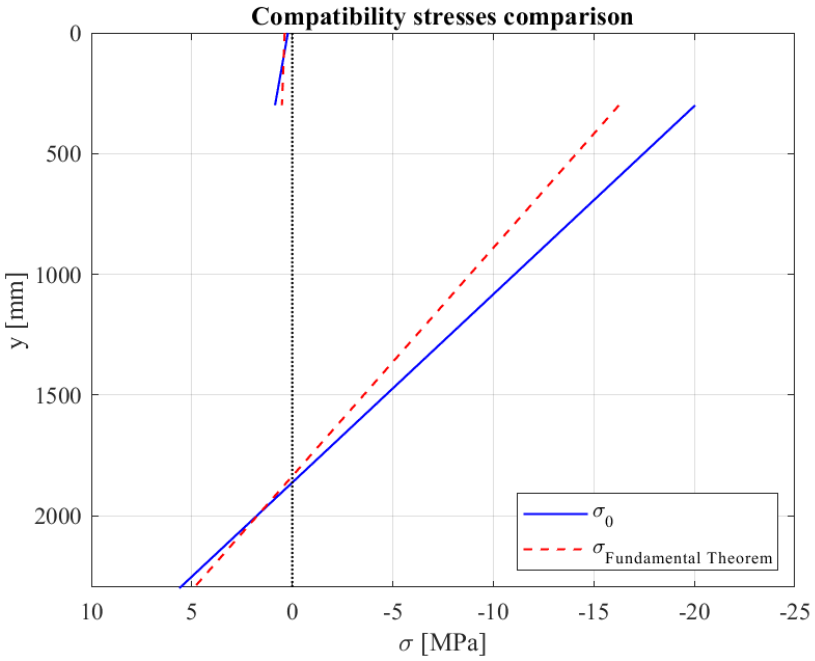

Figure 84 – Compatibility stresses comparison

Moreover the comparison in terms of total deformation of the cross section between the results obtained in the elastic field and the ones obtained in the viscoelastic field at 10000 days is reported in *Figure 85*.

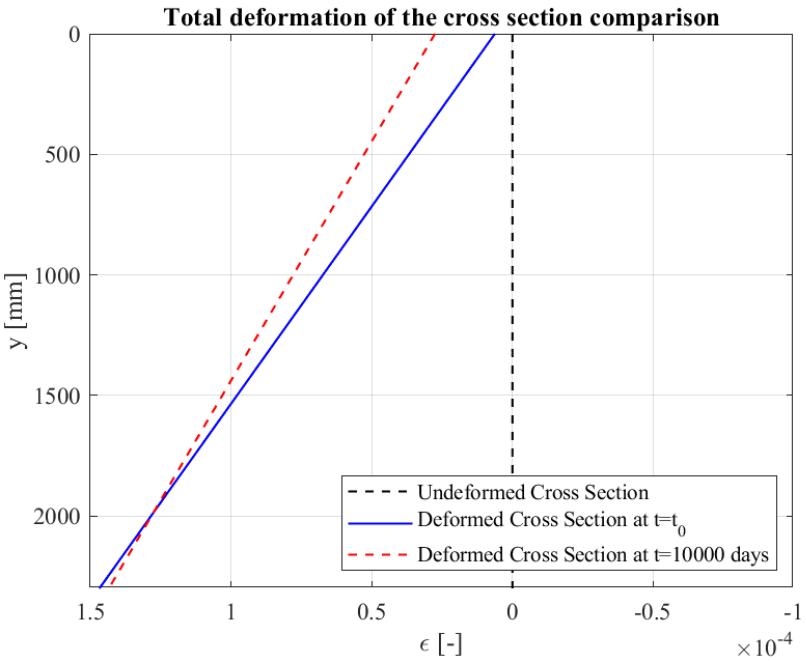

Figure 85– Total deformation of the cross section comparison

7 CONCLUSIONS AND FUTURE RESEARCH

As testified by many references which can be found in literature, the analysis of the response of bridges to thermal actions is a particularly relevant topic, as also confirmed by several cases of damages suffered by this type of structures.

Because of the climatic actions, bridge structures are subject to non-linear temperature distributions which cause the arising of compatibility stresses in order to satisfy the plane section hypothesis under Bernoulli beam bending. Moreover when redundant structures are considered, the effect of thermal actions produces additional stresses due to the reactions of the redundant restraints.

After having discussed in detail the procedure in order to compute the above mentioned stresses in the elastic field, the influence of the long-term behaviour of concrete has been studied with reference to the viscoelastic field. In particular it has been shown that, in order to rigorously treat the problem of the computation of the stresses which arise in bridges due to non-linear temperature distributions in the viscoelastic field, a sinusoidal temperature variation, which reproduces with sufficient precision the seasonal variation of climatic actions, should be considered. In this framework the only solution for the problem is given by the exact formulation, which is based on the numerical integration of a Volterra Integral Equation. However this procedure, in the framework of sinusoidal temperature variations, results to be particularly involved and therefore not suitable for the engineering practice.

Thanks to the analyses performed in the viscoelastic field in presence of simpler variations of the temperature in time, it has been possible to demonstrate the excellent level of accuracy of the Fundamental Theorem in approximating the exact solution given by the numerical integration of the Volterra Integral Equation. This aspect, together with the simplicity of application of the Fundamental Theorem, which basically consists in the superposition of three elastic solutions, makes this procedure a particularly convenient tool for the engineering practice. Moreover this procedure results to be exact in the case of temperature distributions constant in time, such as the ones suggested by national and international code prescriptions, while it becomes approximate when for sake of simplicity $\chi(t, t_0)$ is assumed equal to 0,8. This choice is motivated in practical applications by the fact that the variation in time of the function $\chi(t, t_0)$ can be in many cases neglected by adopting this value and by making the procedure immediately feasible for the engineering practice.

In conclusion, after having discussed in detail all the theoretical aspects characterizing the problem of the evaluation of the long-term response of bridges to thermal actions, the analysis of the real structure of the first case study has allowed to show the applicability of the discussed procedure in presence of the non-linear temperature distribution provided by the Eurocode 1 [11]. Moreover the second real structure analysed has allowed to show the extension of the procedure, previously

discussed with reference to homogeneous cross sections, to the case of non-homogenous cross sections, providing in this way the necessary tools to analyse also bridges with composite reinforced concrete-steel decks.

Future developments in the research for the problems studied in the present work could be oriented to provide additional examples of applications, considering also other non-linear temperature distributions from international standards. For what concerns instead the analysis of bridges characterized by non-homogeneous cross sections, the problem could be approached also by adopting the method of the Reduced Relaxation Functions. Also in this case however, the solution of the problem in presence of temperature distributions varying in time, would be quite involved and therefore not applicable in the engineering practice.

REFERENCES:

[1] M. Froli, *La risposta termica delle strutture interagenti con il clima*. Plus-Pisa University Press, 2006.

[2] F. Leonhardt, "Rißschäden an Betonbrücken - Ursachen und Abhilfe.," *Beton- und Stahlbetonbau*, vol. 74, no. 2, pp. 36–44, Feb. 1979.

[3] "Effetti della temperatura nelle strutture di calcestruzzo. Determinazione della distribuzione della temperatura. CNR DT3/87 | CNR Edizioni." 1994.

[4] "C.E.B.: 'Thermal Effects in Concrete Structures', Bulletin d'Information n°167," 1985. https://www.fib-international.org/publications/ceb-bulletins/thermal-effects-in-concrete-structures-detail.html.

[5] E. Mirambell and A. Aguado, "Acciones térmicas de diseño en puentes cajón de hormigón | Hormigón y Acero," 1987.

[6] A. G. Lanigan, "The Temperature Response of Concrete Box Girder Bridges," 1973.

[7] M. N. Elbadry and A. Ghali, "Non linear Temperature Distributions and its Effects on Bridges," 1983.

[8] A. Ghali and M. N. Elbadry, "Thermal Stresses and Cracking of Concrete Bridges," *ACI J. Proc.*, vol. 83, no. 6.

[9] S. P. Timoshenko and J. N. Goodier, *Theory of Elasticity*, Third Edit. 1985.

[10] E. Mirambell and A. Aguado, "Thermal Response of Concrete Box Girder Bridges," 1988.

[11] "EUROCODE 1, UNI EN 1991-1-5: General actions - Thermal actions." .

[12] M. Emerson, "Temperature Differences in Bridges: Basis of Design Requirements," *Transport and Road Research Laboratory Report TRRL*. 1977.

[13] M. Emerson, "Extreme values of bridge temperatures for design purposes," *TRRL Report LR 744*. 1977.

[14] "BS5400-2 : Steel, Concrete and Composite Bridges Part 2: Specification for Loads," *British Standard Institution*. 1978.

[15] M. Emerson, "Bridge Temperatures Estimated From the Shade Temperature," *TRRL Report LR 696*. 1976.

[16] M. Emerson, "The Calculation of the Distribution of Temperature in Bridges," *TRRL Report LR 561*. 1973.

[17] "NZMWD 1977: Highway Bridge Design Brief Issue C-Amendments," *Office of the Chief Designing Engineer, Ministry of Work and Development*. 1976.

[18] "NAASRA: NAASRA Bridge Design Specification," *National Association of Australian State Road Authorities.* 1976.

[19] D. McHenry, "A new aspect of creep in concrete and its application to design," *Proceedings, Am. Soc. Test. Mater.*, vol. 43, pp. 1069–1084, 1943.

[20] H. Trost, "Auswirkungen des Superpositionsprinzips auf Kriech-und Relaxationsprobleme bei Beton und Spannbeton," *Beton-und stahlbetonbau*, vol. 10, pp. 230-238,261-269, 1967.

[21] Z. P. Bazant, "Prediction of Concrete Creep Effects Using Age-Adjusted Effective Modulus Method," *ACI J.*, vol. 69, pp. 212–217, 1972.

[22] "CEB/FIP Model Code 90 Design Code." T. Telford, London, 1993.

[23] "EUROCODE 2, UNI EN 1992-1-1: General Rules and Rules for Buildings." .

[24] F. Mola, "'New Theoretical Aspects in Linear Viscoelastic Analysis of Concrete Structures' - 32nd Conference on OUR WORLD IN CONCRETE & STRUCTURES: 28-29 August 2007, Singapore."

[25] M. A. Chiorino, M. Koprna, F. Mola, and P. Napoli, "'CEB-FIP Manual on Structural Effects of Time Dependent Behaviour of Concrete' , CEB Bulletin d'Information N°142-142bis." Georgi, St. Saphorin, CH, 1984.

[26] F. Mola and A. Palermo, "Analisi a Lungo Termine di Elementi in Calcestruzzo Armato Soggetti a Variazioni Termiche Stagionali." Studi e Ricerche, Scuola di Specializzazione in Costruzioni in C.A. - Fratelli Pesenti, Milano, 2000.